

WATERSHED-SCALE HYDROLOGY: INFLUENCES OF SPATIAL VARIABILITY
OF SNOWPACK IN A SEMIARID, MOUNTAINOUS ENVIRONMENT


by
Rajiv Prasad

A dissertation submitted in partial fulfillment
of the requirements for the degree


of
DOCTOR OF PHILOSOPHY
in

Civil and Environmental Engineering

Approved:



Dr. David G. Tarboton
Major Professor



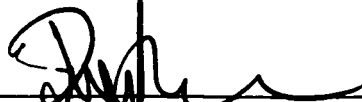
Dr. Christopher M. U. Neale
Committee Member




Dr. Thomas B. Hardy
Committee Member



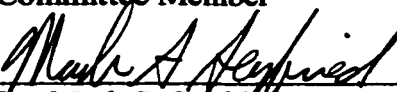
Dr. Gerald N. Flerchinger
Committee Member




Dr. David S. Bowles
Committee Member



Dr. Uppanu Lall
Committee Member



Dr. Mark S. Seyfried
Committee Member



Dr. Thomas L. Kent
Dean of Graduate Studies

UTAH STATE UNIVERSITY
Logan, Utah

2001

ABSTRACT**Watershed-Scale Hydrology: Influences of Spatial Variability
of Snowpack in a Semiarid, Mountainous Environment****by****Rajiv Prasad, Doctor of Philosophy****Utah State University, 2001****Major Professor: Dr. David G. Tarboton
Department: Civil and Environmental Engineering**

Water is a precious resource in the semiarid western U. S. rangeland. In order to effectively develop and allocate water, one needs to accurately know the volume and timing of streamflow from these watersheds. This study used a combination of extensive data analysis and modeling to understand the nature of annual hydrologic mass balance at a range of spatial scales within Reynolds Creek Experimental Watershed (RCEW). The study is presented as a collection of three papers, which focus on building a working hypothesis at a small scale, and then testing its transferability to a larger scale.

The dominant hydrologic process in RCEW is the highly spatially variable surface water input (SWI), a result of wind-induced snow drifting combined with variability of air temperature with elevation and spatial variability of net radiation due to terrain effects. The drift factor approach was used to parameterize wind-induced snow drifting. A quantitative basis was established for subdividing watersheds into modeling elements

based on the distribution of the drift factors. The working hypothesis for the first-order watershed is that most of the runoff is generated by SWI into the deep snowdrift zone located on the north-facing leeward slope, whereas the SWI on the rest of the watershed is used mainly to satisfy evapotranspiration and subsurface storage demands.

It is impractical to conduct manual snow surveys at appreciably sized watersheds. Instead, a physically based, blowing snow model was used to simulate snow drift. Its performance was tested against manually surveyed snow water equivalence maps and the calibrated drift factor map at the first-order watershed. The simulated pattern of snow accumulation did not agree well with observations in a pointwise comparison. It was found, however, that drift factors obtained from the blowing snow model can be used to parameterize the distribution of the drift pattern within an error bound of 25% if the variability of precipitation between measurement sites is of the order of 70%.

The understanding of annual hydrologic mass balance was transferred to a larger, fourth-order watershed within RCEW. Parameters of the above-surface, SWI model calibrated at the first-order watershed could be transferred to the fourth-order watershed. Parameters of the below-surface, hydrologic mass balance model calibrated at the first-order watershed also transferred to the fourth-order watershed with minor modifications. Annual mass balance was found sensitive to two parameters and the initial conditions.

(202 pages)

In memory of three men who taught me to ask “why?”

Dr. Rameshwar Prasad, my father

Dr. Pravin P. Gupta, dear friend

Sri Kedar N. Sonar, loving grandfather

ACKNOWLEDGMENTS

I would like to thank my major professor, Dr. David G. Tarboton, for the opportunity to work with him and the continued financial support. His patience has helped me develop my potential as a researcher, and his insight has guided my quest for answers during the course of this work. I owe a great deal to these excellent teachers and valued members of my dissertation committee: Drs. David S. Bowles, Christopher M.U. Neale, Upmanu Lall, Thomas B. Hardy, Mark S. Seyfried, and Gerald N. Flerchinger. I would also like to thank Drs. Keith R. Cooley, Danny Marks, and Glen E. Liston for providing valuable suggestions. Dr. Liston also provided model runs for Chapter 3.

Several friends and colleagues deserve mention for the help and advice during my stay in Logan: Abhijeet, Abhay, Ashish, Ashutosh, Balaji, Deepa, Charlie, Kevin, Jyotsna, Liji, Pankaj, Sanjay, Shyamal, Shaleen, Umesh, and Unni, among many others. Special thanks are also due to my mother, Mrs. Bharti Prabha, and my brother, Dr. Rakesh Prasad, for extended patience, without which this work could not have been completed.

This work was supported in part by the Environmental Protection Agency (agreement no: R824784) under the National Science Foundation/Environmental Protection Agency Water and Watersheds program. The views and conclusions expressed are those of the author and should not be interpreted as necessarily representing the official policies, either expressed or implied, of the U.S. Government.

Rajiv Prasad

CONTENTS

	Page
ABSTRACT.....	ii
DEDICATION.....	iv
ACKNOWLEDGMENTS	v
LIST OF TABLES.....	ix
LIST OF FIGURES	x
CHAPTER	
1. INTRODUCTION	1
1. Background.....	1
2. Objectives	5
3. Outline.....	6
References.....	9
2. UNDERSTANDING THE HYDROLOGIC BEHAVIOR OF A SMALL SEMIARID MOUNTAINOUS WATERSHED IN IDAHO, UNITED STATES OF AMERICA.....	12
Abstract.....	12
1. Introduction.....	13
2. Study Site and Available Data	14
3. Modeling Surface Water Input.....	16
4. Analysis of Surface Water Input at Upper Sheep Creek.....	28
5. The Dominant Zone Hydrologic Model	30
5.1. Surface Water Input	31
5.2. Evapotranspiration	31
5.3. Soil Zone	32
5.4. Saturated Zone (Baseflow)	34
5.5. Streamflow.....	35
6. Calibration of DZHM	35
7. Model Performance.....	38

7.1. PDIMS	38
7.2. DZHM.....	39
8. Mass Balance Components at USC for 1992-93	39
9. Summary and Conclusions	41
References.....	43
3. TESTING A BLOWING SNOW MODEL AGAINST DISTRIBUTED SNOW MEASUREMENTS AT UPPER SHEEP CREEK, IDAHO, UNITED STATES OF AMERICA	64
Abstract.....	64
1. Introduction.....	65
2. Study Site and Available Data	67
3. The Snow Transport Model	70
4. SnowTran-3D Results.....	74
4.1. Drift Factors	79
4.2. Modeled Basin Average SWE	81
4.3. Scouring and Accumulation Modeled by SnowTran-3D.....	83
4.4. Distribution Function Comparisons.....	86
5. Conclusions.....	90
References.....	92
4. HYDROLOGIC BEHAVIOR OF A FOURTH-ORDER WATERSHED IN REYNOLDS CREEK, IDAHO, UNITED STATES OF AMERICA.....	115
Abstract.....	115
1. Introduction.....	116
2. Study Site.....	118
3. Drift Factors and Surface Water Input Zones for Tollgate	119
4. Interpolation of Precipitation to Obtain Spatial Field.....	121
5. Surface Water Input at Tollgate.....	124
6. Hydrologic Model for Tollgate.....	128
6.1. Performance of Baseline DZHM at Tollgate	132
6.2. Internal Testing	134
7. Sensitivity Analysis	135
8. Summary and Conclusion	141

References.....	144
5. SUMMARY, CONCLUSIONS, AND RECOMMENDATIONS.....	159
1. Summary.....	159
2. Conclusions.....	167
3. Recommendations.....	167
APPENDICES	170
Appendix A: The Radiation Model	171
Appendix B: Permission Letters.....	182
CURRICULUM VITAE.....	188

LIST OF TABLES

Table		Page
2-1	Calibrated Melt Factors at USC (5 Par PDIMS).....	47
2-2	Parameters of DZHM.....	48
2-3	Mass Balance Summary at USC (October 1, 1992 to August 16, 1993)	49
3-1	Cumulative Precipitation Volume in and Around Tollgate	96
3-2	Vegetation Properties for Study Area Defined in Figure 3-1	97
3-3	SWE on Erosion and Deposition Zones at USC	98
3-4	Scouring and Accumulation on the Respective Zones at USC	99

LIST OF FIGURES

Figure	Page
2-1	Reynolds Creek Experimental Watershed and Upper Sheep Creek, the first order subwatershed that is the focus of this study.50
2-2	The measured SWE maps during 1992-93 season.....51
2-3	Drift factors at Upper Sheep Creek calibrated using UEB as the snowmelt model.52
2-4	Time series of basin average snow water equivalence at Upper Sheep Creek during 1992-93.53
2-5	Measured and modeled basin average snow-loss rate between snow survey dates.54
2-6	SWE maps modeled by 5 Par PDIMS during 1992-93 season.55
2-7	Comparison between 5 Par PDIMS modeled and observed SWE at USC.56
2-8	Distribution of drift factors at Upper Sheep Creek.57
2-9	Time series of cumulative surface water input for the three zones at USC during 1992-93 as modeled by 5 Par PDIMS.58
2-10	Observed and modeled outflow hydrographs at Upper Sheep Creek during 1992-93.59
2-11	Moisture content-based reduction function for actual evapotranspiration.60
2-12	Measured streamflow versus inferred storage at USC during 1992-93.61
2-13	Modeled and measured cumulative evapotranspiration.....62
2-14	Cumulative basinwide mass balance plot for 1992-93.63

3-1 Reynolds Creek Experimental Watershed.....100

3-2 The SWE measurements carried out on a 30.48 m grid approximately aligned with the long axis of Upper Sheep Creek watershed.101

3-3 Vegetation map derived from LANDSAT 5 thematic mapper data for August 1, 1993, using a maximum likelihood classification.102

3-4 (a) Key features of the snow-transport model SnowTran-3D [Liston and Sturm, 1998] as applied to topographically variable terrain. (b) Schematic of mass-balance accounting in SnowTran-3D.....103

3-5 (a) SnowTran-3D-modeled snow water equivalence map. Thin lines denote elevation contours. Vegetation was obtained by classifying a LANDSAT image. (b) Pointwise comparison of modeled against observed SWE.104

3-6 (a) SnowTran-3D-modeled snow water equivalence map. Thin lines denote elevation contours. Wyoming big sagebrush was used as uniform vegetation. (b) Pointwise comparison of modeled against observed SWE.....105

3-7 SnowTran-3D-modeled snow water equivalence maps at USC using PG12 precipitation. (a) LANDSAT vegetation scenario, (b) Uniform vegetation scenario. Thin lines denote elevation contours.....106

3-8 USC drift factors obtained by calibration.107

3-9 Comparison between SnowTran-3D predictions with observed snow water equivalence plus UEB modeled melt at Upper Sheep Creek.108

3-10 Distribution of drift factors at Upper Sheep Creek. (a) Observation-based UEB drift factors and SnowTran-3D modeled drift factors using: (b) USC precipitation and LANDSAT vegetation, (c) USC precipitation and uniform vegetation, (d) PG12 precipitation and LANDSAT vegetation, and (e) PG12 precipitation and uniform vegetation, respectively.....109

3-11	Comparison between cumulative distribution functions of observed and SnowTran-3D-modeled SWE at USC. SnowTran-3D used USC precipitation.	110
3-12	Comparison between cumulative distribution functions of observed and SnowTran-3D-modeled SWE at USC. SnowTran-3D used PG12 precipitation.	111
3-13	Comparison between cumulative distribution functions of observation-based and SnowTran-3D-modeled drift factors at USC. SnowTran-3D used USC precipitation.	112
3-14	Comparison between cumulative distribution functions of observation-based and SnowTran-3D-modeled drift factors at USC. SnowTran-3D used PG12 precipitation.	113
3-15	(a) Comparison between distributions of observed and SnowTran-3D-modeled SWE. Sorted modeled SWE is plotted against sorted observed SWE. The 1:1 line indicates perfect agreement between modeled and observed distributions of SWE. It can be seen that the SWE modeled using USC precipitation agrees better than that modeled using PG12 precipitation. (b) Comparison between distributions of observation-based drift factors and SnowTran-3D-modeled drift factors. The plots are constructed in the same manner as in Figure 3-15a. It can be seen that the sensitivity of the distribution of drift factors to the amount of precipitation is less compared with the sensitivity of the distribution of SWE.	114
4-1	Subwatersheds of Tollgate.	146
4-2	Annual precipitation surface from Hanson [1982], precipitation gages and extended Delaunay triangulation.	147
4-3	(a) Drift factor map simulated by the snow transport model. (b) Drift factor zones at Tollgate. White area is zone 1 ($0.0 \leq DF < 0.5$), green area is zone 2 ($0.5 \leq DF < 1.0$), and yellow area is zone 3 ($DF \geq 1.0$).	148
4-4	Snow-covered area at Tollgate obtained from classification of aerial photographs.	149

4-5	Time series of modeled basin average snow water equivalence at Tollgate during 1992-93.	150
4-6	PDIMS modeled snow water equivalence maps at Tollgate.	151
4-7	(a) Measured and DZHM modeled streamflow. (b) Mean air temperature. (c) Mean measured precipitation. (d) Basin average surface water input at Tollgate during 1992-93.	152
4-8	Internal check for DZHM: comparison between measured and DZHM-modeled streamflow at the outlet of Reynolds Mountain East (subwatershed #35 in Figure 4-2).	154
4-9	Sensitivity of modeled ET to DZHM parameters and initial conditions.	155
4-10	Sensitivity of modeled change in soil zone storage to DZHM parameters and initial conditions.	156
4-11	Sensitivity of modeled change in saturated zone storage to DZHM parameters and initial conditions.	157
4-12	Sensitivity of modeled streamflow to DZHM parameters and initial conditions.	158

CHAPTER 1

INTRODUCTION

1. Background

Physically based process description has been a popular approach to develop spatially detailed hydrologic models in recent years like Système Hydrologique Européen [SHE, *Abbott et al.*, 1986a; *Abbott et al.*, 1986b], the Institute of Hydrology Distributed Model [IHDM, *Beven et al.*, 1987], the Hydrologic Simulation Program - FORTRAN [HSPF, *Bicknell et al.*, 1997], the Distributed Hydrology-Vegetation Model [DHVM, *Wigmosta et al.*, 1994], and other terrain-based models [e.g., *Grayson et al.*, 1992; *Jackson*, 1994]. Availability of digital spatial data (e.g., digital elevation data, and remotely sensed images) has also spurred the development and use of these and other spatially distributed models. Many of these models are based on regular grids, which are used to discretize the spatial domain into modeling elements. Some distributed models also use contour-based modeling elements to discretize the spatial domain [e.g., *Moore et al.*, 1988; *Grayson et al.*, 1995]. Typically, physically based, spatially distributed hydrologic models try to include as many hydrologic processes in the model as possible (e.g., SHE). The underlying idea is that a subset of these processes would be able to capture the overall hydrologic behavior at any watershed, thus allowing the model to be universally applicable. However, there has been growing concern that these distributed models may be limited by (1) assumption that mathematical description of point processes are applicable at the grid scale [or any other spatial discretization, see *Beven*, 1989; *Beven*, 1995], (2) it may be impossible to estimate effective parameters at the grid

scale [Beven, 1995; Beven, 1996], and (3) lack of appropriate measurement techniques, which could be used to estimate parameters and initial conditions over the scales required by these models. Most of the above concerns arise out of scaling problems [Blöschl, 1996], the strong nonlinearity of hydrologic processes and the so-called “unknowable” characteristics of the hydrologic system [Beven, 1996].

Scale issues are important in hydrologic modeling, as shown by Seyfried and Wilcox [1995]. In the context of physical processes, the term *scale* refers to a characteristic time or length (*temporal* or *spatial* scale) of a process or observation [Blöschl, 1996]. In practice, processes are observed at short time and space scales (e.g., an infiltration experiment to determine soil infiltration characteristics). A model may then be developed that fits the observation nicely. This process then is modeled at its observational scale. The point to note here is that the developed model represents the process at the spatial and temporal scale at which the experiment was carried out. Frequently, this model needs to be applied to a larger scale; e.g., the infiltration model may be employed to compute infiltration over a watershed (larger spatial scale, when the experiment was essentially conducted at a point), for the duration of a storm (larger temporal scale; the storm may last for several hours while the experiment was carried over several minutes). This process invariably involves some extrapolation or transfer of information across scales. This transfer of information is called *scaling* and the problems associated with it are called *scale issues*.

An important concept with respect to scale is the notion of a *scale-triplet* [Blöschl, 1996]. Three quantities are necessary to completely characterize the scale properties of a

measurement: the *spacing* between measurements, the *support* or integration volume of the measurement, and the *extent* or coverage of the measurement. Scale-triplets can refer either to time or to space.

Scaling can be carried out in either direction: from a small scale to a large scale, we *upscale*, and the inverse is called *downscaling*. An example of upscaling is the derivation of a catchment-average albedo given a remotely sensed reflectance map. The steps involved in this upscaling exercise may involve aggregating the distributed values into one single value, possibly based on an appropriate weighting scheme. Downscaling involves disaggregation of a large-scale average value into several small-scale values, and then singling out one value as the representative value at the small-scale location of interest. An example of downscaling is the derivation of catchment-wide local groundwater depths given a catchment average groundwater depth [e.g., *Beven and Kirkby, 1979*].

Scaling in a hydrologic modeling framework involves much more than just aggregating or disaggregating inputs and parameters. It may also involve scaling the mathematical description of the processes included in the model [*Blöschl, 1996*], especially in the light of the relative importance of processes changing with scale [*Seyfried and Wilcox, 1995*]. Often only the inputs and parameters are scaled, and it is assumed that the process descriptions themselves do not change across scales. For example, it may be wrong to assume that Darcy's law is applicable at scales where macropores start dominating flow and preferential flow becomes important. This is the classic effective parameter approach to scaling, and may not be appropriate in all

instances [Beven, 1995; Beven, 1996], although some exceptions to this general rule exist. Effective hydraulic conductivity values can be derived for heterogeneous soils under specific flow conditions [Dagan, 1986]. Mathematically scaling the process description appears to be the most complicated, especially in a numerical modeling framework.

At this time, we do not know of any universally applicable, completely general way to derive parameters, state variables and process descriptions at an arbitrary scale [e.g., modeling scale, see Blöschl, 1996] given the values (for parameters and state variables) or equations (for process descriptions) at another scale [e.g., measurement scale, see Beven, 1996; Blöschl, 1996]. Some recent approaches that use generalized distribution functions to parameterize subgrid variability of state variables and model parameters [e.g., Beven, 1995; Luce *et al.*, 1999] are attempts towards this goal.

An alternative to explicit scaling was proposed by Beven [1989; 1995; 1996] which argues that all process descriptions, no matter how detailed in space, are lumped descriptions of physical processes at that scale. Recognizing that the overall hydrologic behavior at the watershed scale may be explained to a large extent by only a few processes (the so-called dominant processes) allows us to take another approach toward building hydrologic models. This approach only parameterizes the dominant processes for a given watershed, at the scale of the watershed. There are two important consequences of this approach: (1) the model is specific to the region, possibly even specific to the watershed where it is developed, thereby abandoning the long-sought hope of a universal hydrologic model, but (2) the model is simply parameterized and driven with typically available data. In this approach (henceforth called dominant processes

modeling or DPM), spatial variability of processes and parameters can still be maintained if sufficient supporting data is available. The difference between grid-based formulation and the DPM approach is that the spatial discretization in the former often is arbitrary (e.g., controlled by the resolution of gridded spatial data sets such as DEMs), whereas in the latter it is determined by the overall watershed behavior in a natural way. The philosophy of hydrologic modeling in the DPM approach is universally applicable to any region, but at the same time calls on the hydrologist to minutely investigate and understand the hydrologic behavior in order to identify dominant processes. Physically based, detailed spatially distributed models can be used in data analysis at this early identification stage in order to investigate the relative importance of competing processes. An example of the DPM approach is presented in Chapter 2.

2. Objectives

The objectives of this work were (1) to understand the hydrologic processes acting in the watershed at a range of scales, (2) to identify dominant hydrologic processes at these scales, and (3) to develop quantitative models of the watershed behavior. The approach adopted was to treat a first-order, small-scale, intensively monitored subwatershed as a prototype to test hypotheses regarding the hydrologic behavior in the region, to transfer the insights gained from the small-scale work to explain the hydrology and to develop quantitative models at larger watersheds. The study of larger watersheds was expected to test the hypothesis that the hydrologic behavior inferred at the small-scale watershed was also applicable at larger scales.

3. Outline

This dissertation is presented in multiple-paper format. A comprehensive radiation model was used in the first paper and is briefly described in Chapter 2. The details of the radiation model are included in Appendix A. Appendix B contains the permission letters obtained from the coauthors.

Chapter 2 of this dissertation describes the work done at a small-scale, intensively monitored, first-order subwatershed. This work describes the process of identification of dominant hydrologic processes in the watershed, and then shows that a simple hydrologic model is sufficient to parameterize the overall watershed behavior in terms of annual mass balance. During this study, spatial variability of snow water equivalence (SWE), which resulted from wind-blown redistribution of snow in the watershed, was identified as the dominant hydrologic process. Wind-induced redistribution was parameterized using the drift factor concept. The drift factors were obtained by calibration against a set of manually measured SWE maps. During spring, the highly spatially variable snowpack melts and provides surface water input (SWI) to the soil. Analysis of spatial variability of SWI suggested that the watershed could be divided into three SWI zones. Comparison of the timing of SWI with the outflow hydrograph suggested that almost all of the measured streamflow at the outlet resulted from the SWI on the north-facing, leeward slope of the watershed. SWI on the other two zones was used mainly to satisfy evapotranspiration and soil storage demands. The insights from the working of this watershed provided a hypothesis of the overall hydrologic behavior at the scale of a first-order subwatershed in the study region.

Manual measurement of SWE over large areas is impractical, and less expensive techniques are needed to establish the spatial pattern of SWE over larger areas. Chapter 3 applied a wind-blowing snow transport model to the study region in order to test the appropriateness of this model in describing the spatial pattern of snow accumulation at the end of winter. The snow transport model parameterizes processes related to wind flow over rugged terrain and erosion, transport and deposition of snow by wind. The results from this study suggested that the distribution of drift factors obtained from the snow transport model simulations were reasonably independent of the amount of precipitation, allowing the use of the same drift factor pattern for different years. Pointwise comparison between modeled and measured SWE grids at the intensively monitored first-order watershed yielded poor results, mainly due to a pattern shift and potential limitations of wind data which led to limitations in wind flow parameterization in the snow transport model. However, since the distributions of the drift factors were reasonable, these results could still be utilized to partition first-order subwatersheds into SWI zones, and to specify drift patterns.

Chapter 4 describes an attempt to transfer the understanding gained during the studies described in Chapters 2 and 3 to a larger scale. The study is carried out at a fourth-order watershed, which is composed of 153 subwatersheds. The main goal of this study was to determine whether the subwatersheds of the larger watershed behave similarly compared to the intensively monitored first-order subwatershed that was the focus of Chapter 2. The hydrologic model constructed for the fourth-order subwatershed consisted of two main components: (1) the above-surface component, which included a

spatially distributed precipitation interpolation scheme, a spatially distributed radiation model and a snow accumulation and melt model used to compute surface water input to the soil, and (2) the below-surface component, which included a soil-vegetation-groundwater model, used to partition the surface water input into evapotranspiration (ET), surface runoff, soil zone storage, saturated zone storage and baseflow. During this study, it was found that snowmelt characteristics were similar between the first-order watershed used in Chapter 2 and the fourth-order watershed used in Chapter 4. The above-surface component was shown transferable from the first-order watershed to the fourth-order watersheds in the study region.

The below-surface component, with parameters calibrated at the intensively monitored first-order watershed (Chapter 2), was sufficient to parameterize the annual mass-balance at the fourth-order watershed. The only change required was specification of different initial conditions, and one model parameter. The parameters and initial conditions were kept uniform in a zone-wise fashion for all subwatersheds of the fourth-order watershed because of lack of supporting data for their determination. It was concluded that the below-surface component was mostly transferable from the first-order watershed to the fourth-order watershed.

A sensitivity analysis was also carried out to better understand the relative importance of model parameters and initial conditions. This analysis revealed that the annual mass balance components are most sensitive to two model parameters and two initial condition variables. The two parameters are used in the computation of ET and baseflow, respectively. The two initial condition variables specify initial soil moisture

content and initial depth to the water table. All of these variables are highly spatially variable and very difficult to measure, especially for large watersheds. It may be possible to obtain reasonable values for the basin average of initial condition variables based on antecedent conditions. Reasonable values of the vegetation parameter could in theory be obtained from remotely sensed data. There is no known way to accurately determine water table depth over large areas. This problem is further complicated by the simplifying assumptions made while developing the subsurface component, and correlation between field measurements such as piezometer data and water table depth required by the subsurface model may not work satisfactorily. These issues are recommended for further research.

References

- Abbott, M. B., J. C. Bathurst, J. A. Cunge, P. E. O'Connell, and J. Rasmussen, An introduction to the European hydrological system -- Système Hydrologique Européen, "SHE", 1: History and philosophy of physically-based, distributed modelling system, *J. Hydrol.*, 87, 45-59, 1986a.
- Abbott, M. B., J. C. Bathurst, J. A. Cunge, P. E. O'Connell, and J. Rasmussen, An introduction to the European hydrological system - Système Hydrologique Européen, "SHE", 2: Structure of a physically-based, distributed modeling system, *J. Hydrol.*, 87, 61-77, 1986b.
- Beven, K., Changing ideas in hydrology -- The case of physically-based models, *J. Hydrol.*, 105, 157-172, 1989.
- Beven, K., Linking parameters across scales: Subgrid parameterizations and scale dependent hydrological models, *Hydrol. Processes*, 9, 507-525, 1995.
- Beven, K. J., A discussion of distributed hydrological modelling, in *Distributed Hydrological Modelling*, edited by M. B. Abbott and J. C. Refsgaard, pp. 289-295, Kluwer Academic Publishers, Dordrecht, The Netherlands, 1996.

- Beven, K., A. Calver, and E. M. Morris, The Institute of Hydrology distributed model, *Rep. 98*, Inst. of Hydrol., Wallingford, Oxon, England, 1987.
- Beven, K. J., and M. J. Kirkby, A physically based variable contributing area model of basin hydrology, *Hydrol. Sci. Bull.*, 24(1), 43–69, 1979.
- Bicknell, B. R., J. C. Imhoff, J. L. Kittle, A. S. Donigan, and R. C. Johanson, Hydrologic simulation program -- Fortran, user's manual for version 11, *Rep. EPA/600/R-97/080*, U.S. EPA, Ecosystems Research Division, Environmental Research Laboratory, Athens, Geog., 1997.
- Blöschl, G., *Scale and Scaling in Hydrology (Habilitationsschrift)*, 346 pp., Institut für Hydraulik, Gewässerkunde und Wasserwirtschaft. Wiener Mitteilungen, Wasser-Abwasser-Gewässer, Band 132, Tech. Univ. of Vienna, Vienna, Austria, 1996.
- Dagan, G., Statistical theory of groundwater flow and transport: Pore to laboratory, laboratory to formation and formation to regional scale, *Water Resour. Res.*, 22(9), 120s–134s, 1986.
- Grayson, R. B., G. Blöschl, and I. D. Moore, Distributed parameter hydrologic modelling using vector elevation data: THALES and TAPES-C, in *Computer Models of Watershed Hydrology*, edited by V. P. Singh, pp. 669–696, Water Resources Publications, Littleton, Colo., 1995.
- Grayson, R. B., I. D. Moore, and T. A. McMahon, Physically based hydrologic modeling 1. A terrain-based model for investigative purposes, *Water Resour. Res.*, 28(10), 2639–2658, 1992.
- Jackson, T. H. R., A spatially distributed snowmelt-driven hydrologic model applied to the Upper Sheep Creek watershed, Ph.D. dissertation, 323 pp., Utah State Univ., Logan, 1994.
- Luce, C. H., D. G. Tarboton, and K. R. Cooley, Subgrid parameterization of snow distribution for an energy and mass balance snow cover model, *Hydrol. Processes*, 12(10–11), 1671–1683, 1999.
- Moore, I. D., E. M. O'Loughlin, and G. J. Burch, A contour-based topographic model for hydrological and ecological applications, *Earth Surface Processes and Landforms*, 13, 305–320, 1988.
- Seyfried, M. S. and B. P. Wilcox, Scale and the nature of spatial variability: Field examples having implications for hydrologic modeling, *Water Resour. Res.*, 31(1), 173–184, 1995.

Wigmosta, M. S., L. W. Vail, and D. P. Lettenmaier, A distributed hydrology-vegetation model for complex terrain, *Water Resour. Res.*, 30(6), 1665–1679, 1994.

CHAPTER 2
UNDERSTANDING THE HYDROLOGIC BEHAVIOR OF A
SMALL SEMIARID MOUNTAINOUS WATERSHED IN
IDAHO, UNITED STATES OF AMERICA¹

Abstract

The purpose of this study is to understand hydrologic behavior at a small (0.25 km²) semiarid mountainous watershed. A quantitative basis for subdividing the watershed into modeling zones based on dominant processes was established. A data intensive approach was used to understand the hydrologic processes acting in the watershed. Measurements used included maps of snow water equivalence surveyed manually on a 30-m grid, streamflow, and weather variables. Wind-driven snow drifting combined with variable radiation exposure on rough terrain produces a consistent (from year to year) spatial distribution of snowpack in the watershed. Spatially varying surface water input (SWI) was identified as the dominant hydrologic process in this watershed. The drift factor approach was used to parameterize wind-blown snow drifting in the watershed. The drift factors were obtained by calibration using manually surveyed snow water equivalence maps during the accumulation and drift period. Earlier studies have examined annual water balance at this watershed by dividing the watershed into three zones based on drift patterns, soil types, and vegetation. We show that these zones can

¹ Coauthored by Rajiv Prasad, David G. Tarboton, Gerald N. Flerchinger, Keith R. Cooley, and Charles H. Luce.

be obtained from the distribution of calibrated drift factors. The timing of SWI on the zone corresponding to deep drifts on the north-facing, leeward slope corresponded closely with the timing of streamflow at the outlet. A lumped hydrologic model was developed which consists of (1) simple parameterization of evapotranspiration, (2) infiltration into soil and recharge to groundwater, and (3) subsurface storage-discharge function. This model, applied to each of the three SWI zones individually was shown to be sufficient to parameterize the volume and timing of runoff from this watershed.

1. Introduction

The surface water input (SWI) into a watershed consists of rainfall and/or snowmelt. The correct estimation of the spatio-temporal distribution of SWI is especially important in semiarid mountainous watersheds where most of the precipitation falls as snow and its accumulation and melt is strongly influenced by terrain properties and other weather variables. Snowpack formed during the accumulation period acts as surface water storage, delaying the infiltration of precipitation into the subsurface. Wind driven drifting in mountainous watersheds erodes snow from windward slopes and deposits it on the leeward slopes, creating a consistent spatial distribution of snowpack every year. The resulting SWI is influenced primarily by the location of the deep drifts on the leeward slopes. Windward slopes accumulate relatively shallow snowpacks, which tend to melt early in the melt season, in contrast to deep drifts on leeward slopes, which melt late in the season. Previous works in this watershed [*Jackson, 1994; Tarboton et al., 1995b*] have developed spatially distributed models that work on a regular grid. In these models,

each grid cell was modeled as a snow-soil system. Snowmelt infiltrating into the soil modified the water held by the soil column at each grid cell. Lateral flow in the soil was modeled explicitly using grid cell to grid cell connectivity, driven by a topographic gradient [similar to *Wigmosta et al.*, 1994]. These models were shown to simulate the watershed behavior reasonably well. However, these models had large data requirements and proved impractical in modeling larger scale watersheds without moving to coarser grid sizes. In this paper we use the knowledge gained from earlier studies and results obtained from extensive data analysis to identify important hydrologic processes at scales larger than a grid cell and to develop a methodology to build simpler hydrologic models, which describe the hydrologic behavior at the watershed scale. A simple hydrologic model that is driven by SWI computed from the spatially distributed snowpack is shown to be sufficient to parameterize the volume and timing of runoff from a first-order watershed. This approach will be used in forthcoming papers to upscale our modeling to larger watersheds.

2. Study Site and Available Data

Reynolds Creek Experimental Watershed (RCEW) is a 233.5-km² semiarid mountainous watershed located in southwestern Idaho (Figure 2-1) and has been the focus of intensive hydrometeorologic and geologic instrumentation and investigation over the last three decades [*Hamon*, 1973; *Stephenson and Freeze*, 1974; *Winkelmaier*, 1987; *Hanson*, 1989; *Duffy et al.*, 1991; *Stevens*, 1991; *Flerchinger et al.*, 1992]. The watershed is maintained by the Northwest Watershed Research Center (NWRC), Boise,

Idaho, a part of the Agricultural Research Service, U. S. Department of Agriculture. Elevations in the watershed range from 1097 to 2237 m. Mean annual precipitation varies with elevation and ranges from 229 to 1107 mm. The watershed is almost entirely sagebrush rangeland. Approximately 9% of the area is cultivated/burned/seeded and about 5% is forested with scattered Douglas fir, aspen, and alpine fir. The main waterway of Reynolds Creek has a length of 25.1 km and overall slope of 4%. The hydrology of the watershed is mainly snowmelt driven. Channel flow is sustained by groundwater recharged by infiltration of snowmelt.

Upper Sheep Creek (USC) is a 0.25-km² first-order watershed within Reynolds Creek Experimental Watershed (Figure 2-1). This watershed has been the location of intensive study of the distribution of snow over the period 1982 to 1996. A 30.48-m grid over the watershed defines 255 locations where snowpack has been measured at approximately 2-week intervals during the winter [Cooley, 1988]. In particular, nine snow surveys were conducted during water year 1992-93, thereby establishing the spatio-temporal distribution of snow accumulation and melt at USC. Snow water equivalence maps derived from the snow surveys are shown in Figure 2-2. This study focused on the water year 1992-93. The hydrometeorologic instrumentation network at USC is described in detail by *Flerchinger et al.* [1998].

Point data used in this study consisted of time series of precipitation, radiation, wind speed and direction, air temperature, and relative humidity. These variables were collected at PG8 (Figure 2-1). There is some variability in precipitation within the watershed as measured by the dual-gage system described by *Hanson* [1989]. In this

study, precipitation measured only at PG8 was available, and we used precipitation data from this location to specify a uniform precipitation field over the watershed.

The topography depicted in Figures 2-1 and 2-2 was obtained from a 30-m digital elevation model (DEM) of the watershed. This DEM was obtained from averaging a commercial, high-resolution 10-m DEM developed from USGS 1:24,000 maps for Reynolds Creek Experimental Watershed.

3. Modeling Surface Water Input

The field snow surveys provided snapshots in time of the spatial pattern of snow accumulation and ablation (Figure 2-2). In order to relate observed changes in snowpack to SWI, which drives the hydrologic response, we need to estimate and interpolate melt rates between these measurements. A snowmelt model was used for this interpolation. Apart from some specialized wind blowing models [e.g., *Pomeroy and Gray, 1995; Liston and Sturm, 1998*] most physically based snowmelt models do not include a description of wind-driven drift; indeed, they are point models, and application of these models to a regular grid needs to account for lateral snow exchanges.

Wind-induced drifting usually occurs after the snowfall during periods of relatively high wind speeds, when the wind-induced shear stress on the surface of the snowpack exceeds the threshold and snow particles can be detached from the surface. The timescale of the drifting process can be short, of the order of a few minutes to a few hours, depending on the prevailing wind conditions. This process occurs throughout the winter. As spring approaches, temperatures get warmer and the snowpack starts to ripen.

Snow densification and other morphologic processes also increase grain size, limiting drifting as spring progresses. The goal here was to simulate the end-of-winter snowpack pattern within the watershed as accurately as possible, for subsequent computation of spatially varying snowmelt and infiltration during spring.

Our approach was to apply a point snowmelt model to represent snowmelt, and absorb the effects of wind-driven drift into a drift factor [Jackson, 1994]. The drift factor at a point is defined as a factor by which gage snowfall must be multiplied to equate measured and modeled snow water equivalence on the ground. The drift factor is used to describe the propensity of a location to accumulate extra snow through drifting (drift factor > 1), or to lose snow due to scouring (drift factor < 1). These drift factors vary spatially over the domain and are multiplied with observed snowfall to model snowfall redistribution by wind. This approach approximates drifting which follows snowfall as occurring concurrently with snowfall. This approach also amounts to an assumption of linearity in the spatial pattern of snow accumulation. If precipitation is doubled, the spatial pattern is assumed to remain the same with double the amount at each location. The drift factor approach assumes that spatial patterns of snow accumulation are consistent from year to year. At Upper Sheep Creek data from 9 years of snow surveys has shown the consistency of drifting patterns [Luce, 2000; Luce and Tarboton, 2001]. In order to estimate the drift factors over the watershed, a physically based point snowmelt model called the Utah Energy Balance (UEB) snow accumulation and melt model [Tarboton *et al.*, 1995a; Tarboton and Luce, 1996] was applied to each grid cell at USC. Using the model in this way provides an approach to account for the melt that occurs

during accumulation and drifting. Snowmelt during the accumulation and drift period is usually small, yet significant. The first three manually surveyed snow water equivalence maps during 1992-93 (dates February 10, 1993, March 3, 1993 and March 23, 1993) were used to carry out a point-by-point calibration. These three snow water equivalence maps were chosen because they were measured before the onset of substantial snowmelt, which was the period when snow drifting was expected to be important.

The objective function used for calibration was the sum of the signed differences between modeled and measured snow water equivalence on these three dates. The objective function was monotonic with respect to the drift factor. Drift factor at each grid cell was thus obtained as the value that made the objective function equal to zero at that grid cell. The snowmelt model was run at an hourly time step driven by observations of radiation, precipitation, air temperature, humidity, and wind speed. Other parameters of the UEB model were fixed at their recommended values [Tarboton and Luce, 1996]. Figure 2-3 shows the map of calibrated drift factors. These drift factors differ from those previously reported [Jackson, 1994; Tarboton et al., 1995b] because the drift factors reported here were referenced on a north-aligned grid (which required interpolation of snow water equivalence measurements made on the skewed grid to the north-aligned grid, resulting in some smoothing) and were calibrated to the 1992-93 observations. The previously reported drift factors were calibrated against 1985-86 data on a skewed grid and used in a split sample test to compare against data from 1992-93. The 1992-93 drift factors reported here were slightly smaller than the 1985-86 drift factors consistent with the meteorologic records of less wind in 1992-93, relative to 1985-86. Drift factors

calibrated to the year of interest (1992-93) were used here because our intent was to obtain the best estimates of SWI based on all information available for this year so we can understand and model the hydrologic response.

The physically based point snowmelt model, UEB [*Tarboton and Luce, 1996*], could also have been used to estimate SWI. However, even with calibrated drift factors we found that our current physically based model still differs noticeably from the measurements in its reproduction of measured snow water equivalence (see Figures 2-4 and 2-5) during the melt period for which it was not calibrated. Figure 2-4 shows the time series of observed and modeled basinwide average snow water equivalence. Figure 2-5 shows the comparison between observation-based and modeled watershed snow loss rates over the intermeasurement periods. Observation-based SWI was calculated as the difference between basinwide cumulative precipitation estimated from measurements and drift factors and measured snow water equivalence on any date. The basinwide cumulative precipitation above refers to the drift factor adjusted basin average precipitation accumulated until the specified date, which was the precipitation input to the snowmelt model (UEB). The observation-based average snow loss rates for intermeasurement periods were then calculated from the cumulative values. Figure 2-5 shows that UEB underestimated the snow loss rate during the first intermeasurement period (February 10 – March 3, 1993). Snow loss rates computed during the next two intermeasurement periods (March 3 – March 23, 1993, and March 23 – April 8, 1993) were overestimated by UEB. Approximately two-thirds of the snow modeled by UEB at the start of these two intermeasurement periods (approximately 0.3 m on March 3, 1993,

as shown by the dotted line in Figure 2-4) melted during this time (UEB modeled basin average SWE on April 8 is about 0.1 m, as shown by the dotted line in Figure 2-4). UEB underestimated the snow loss rate during the intermeasurement periods April 8 – April 15, 1993, overestimated it slightly during April 15 – April 29, 1993, was very close during April 29 – May 12, 1993, and underestimated the snow loss rates during the last two intermeasurement periods, May 12 – May 19, 1993, and May 19 – May 25, 1993. The underestimation of snow loss rate during the last two intermeasurement periods was partly due to the fact that as per UEB, almost all snow had melted by that time. As shown in Figure 2-5, the snow loss rate predicted by an index-based snowmelt model was closer to the observation-based average snow loss rates for all intermeasurement time periods except the three during April 8 – May 12. The index-based snowmelt model was calibrated to the measured snow water equivalence data and is described below. It can be seen that the index-based model tracks the basin average snow water equivalence more accurately than UEB (see Figure 2-4).

Since the focus of this study was to understand the hydrologic response due to SWI patterns, we wanted to ensure that SWI corresponded as closely with measurement as possible. Therefore we chose to sidestep the discrepancies with the physically based model and develop an index-based approach to estimate snowmelt and SWI. We are thus replacing the physical rigor, transportability and generality of the UEB model, with simplicity and accuracy for this specified setting. The index-based snowmelt model still uses the drift factors calibrated using UEB. Early in the season, drifting and accumula-

tion dominate, and melting is a secondary effect. Therefore the drift factors estimated with UEB were still felt to be our best estimate of actual drift effects.

The index-based approach used air temperature and net radiation to estimate snowmelt at each grid cell.

$$M = m_f \cdot \max[R \cdot (T_a - T_b), 0] \quad (2.1)$$

where M is rate of snowmelt in m/hr, m_f is a parameter (the melt factor, m/hr/(W/m²)/°C), T_a is air temperature (°C), T_b is a reference base temperature (0 °C), and R is net radiation. This multiplicative form of the index model was the best of several we tried and has also been used by others previously [Riley *et al.*, 1966; Sharma and Tarboton, 1995]. Air temperature at each grid cell was adjusted from measurement at a reference location (PG8, see Figure 2-1) using an average lapse rate. Other index models evaluated included a simple temperature only index model (degree-day model) and an additive temperature and radiation index model. The evaluation was in terms of the ability to represent the observed snowmelt patterns with spatially constant parameters. Since temperature was related to elevation only, the temperature only index model failed to capture the slope aspect effects of the snowmelt patterns that the models that used radiation, did.

Measured incoming solar radiation was split into direct and diffuse components as described by Erbs *et al.* [Erbs *et al.*, 1982]. Incident radiation at a grid cell was composed of incoming direct shortwave, incoming diffuse sky and incoming longwave

radiation. Direct radiation was adjusted for terrain slope, aspect and shading [see Appendix E in *Dingman*, 1994]. Diffuse and longwave radiation components were adjusted for sky view factor [*Dozier and Frew*, 1990] at each grid cell. We estimated net radiation using

$$R = (1 - A) \cdot (R_{dir} + R_{dif}) + R_{lw,net} \quad (2.2)$$

where A is snow surface albedo taken as 0.85. R_{dir} and R_{dif} (W/m^2) are the direct and diffuse components of incident solar radiation adjusted for terrain effects, and $R_{lw,net}$ (W/m^2) is the net longwave radiation, estimated using

$$R_{lw,net} = R_{lwi} - R_{lw,out} + R_{lwi,terrain} \quad (2.3)$$

In equation 2.3, the incoming atmospheric longwave radiation R_{lwi} (W/m^2) was estimated as

$$R_{lwi} = \{f_{cloud} \cdot \varepsilon_{cloud} + (1 - f_{cloud}) \cdot \varepsilon_{air}\} \cdot \sigma \cdot T_a^4 \cdot V_d \quad (2.4)$$

In equation 2.4, σ is Stefan-Boltzmann constant, T_a is air temperature in Kelvin, V_d is the sky view factor, and f_{cloud} is the cloudiness factor, estimated from atmospheric transmission factor which itself was deduced by comparing measured global radiation

with extra-terrestrial solar radiation estimated using sun-earth geometry. Emissivities of air and clouds are denoted by ε_{air} and ε_{cloud} . The emissivity of clouds was set to 1.0, and that of air was computed using *Satterlund's* [1979] formula based on humidity and air temperature. The outgoing longwave radiation flux $R_{lw,out}$ (W/m^2) in equation 2.3 is the longwave radiation flux emitted by snow ($R_{lw,snow}$, in W/m^2) if the ground is snow covered, or the longwave radiation flux emitted by the ground ($R_{lw,ground}$, in W/m^2), which were computed as:

$$\begin{aligned} R_{lw,snow} &= \varepsilon_{snow} \cdot \sigma \cdot T_{snow}^4 \\ R_{lw,ground} &= \varepsilon_{ground} \cdot \sigma \cdot T_{ground}^4 \end{aligned} \tag{2.5}$$

The emissivity of snow ε_{snow} was taken as 0.99 [*Tarboton and Luce*, 1996], and that of the ground ε_{ground} was taken as 0.97 [see Table D-1 in Appendix D, *Dingman*, 1994].

T_{snow} is surface temperature of snow in Kelvin, taken as the smaller of air temperature and 0 °C, and T_{ground} is surface temperature of bare ground in Kelvin, approximated by the air temperature. Longwave radiation flux emitted by surrounding terrain $R_{lw,terrain}$ (W/m^2) in equation 2.3 was computed as:

$$R_{lw,terrain} = \{A_f \cdot \varepsilon_{snow} \cdot \sigma \cdot T_s^4 + (1 - A_f) \cdot \varepsilon_{ground} \cdot \sigma \cdot T_a^4\} \cdot (1 - V_d) \tag{2.6}$$

In equation 2.6 A_f is snow covered area fraction.

Air temperature was used to partition precipitation into snow and rain [U.S. Army Corps of Engineers, 1956]. The fraction of precipitation falling as snow, f_{snow} , was computed as:

$$\begin{aligned} f_{snow} &= 1.0 & T_a < T_s \\ &= \frac{T_r - T_a}{T_r - T_s} & T_s \leq T_a \leq T_r \\ &= 0.0 & T_a > T_r \end{aligned} \quad (2.7)$$

where T_r ($= 1$ °C) is the air temperature above which all precipitation is assumed to fall as rain, and T_s ($= -3$ °C) is the air temperature below which all precipitation is assumed to fall as snow. Rain is assumed to pass through any snow already present on the ground and immediately add to SWI. Snowfall P_{snow} (m) was adjusted for wind-induced drifting using the drift factor f_{drift} for each grid cell, computed as:

$$P_{snow} = f_{snow} \cdot f_{drift} \cdot P \quad (2.8)$$

where P is the measured precipitation (m).

$W(t)$ (m) is defined as the snow water equivalence at a grid cell at the end of a computation time step indexed as t , and was determined from the mass balance equation:

$$W(t) = W(t-1) + [P_{snow}(t) - M(t)] \cdot \Delta t \quad (2.9)$$

where $M(t)$ (m) refers to the snowmelt computed during the time step indexed as t , and Δt (h) is the length of the modeling time step.

This snowmelt model (Pseudo-Distributed Index-based Model for Snowmelt, PDIMS) was calibrated at USC to obtain the melt factor m_f . The spatial distribution of snowmelt is influenced largely by spatial variation in radiation and air temperature, which have strong diurnal cycles and vary on a short time scale. Radiation and air temperature are also strongly influenced by terrain properties such as sky view factor and terrain shading. We assumed that the incorporation of topographic effects into R and T_a accounts for these effects. Therefore melt factors were assumed to be uniform in space and to vary on a much longer time scale. Here we assumed melt factors to be constant on a monthly time scale. This assumption gave us five melt factors, one each for January through May. We found that the model was insensitive to the values of melt factor during other months when there was minimal snowmelt (June through December). The objective function used during calibration was the sum of square of differences between the modeled and measured snow water equivalence at each grid cell in the watershed for each of the nine snow water equivalence measurements:

$$F(\{m_f\}) = \sum_{\bar{x} \in \bar{X}} \sum_{t=1}^9 \{W_{mod}(\bar{x}, t) - W_{obs}(\bar{x}, t)\}^2 \quad (2.10)$$

where $\{m_f\}$ is the set of melt factors being calibrated, \bar{x} refers to the location of a specific grid cell, \bar{X} is the set of all grid cells that constitute the watershed, and t is the

index identifying a snow water equivalence map measured by the snow surveys at USC.

Parameters of PDIMS were calibrated for three configurations:

- (1) melt factor varying for each month during January through May (5 Par PDIMS)
- (2) one melt factor during January and February which were primarily accumulation months, and another during March through May which were primarily melt months (2 Par PDIMS), and
- (3) temporally constant melt factor (1 Par PDIMS).

These configurations result in the calibration of 5, 2, and 1 parameters, respectively, against 2475 observations (9 dates times 275 grid locations).

Calibration was carried out using an interactive program called NLFIT [*Kuczera, 1994; Kuczera, 1997*] for each of the three configurations. During calibration, PDIMS was run on an hourly time step. Modeled snow water equivalence maps at 1300 hours on the dates when snow water equivalence measurements were carried out were used to compute the objective function. The search algorithm used during this calibration was the Gauss-Marquardt algorithm with a scalar parameter that controlled the direction of descent on the parameter surface between the Gauss-Newton direction and the direction of steepest descent. During calibration of the 5 Par PDIMS configuration, the scaled objective function (1.0 before the start of the optimization) reduced with each iteration of the interactive search. The search vector was recomputed at the start of each iteration. After eight iterations, the scaled objective function reduced from 1.0 at the start of the calibration to less than 0.02, and the relative reduction at this stage was less than 0.001.

The coefficient of determination reported by NLFIT was 0.937. The calibration was terminated at this point.

It was found that in the one- and two-parameter configurations, PDIMS gave noticeably poor time history of basin average snow water equivalent as compared to the five-parameter configuration. Since we needed an accurate SWI time series to assess the hydrologic behavior of the watershed, we chose to use 5 Par PDIMS as the snowmelt model. Table 2-1 shows the calibrated melt factors for 5 Par PDIMS configuration. Figure 2-4 includes the time history of observed and modeled basinwide average snow water equivalence from PDIMS. The PDIMS simulation tracked the observations more closely than the UEB simulation. Figure 2-5 shows snow loss rates from the PDIMS model. Again PDIMS simulation more closely matched the observation based loss rate estimates compared to the UEB simulation. Figure 2-6 shows the modeled (5 Par PDIMS) snow water equivalence maps. Figure 2-7 shows the pointwise comparison between the observed and modeled snow water equivalence. The Nash-Sutcliffe measure for goodness-of-fit [Gupta *et al.*, 1998] was computed for the modeled snow water equivalence maps as:

$$NS = 1 - \frac{\sum_{\bar{x} \in \bar{X}} [W_{mod}(\bar{x}) - W_{obs}(\bar{x})]^2}{\sum_{\bar{x} \in \bar{X}} [W_{obs}(\bar{x}) - \bar{W}_{obs}]^2} \quad (2.11)$$

where \bar{W}_{obs} is the mean of the observed snow water equivalence map.

The calibrated melt factors show a large variation. We do not have sufficient information to pinpoint what may be responsible for such a large variation in the melt factor. One probable reason can be deduced from the nature of the melt equation. Net radiation multiplied by the air temperature tends to grow rapidly in spring as temperatures above 0 °C occur more frequently (during more time steps). Also, air temperatures above 0 °C occur more extensively as more of the grid cells comprising the zone are assigned temperatures above 0 °C, due to linear scaling of air temperature with elevation. The tendency of the driving index $R \cdot (T_a - T_b)$ to grow rapidly as spring progresses means smaller melt factors may produce the same amount of melt compared to earlier in winter. Similar argument can also be made for increasing melt factors as fall progresses into winter. We have not evaluated the melt factors with sufficiently temporal resolution here to conclusively demonstrate this point. However, evidence points that this reasoning is plausible since the melt factor for January was less than that for February, and then after March we saw a sharp decline in the value of the monthly melt factors.

4. Analysis of Surface Water Input at Upper Sheep Creek

Surface water input is defined as the sum of rainfall and snowmelt at a given time step at any grid cell. SWI at USC for 1992-93 water year was computed using the 5 Par PDIMS. Research in the past has indicated three snowmelt zones at USC [Cooley, 1988]. Snow on the windward, southwest-facing slope melts early in the season. Snow on the leeward, northeast-facing slope melts in two stages – a general melt period when most of

the relatively shallow snowpack on the northeast-facing slope is consumed, and a drift melt period when the deep drift which forms on the leeward, northeast-facing slope melts. In order to identify these three SWI zones at USC, we examined the distribution of the drift factors at USC (Figure 2-8). It can be seen that there are roughly three modes on this histogram that can be used to cluster or group the grid cells of USC into SWI zones. The first cluster extends from drift factor values of 0.0 to about 0.5, the second cluster extends from 0.5 to 1.0 and the third for all drift factors greater than 1.0. This observation gave us a basis for subdividing USC into three zones based on drift factors. These three zones are zone 1: early snowmelt on southeast-facing slope corresponding to drift factors between 0.0 and 0.5; zone 2: general snowmelt on northeast-facing slope corresponding to drift factors between 0.5 and 1.0, and zone 3: drift snowmelt on northeast-facing slope corresponding to drift factors greater than 1.0. Subdividing USC using the criterion outlined above led to the three zones shown in Figure 2-8. These zones do correspond approximately to the three snowmelt zones described by *Cooley* [1988] and *Flerchinger et al.* [1998]. The importance of this subdivision becomes apparent when we examine the time series of cumulative SWI into each of these zones (Figure 2-9). The solid line in Figure 2-9 is the basinwide SWI (area weighted average of SWI for the three zones). Measured runoff at USC during 1992-93 is shown in Figure 2-10. Outflow starts around the beginning of May. The whole watershed becomes snow free at the beginning of June. It can be seen on Figure 2-9 that zones 1 and 2 do not get any appreciable SWI during May, in contrast to zone 3, which showed a rapid rise in SWI

during this time period, and corresponded closely with the rise in the outflow hydrograph. The rise in cumulative graphs of SWI beyond June is all due to rainfall.

Furthermore, the potential evapotranspiration (ET) for this period (October 1, 1992 to August 16, 1993), evaluated using the model described below, was 968 mm, 862 mm and 724 mm for zones 1 to 3, respectively. These potential ET values were greater than the corresponding SWI on zones 1 (460 mm) and 2 (665 mm), but less than the SWI on zone 3 (1263 mm), indicating that zone 3 may generate runoff, but on zones 1 and 2 potentially all SWI may be lost to evapotranspiration.

This behavior leads us to suggest that almost all of watershed outflow was generated by the SWI that occurred on zone 3 during May generated by the melting of the deep snowdrift on this zone. These insights suggested separate lumped hydrologic models for each of these three SWI zones as an approach for predicting watershed outflow at USC.

5. The Dominant Zone Hydrologic Model

Based on insights gained from the distribution of SWI at USC, we developed a hydrologic model, which works on what we call dominant zones of the watershed. The overall behavior of the watershed is determined by the aggregation of individual zone behavior. In our case, these dominant zones are identified as the three SWI zones described above. In general, these zones should be determined from important hydrologic behavior in the watershed of interest. The components of the dominant zone hydrologic model (DZHM) are described here.

5.1. Surface Water Input

Surface water input into the soil is computed using PDIMS, as described in earlier sections.

5.2. Evapotranspiration

Potential evapotranspiration was computed from Priestley-Taylor equation. Actual evapotranspiration was then computed depending on moisture availability in the soil store. No ET was allowed from snow covered area. This assumption amounts to inactive vegetation during periods of snow cover.

$$PET = \alpha \frac{\Delta}{\Delta + \gamma} \frac{R_a}{\lambda \cdot \rho_w} \quad (2.12)$$

$$ET = K_{veg} \cdot f_{AET} \cdot PET \quad (2.13)$$

where α is the Priestly-Taylor coefficient [1.74 for arid climate, *Shuttleworth*, 1993], Δ is the gradient of the saturated vapor pressure – temperature curve at air temperature, γ is the psychometric constant at air temperature and pressure, λ is the latent heat of vaporization of water (kJ/kg), ρ_w is the density of water (kg/m³), R_a is a measure of available energy (net short- and long-wave radiation, kJ/m²/hr), f_{AET} is the soil moisture dependent ratio of actual to potential evapotranspiration parameterized as shown in Figure 2-11 similar to *Shuttleworth* [1993, Fig 4.4.3, p. 4.46], and the coefficient K_{veg}

accounts for vegetation type. The parameters involved in the evapotranspiration component are K_{veg} , and moisture contents at saturation θ_s , field capacity θ_r and permanent wilting point θ_w .

It is worth mentioning here that the Priestley-Taylor method ignores the effects of advection, and may only be applicable for time periods of a week or more [Jensen *et al.*, 1990]. Combination methods like Penman-Monteith [Monteith, 1965] may be more general. Since we had measured data to calibrate the vegetation coefficients, this approach may be acceptable for this study.

5.3. Soil Zone

The soil zone acts as a temporary store for infiltrated water. Evapotranspiration extracts moisture from this store. The soil zone drains to the saturated zone. Hydraulic conductivity in the soil zone was assumed to decrease exponentially with depth. The active capacity of the soil zone was divided into components between the volumetric moisture content at saturation θ_s , field capacity θ_r and permanent wilting point θ_w . We define $\Delta\theta_1 = \theta_s - \theta_r$, $\Delta\theta_2 = \theta_r - \theta_w$ and $\Delta\theta = \Delta\theta_1 + \Delta\theta_2$. The soil zone was characterized by a depth z_r (m), which gives a capacity parameter C_{soil} :

$$C_{soil} = z_r \cdot (\theta_s - \theta_w) = z_r \cdot (\Delta\theta_1 + \Delta\theta_2) = z_r \cdot \Delta\theta \quad (2.14)$$

The state of the soil zone is denoted by S (m), which represents the depth of water

stored in the soil zone. Potential rate of infiltration is computed using a Green-Ampt like formulation:

$$i = K_0 \cdot e^{-f \cdot z_f} \frac{z_f + \psi_f}{z_f} \quad (2.11)$$

with

$$z_f = \frac{S}{\Delta\theta} \quad (2.16)$$

where K_0 is the hydraulic conductivity of soil at the surface (m/hr), f is the parameter that defines the rate of exponential decrease of hydraulic conductivity with depth (1/m) and ψ_f is the wetting front soil suction head (m). This formulation assumed that for the purposes of infiltration excess calculation all moisture in the soil zone was in a saturated wedge at the surface above a wetting front.

Drainage from the soil zone to the saturated zone was computed using:

$$r_d = K_o \cdot e^{-f \cdot z_r} \left(\frac{\max(0, S - z_r \cdot \Delta\theta_2)}{z_r \cdot \Delta\theta_1} \right)^c \quad (2.17)$$

This formulation assumed that for the purposes of drainage calculations, the

moisture content is uniform over the soil zone. Drainage only occurred when moisture content was in excess of field capacity. The maximum drainage rate was assumed equal to the hydraulic conductivity at the base of the soil zone with drainage reducing as moisture content reduces according to a pore disconnectedness parameter c . These approximations are recognized to be gross simplifications of point-scale soil water processes. Nevertheless they capture the major sensitivities in a relatively simple way. The parameters involved in the soil zone component are K_0, f, z_r, ψ_f, c , and moisture contents at saturation θ_s , field capacity θ_r , and permanent wilting point θ_w .

5.4. Saturated Zone (Baseflow)

Our analysis of saturated zone storage and measured discharge showed evidence that the saturated zone at USC acts as a bucket-like store, which overflows when storage exceeds a threshold. In order to decipher the nature of the storage discharge relationship of the saturated zone, we plotted measured streamflow at USC versus inferred storage at USC. This plot is shown in Figure 2-12. Storage during the simulation period was estimated by subtracting modeled ET and measured runoff from the surface water input. The threshold behavior can be seen in the plot. There is suggestion that the storage discharge relationship is complicated, even hysteretic.

Since the relationship between storage and discharge beyond the threshold was not clearly established from analysis of data, we chose to employ a general power-function and exponential relationship to describe the baseflow generated by the saturated zone. The baseflow is computed as:

$$\begin{aligned}
 Q_b &= 0 && \text{if } \bar{z} > z_i \\
 &= K_0 \cdot e^{-f \cdot \bar{z}} \cdot \left(\frac{z_i - \bar{z}}{z_i} \right)^\eta && \text{if } \bar{z} \leq z_i
 \end{aligned}
 \tag{2.18}$$

where Q_b is baseflow (m/hr), z_i is the threshold (m), and η is the parameter of the saturated zone storage-discharge relationship. The state of the subsurface storage is denoted by \bar{z} (m), which is the average depth to the water table measured from the soil surface. Parameters involved in saturated zone flow are z_i , η , K_0 , and f .

5.5. Streamflow

In this model, we did not use an explicit streamflow routing scheme. Rainfall excess surface runoff may be generated at the soil zone surface if SWI during a time step exceeds the net water holding capacity of the soil zone or potential infiltration rate. In USC essentially no overland flow is observed and in the model runs surface runoff was rarely generated. Therefore we decided that effort to model routing of overland flow was not warranted and held this excess water in a surface store for reinfiltration during subsequent time steps. The streamflow at the outlet of the watershed was taken as the sum of the baseflows generated from the three zones. The time delay between the baseflow response and its appearance at the basin outlet was assumed to be zero.

6. Calibration of DZHM

DZHM is used to implement a 3-zone model for USC. The modeling time step was 1 hour. The parameters θ_s , θ_r , θ_w , z_r , and c were not calibrated. They were set at

values given in Table 2-2. The soil moisture content parameters were estimated for each zone based on soil texture information. *Rawls et al.* [1982] reported and used an extensive soil data set to estimate regression relationships for water content based on soil texture. Using the above database, *Saxton et al.* [1986] estimated continuous drainage curves over the hydraulically useful moisture range. These empirical equations were used to compute the moisture contents for representative soils using the corresponding texture information for the three SWI zones at USC.

The initial moisture content on October 1, 1992 for each zone was set to the wilting point. The preceding year 1991-92 was the driest year on record and we used the wilting point, θ_w , as a reasonable approximation for the dry conditions.

We did not have enough information to determine the drainage properties of the soils at USC, and so we decided to set c to 1.0, which results in linear scaling of the drainage rate by the ratio of available moisture ($S - z_r \cdot \Delta\theta_2$) to drainable capacity ($z_r \cdot \Delta\theta_1$). NLFIT was used to calibrate the remaining parameters: K_{veg} for each of the three zones, and K_0, f, z_i , and η which were assumed to be identical across the three zones. The variation in K_{veg} was used to characterize the vegetation differences between zones. The calibration was carried out in two phases. In the first phase, the parameter K_{veg} was calibrated for each zone, while keeping the values of K_0 and f fixed at some nominal values. This calibration used measured ET data at USC [*Flerchinger et al.*, 1998]. Figure 2-13 shows modeled and measured cumulative ET after this calibration for each zone.

The model needed initial average depth to the water table specified as an initial condition. We had some piezometer data at USC for 1992-93. However, there were practical difficulties associated with interpreting this data in terms of average depth to saturated zone at USC. The subsurface at USC is more complicated than the simplifying assumptions used in developing DZHM. We decided, therefore, to find reasonable values of initial average depth to the water table by trial and error. During this process, we tried to match the volume of simulated outflow to that of measured outflow from USC. We also assumed that the initial average depth to the water table was spatially uniform across the three zones. There is also the possibility of obtaining reasonable values of initial conditions by running the model in warming-up mode. We have not tried this procedure here. Specification of initial conditions is one of the challenging problems in hydrology, and we recommend further research on this topic.

In the second phase of calibration, the saturated zone parameters z_i and η were calibrated along with K_0 and f . These parameters were assumed to be uniform across the three zones. This phase of calibration used measured 1992-93 streamflow at the outlet of USC. Computed ET after the second phase of calibration was found to be insensitive to changes in the values of K_0 and f , which occurred during the transition from phase one to phase two. We decided, therefore, not to iterate on the two phases of the calibration. The values of all parameters after calibration are shown in Table 2.

Another issue deserves mention here. It has been pointed out in literature over the last few years that for complicated model structures, there may exist several sets of parameter values that perform equally well given a set of observations [e.g., *Beven and*

Binley, 1992]. It is therefore desirable to obtain uncertainty bounds on model parameters within which any parameter value is equally likely. This topic is broad enough to deserve a complete study in itself. We have not addressed this issue here but it is recommended for further research.

7. Model Performance

Two different models, PDIMS and DZHM, were presented in this paper. In this section we discuss the performance of these models.

7.1. PDIMS

In spite of the simplifying assumptions made during the formulation of PDIMS, this model performed well given the goal we set for it. The principal goal of PDIMS was to provide accurate surface water input at the watershed scale. One of the great challenges in hydrology is to upscale model structure along with parameters, inputs, and state variables. In other work [*Luce et al., 1999; Luce, 2000; Luce and Tarboton, 2001*] some of us have explored the use of depletion functions as a parameterization for the scaling up of snowmelt models. Here PDIMS was run on each grid cell with varying radiation and air temperature, and the SWI for the zone was computed by aggregating SWI computed at the grid scale. We evaluated the performance of PDIMS both at the grid scale (Figure 2-7) as well as at the watershed scale (Figure 2-4). There was some scatter in the predictions made by PDIMS at the grid scale, especially later in spring (Figure 2-7). This observation was not completely unexpected given the simplifying assumptions. Also, when the snowmelt model seems to perform poorly at the grid scale,

i.e., in the second half of May, most of the snow has already melted, and has been accounted for accurately at the watershed scale (see Figure 2-4).

7.2. DZHM

The primary goal of DZHM was to demonstrate if a relatively simple hydrologic model could be developed to adequately transform the SWI computed by PDIMS into annual water balance components. Predictions made by DZHM agree favorably in terms of water balance components at USC (see below). There are, however, differences between DZHM predictions and observations made at USC. Figure 2-10 shows the measured hydrograph and the DZHM modeled hydrograph. The measured hydrograph shows spikes indicating short duration streamflow response to events like surface runoff from frozen ground or from partially saturated area. The three-zone structure of DZHM does not include parameterization for runoff from frozen ground or from partially saturated area. Rain on snow or on potentially frozen ground is assumed to pass immediately to the soil surface and be available for infiltration or surface runoff. This behavior might result in the smoothing of streamflow response as indicated by the modeled hydrograph. Although DZHM seems to capture some of the major behavior of the subsurface response, there are some missing process parameterizations that may be required for better streamflow modeling.

8. Mass Balance Components at USC for 1992-93

Basinwide mass balance components as simulated by the calibrated DZHM are

shown in Table 2-3 and Figure 2-13. There was 715 mm of surface water input (rainfall + snowmelt) during the simulation period (October 1, 1992 – August 16, 1993). The simulated ET accounted for 408 mm, which was reasonably close to the estimate given by Flerchinger et al. [see Table II in *Flerchinger et al.*, 1998]. Runoff accounted for 61 mm, which compared favorably with the measured volume of runoff (60 mm). The rest of the water was stored in the soil zone (20 mm) and the saturated zone (227 mm). These storage component values differ from those reported by Flerchinger et al. [20 mm vs. 100 mm for soil zone and 227 mm vs. 75 mm for the saturated zone, see Table II in *Flerchinger et al.*, 1998]. These discrepancies may be due to difficulties associated in interpreting point measurements to estimate zonal averages, differences in definition of soil and saturated zones, interpretation of model state variables compared to measurements, and due to the simple structure of the subsurface model used in DZHM. Overall, basinwide mass balance components agree well with observations. Table 2-3 also shows zonal mass balance components. Surface water inputs on zones 1 and 2 were substantially less than the potential evapotranspiration. For zone 3, however, surface water input was greater than potential evapotranspiration. On zones 1 and 2, a large fraction of surface water input was used to satisfy the evapotranspiration demand, and the rest of the water was not sufficient to raise the water table to the threshold in order to produce runoff. On zone 3, although the absolute modeled evapotranspiration was larger than those on zones 1 and 2, it was a smaller fraction of the surface water input compared to the other zones. The relatively large fraction of surface water input available for infiltration on zone 3 raised the water table to the threshold, and resulted in all runoff

produced from USC. The spatially varying surface water input, which was a result of the wind-induced snow drifting, controlled the amount and timing of recharge at USC, and is thus identified as the dominant hydrologic process.

9. Summary and Conclusions

In this paper, we used an extensive hydrometeorological dataset to identify hydrologic behavior at a small semiarid mountainous watershed. The hydrologic behavior of the watershed was mainly influenced by the spatial variability of surface water input. The variability of surface water input was a direct result of the wind-driven redistribution of snow. Wind-induced drifting was parameterized by the drift factor concept. Drift factors were obtained by calibration against measured snow water equivalence maps. A physically based, energy-balance snowmelt model was used to estimate early season melt during the calibration. This drift factor map was used to parameterize the wind-induced snow drifting over the watershed in absence of explicit lateral snow exchange over the grid cells.

Surface water input was computed using a simple, index-based snowmelt model, PDIMS. The parameters of PDIMS were obtained by calibration against measured snow water equivalence maps. The calibration was carried out using an interactive optimization software, NLFIT. The space-time evolution of snowpack and surface water input during one snow accumulation, drift, and melt season was excellently modeled at the watershed scale using the UEB calibrated drift factors and 5 Par PDIMS. The distribution of drift factors was used to delineate zones of surface water input. These zones corresponded

well with snowmelt zones described by past investigations at USC. Comparison of the cumulative surface water input time series with the measured runoff from USC suggested that almost all of the measured outflow resulted from the surface water input from the deep drifts which formed on the leeward, northwest-facing slope of USC. The timing of measured USC outflow also corresponded closely with the timing of SWI into the zone corresponding to leeward, northwest-facing slope where the deep drifts form. The above observations are very important because they reveal the internal dynamics of a snowdrift and snowmelt-driven semiarid watershed, and may be used to build simpler hydrologic models that capture the important dynamics of the processes in spite of simplifying assumptions.

Based on these insights, we developed a simple lumped hydrologic model, DZHM, which was applied to each of the three SWI zones individually. NLFIT was used to calibrate DZHM in two phases, first against ET data and then against measured streamflow. The aggregate water balance values reported in Table 2-3 agree favorably with those reported by *Flerchinger et al.* [1998], except for the aggregate storage changes in the soil zone and in the saturated zone. We suspect that these discrepancies may be partly due to difficulties inherent in interpreting point-scale measurements to estimate zonal average conditions, differences in definition of soil and saturated zones, interpretation of model state variables compared to measurements, and partly due to the simplified structure of the soil zone representation in DZHM.

We have shown in this paper that small-scale hydrology at a first-order subwatershed in Reynolds Creek Experimental Watershed is controlled by the magnitude

and timing of surface water input into the soil, which depends on the spatial variability of snowpack accumulation during winter. Once we correctly identified and represented the spatial variability of surface water input, a relatively simple lumped hydrologic model was sufficient to parameterize the hydrologic behavior at the scale of the first-order subwatershed. In order to upscale our understanding to model the hydrologic behavior of larger watersheds within RCEW, we believe it is necessary to establish the spatial variability of snowpack accumulation and melt. At scales larger than Upper Sheep Creek, it is impractical to conduct manual snow surveys. Wind-blowing snow transport models [e.g., *Pomeroy and Gray, 1995; Liston and Sturm, 1998*] may be a viable alternative for estimating terrain related drift factors. Some work in this direction has already been reported in Chapter 3.

References

- Beven, K., and A. Binley, The future of distributed models: Model calibration and uncertainty prediction, *Hydrol. Processes*, 6, 279–298, 1992.
- Cooley, K. R., Snowpack variability on western rangelands, paper presented at Western Snow Conference, Kalispell, Mont., April 18–20, 1988.
- Dingman, S. L., *Physical Hydrology*, 575 pp., Macmillan, New York, 1994.
- Dozier, J., and J. Frew, Rapid calculation of terrain parameters for radiation modeling from digital elevation data, *IEEE Trans. on Geosci. and Rem. Sens.*, 28(5), 963–969, 1990.
- Duffy, C. J., K. R. Cooley, N. Mock, and D. Lee, Self-affine scaling and subsurface response to snowmelt in steep terrain, *J. Hydrol.*, 123, 395–414, 1991.
- Erbs, D. G., S. A. Klein, and J. A. Duffie, Estimation of the diffuse radiation fraction for hourly, daily and monthly-average global radiation, *Solar Energy*, 28, 293–302, 1982.

- Flerchinger, G. N., K. R. Cooley, C. L. Hanson, and M. S. Seyfried, A uniform versus an aggregated water balance of a semi-arid watershed, *Hydrol. Processes*, 12, 331–342, 1998.
- Flerchinger, G. N., K. R. Cooley, and D. R. Ralston, Groundwater response to snowmelt in a mountainous watershed, *J. Hydrol.*, 133, 293–311, 1992.
- Gupta, H. V., S. Sorooshian, and P. O. Yapo, Toward improved calibration of hydrologic models: Multiple and noncommensurable measures of information, *Water Resour. Res.*, 34(4), 751–763, 1998.
- Hamon, W. R., Computing actual precipitation, in *Proceedings of WMO-IDHS Symposium, Distribution of Precipitation in Mountainous Areas, Geilo, Norway, Rep. 326*, pp. 159–174, World Meteorol. Organ., Geneva, 1973.
- Hanson, C. L., Precipitation catch measured by the Wyoming shield and the dual-gage system, *Water Resour. Bull.*, 25, 159–164, 1989.
- Jackson, T. H. R., A spatially distributed snowmelt-driven hydrologic model applied to the Upper Sheep Creek watershed, Ph.D. dissertation, 323 pp., Utah State Univ., Logan, 1994.
- Jensen, M. E., R. D. Burman, and R. G. Allen, ed., *Evapotranspiration and Irrigation Water Requirements, ASCE Manuals and Reports on Engineering Practice No. 70*, 332 pp., Am. Soc. Civ. Eng., New York, 1990.
- Kuczera, G., *NLFIT, A Bayesian Nonlinear Regression Program Suite, Rep. Version 1.00g*, Department of Civil Engineering and Surveying, Univ. of Newcastle, N.S.W., Australia, 1994.
- Kuczera, G., Efficient subspace probabilistic parameter optimization for catchment models, *Water Resour. Res.*, 33(1), 177–185, 1997.
- Liston, G. E., and M. Sturm, A snow-transport model for complex terrain, *J. Glaciol.*, 44(148), 498–516, 1998.
- Luce, C. H., Scale influences on the representation of snowpack processes, Ph.D. dissertation, 202 pp., Utah State Univ., Logan, 2000.
- Luce, C., and D. Tarboton, Scaling up snowpack accumulation and melt models, *Submitted to Water Resour. Res.*, 2001.

- Luce, C. H., D. G. Tarboton, and K. R. Cooley, Subgrid parameterization of snow distribution for an energy and mass balance snow cover model, *Hydrol. Proc.*, 12(10–11), 1671–1683, 1999.
- Monteith, J. L., Evaporation and environment, in *State and Movement of Water in Living Organisms*, Proc. 19th Symp. of the Soc. for Exp. Biol., pp. 205–234, Cambridge Univ. Press, Cambridge, U.K., 1965.
- Pomeroy, J. W., and D. M. Gray, Snowcover: Accumulation, relocation and management, *Sci. Rep.* 7, 144 pp., Natl. Hydrol. Res. Inst., Saskatoon, Sask., Canada, 1995.
- Rawls, W. J., D. L. Brakensiek, and K. E. Saxton, Estimation of soil water properties, *Trans. ASAE*, 25, 1316–1320, 1982.
- Riley, J. P., D. G. Chadwick, and J. M. Bagley, Application of electronic analog computer to solution of hydrologic and river basin planning problems: Utah simulation model II, *Rep. PRWG32-1*, Utah Water Res. Lab., Utah State Univ., Logan, 1966.
- Satterlund, D. R., An improved equation for estimating long-wave radiation from the atmosphere, *Water Resour. Res.*, 15, 1643–1650, 1979.
- Saxton, K. E., W. J. Rawls, J. S. Romberger, and R. I. Papendick, Estimating generalized soil-water characteristics from texture, *Soil Sci. Soc. Am. J.*, 50(4), 1031–1036, 1986.
- Sharma, A., and D. G. Tarboton, Conceptual models of snowmelt processes, *Eos Trans. AGU*, Fall Meeting Suppl., 76(46), Abstract H21A-09, 1995.
- Shuttleworth, W. J., Evaporation, in *Handbook of Hydrology*, edited by D. R. Maidment, pp. 4.1–4.53, McGraw-Hill, New York, 1993.
- Stephenson, G. R., and R. A. Freeze, Mathematical simulation of subsurface flow contributions to snowmelt runoff, Reynolds Creek Watershed, Idaho, *Water Resour. Res.*, 10(2), 284–294, 1974.
- Stevens, G. R., A geophysical investigation of the Upper Sheep drainage, Reynolds Creek Experimental Watershed, Owyhee County, Idaho, M.S. thesis, 119 pp., Univ. of Idaho, Moscow, 1991.
- Tarboton, D. G., T. G. Chowdhury, and T. H. Jackson, A spatially distributed energy balance snowmelt model, in *Biogeochemistry of Seasonally Snow-Covered*

Catchments, edited by K. A. Tonnessen et al., *IAHS Publ. 228*, pp. 141–155, 1995a.

Tarboton, D. G., T. H. Jackson, J. Z. Liu, C. M. U. Neale, K. R. Cooley, and J. J. McDonnell, A grid based distributed hydrologic model: Testing against data from Reynolds Creek experimental watershed, in *Preprint Volume, Am. Meteorol. Soc. Conf. on Hydrol.*, pp. 79–84, Am. Meteorol. Soc., Dallas, Tex., 1995b.

Tarboton, D. G., and C. H. Luce, *Utah Energy Balance Snow Accumulation and Melt Model (UEB), Computer Model Technical Description and Users Guide*, Utah Water Res. Lab., Logan, 1996.

U.S. Army Corps of Engineers, *Snow Hydrology, Summary Report of the Snow Investigations*, 437 pp., N. Pac. Div., Portland, Oreg., 1956.

Wigmosta, M. S., L. W. Vail, and D. P. Lettenmaier, A distributed hydrology-vegetation model for complex terrain, *Water Resour. Res.*, 30(6), 1665–1679, 1994.

Winkelmaier, J. R., Ground-water flow characteristics in fractured basalt in a zero-order basin, M.S. thesis, 128 pp., Univ. of Idaho, Moscow, 1987.

Table 2-1. Calibrated Melt Factors at USC (5 Par PDIMS)

Configuration	January	February	March	April	May
5 Par PDIMS	0.106	0.635	0.063	0.065	0.045

Units are $\text{m/h}/(\text{W/m}^2)^{\circ}\text{C}$

Table 2-2. Parameters of DZHM

Parameter	Calibrated Value	Parameter	Prescribed Value
K_{veg} (Zone 1)	1.3960	θ_s (Zone 1)	0.54
K_{veg} (Zone 2)	1.4990	θ_s (Zone 2)	0.61
K_{veg} (Zone 3)	1.5999	θ_s (Zone 3)	0.70
K_0	0.2 m/hr	θ_r (Zone 1)	0.39
F	2.156 1/m	θ_r (Zone 2)	0.46
Z_l	1.335 m	θ_r (Zone 3)	0.50
η	2.156	θ_w (Zone 1)	0.14
		θ_w (Zone 2)	0.21
		θ_w (Zone 3)	0.18
		z_r	0.75 m
		c	1.0

Table 2-3. Mass balance summary at USC (October 1, 1992 to August 16, 1993)

Mass Balance Components	Basinwide Average	Zone 1	Zone 2	Zone 3
Surface Water Input (mm)	715	460	665	1263
Potential Evapotranspiration (mm)	878	968	862	724
Modeled Evapotranspiration (mm)	408	395	384	460
Change in Soil Storage (mm)	20	19	18	25
Inferred Change in Soil Storage (mm)**	100	37	162	240
Change in Ground Water Storage (mm)	227	46	264	533
Inferred Change in Ground Water Storage (mm)**	75	--	--	--
Modeled Runoff (mm)	61	0	0	245
Measured Runoff (mm)*	59.7	--	--	--

* measured basin average outflow

** as reported by Flerchinger et al., 1998

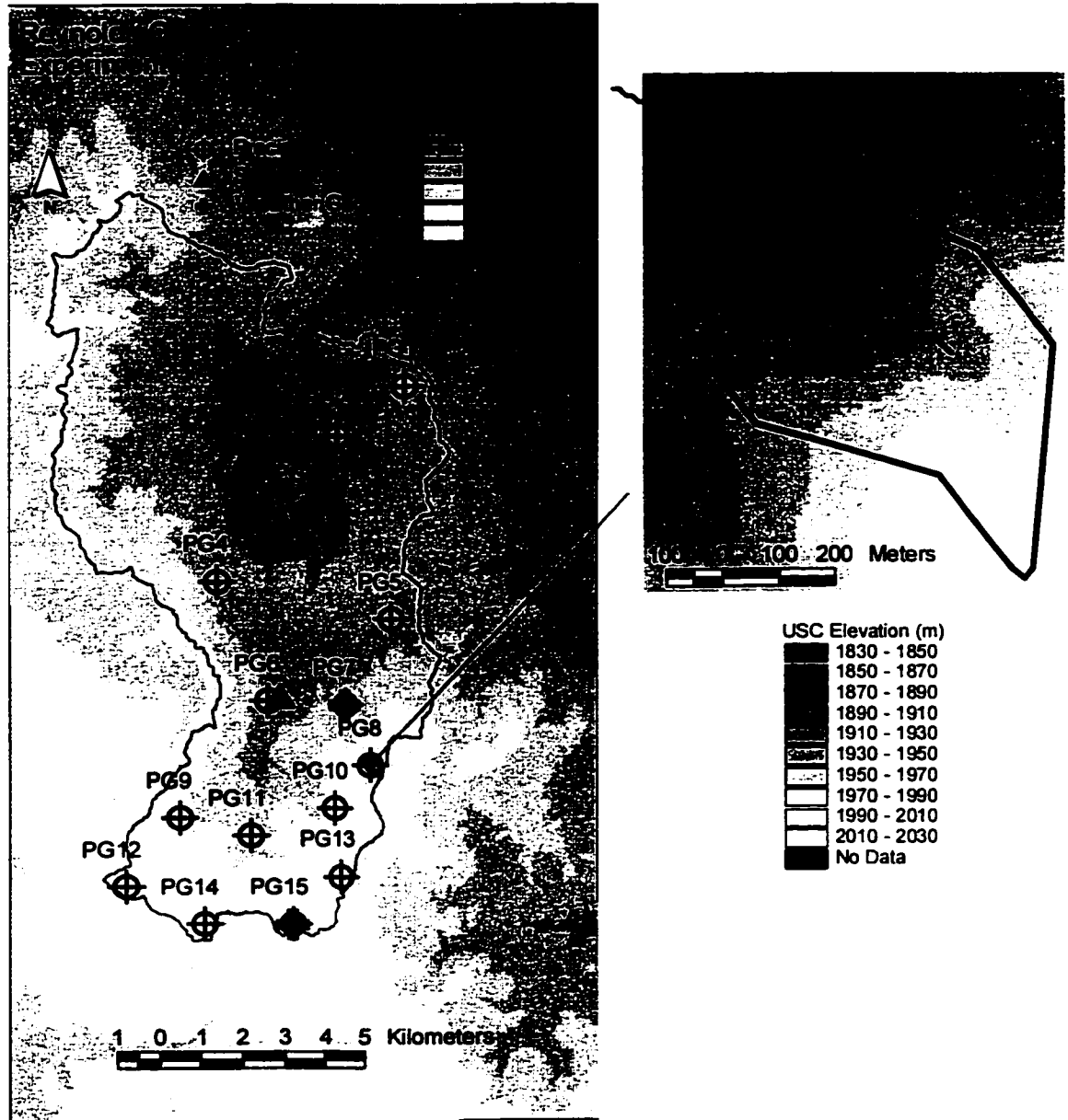


Figure 2-1. Reynolds Creek Experimental Watershed and Upper Sheep Creek, the first order subwatershed that is the focus of this study.

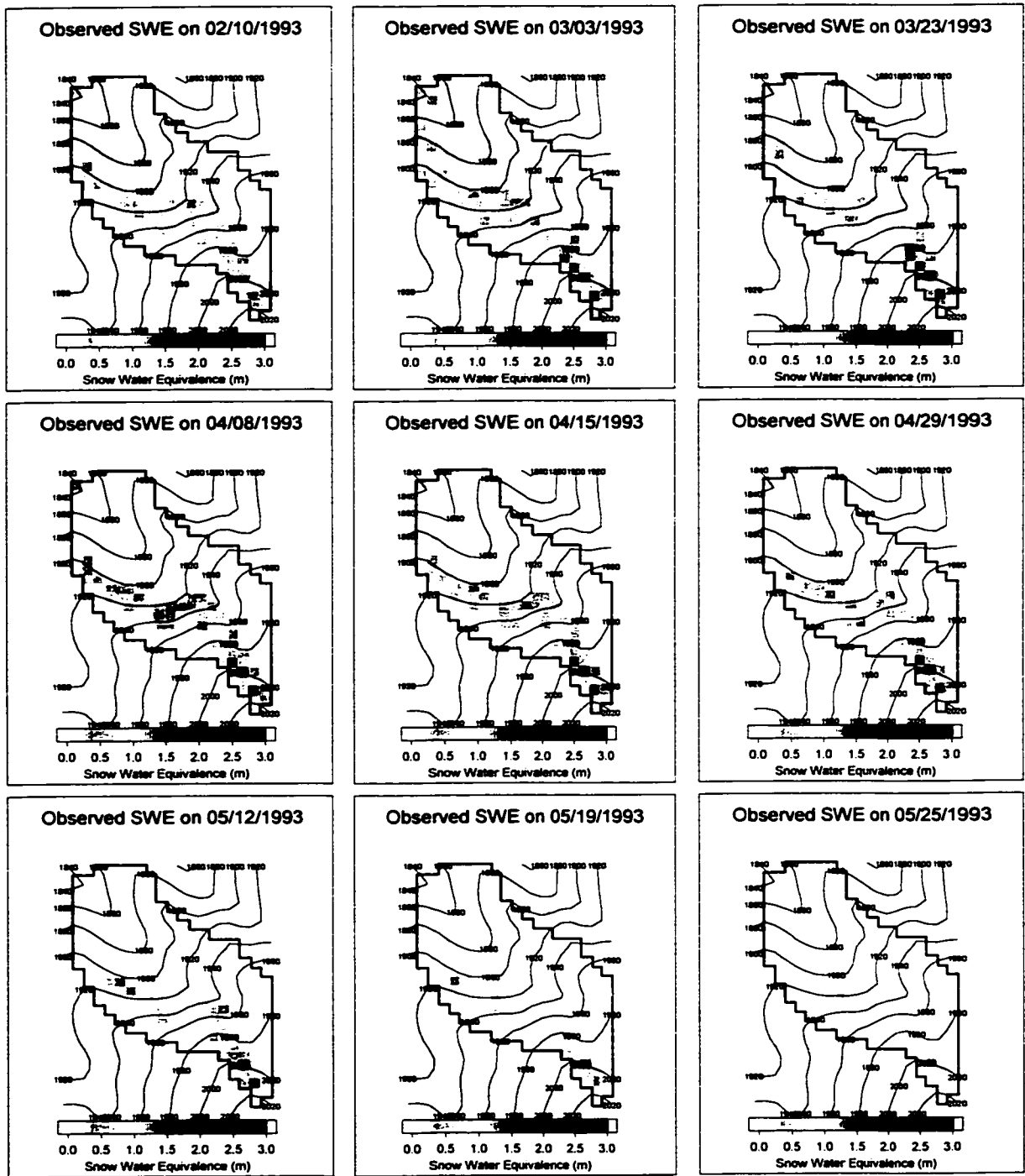


Figure 2-2. The measured SWE maps during 1992-93 season. Thin lines denote elevation contours. Measurements were made on a 30.48 m grid approximately aligned with the long axis of USC. These maps were produced by interpolation of measured data on to the 30 m north-aligned DEM grid.

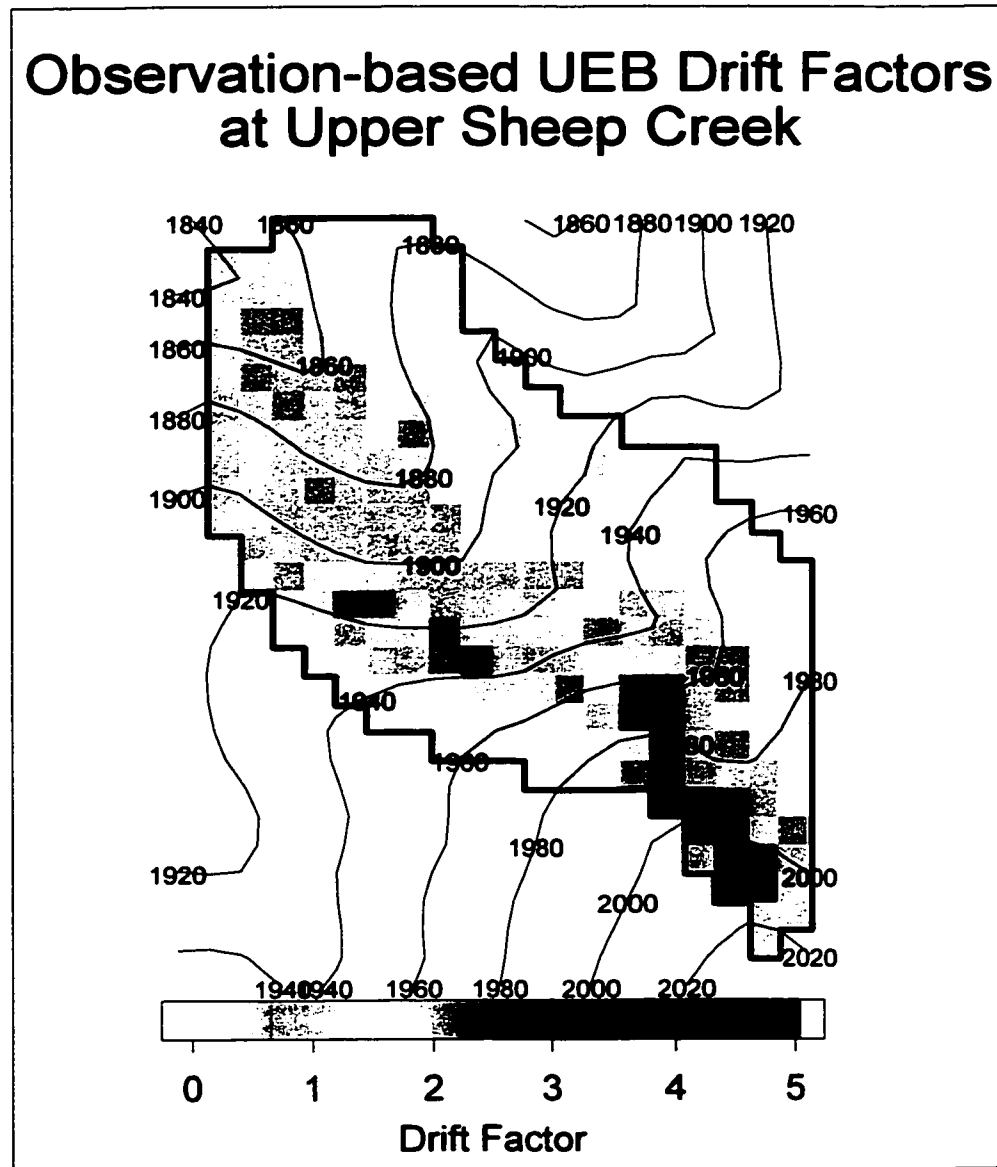


Figure 2-3. Drift factors at Upper Sheep Creek calibrated using UEB as the snowmelt model. The calibration used the first three measured SWE maps during 1992-93. Thin lines denote elevation contours.

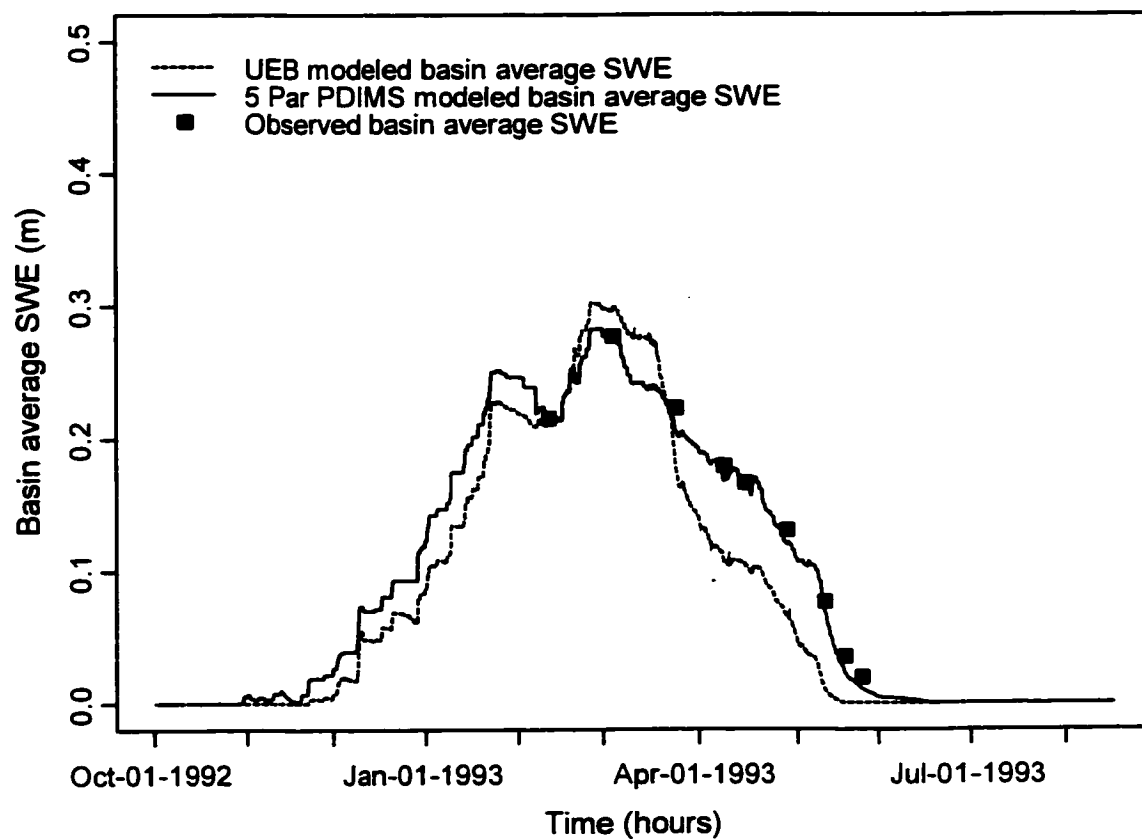


Figure 2-4. Time series of basin average snow water equivalence at Upper Sheep Creek during 1992-93.

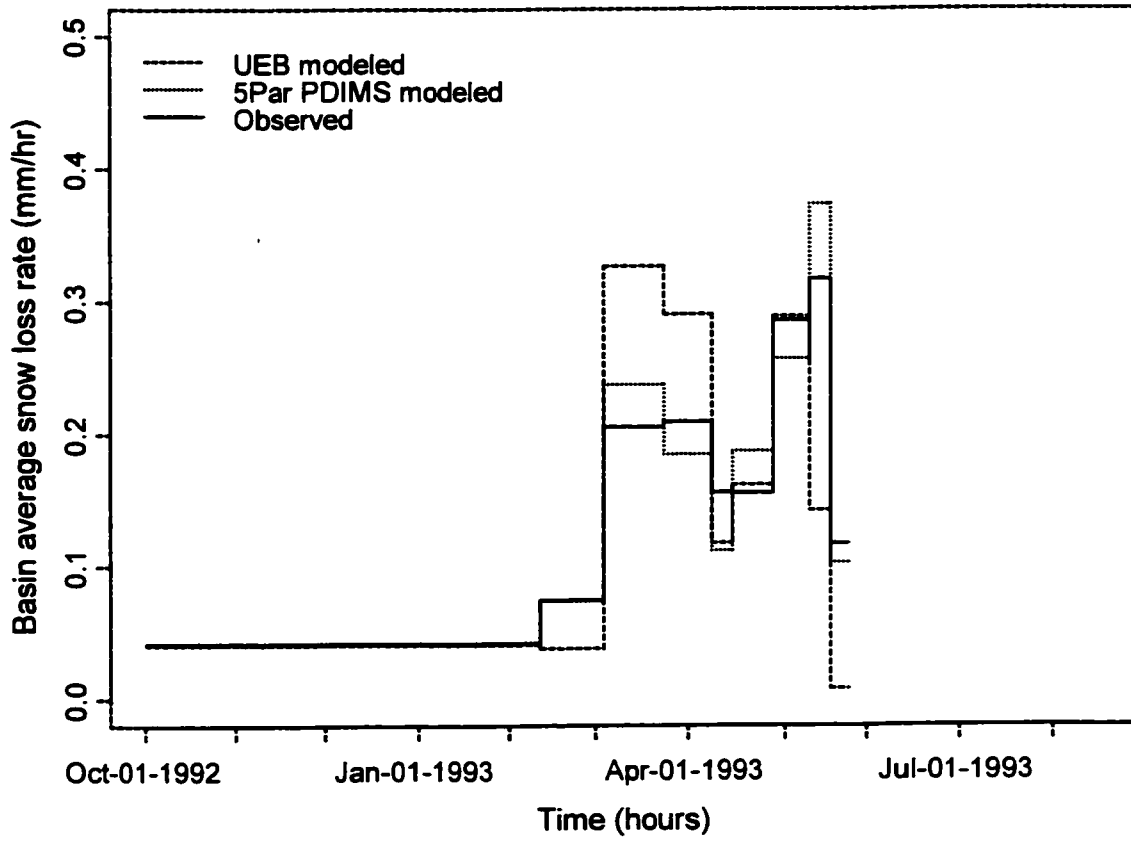


Figure 2-5. Measured and modeled basin average snow-loss rate between snow survey dates.

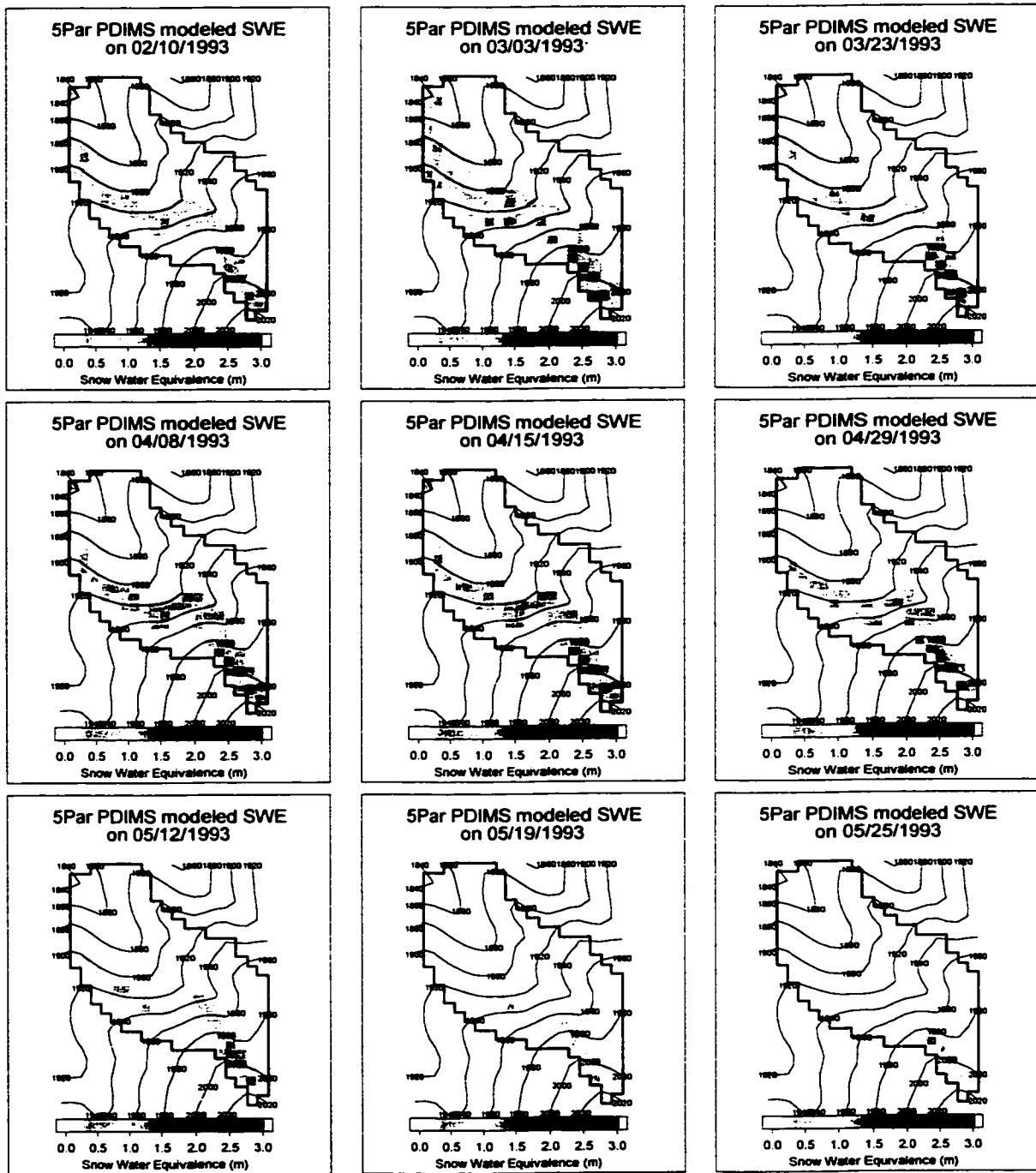


Figure 2-6. SWE maps modeled by 5 Par PDIMS during 1992-93 season. Thin lines denote elevation contours.

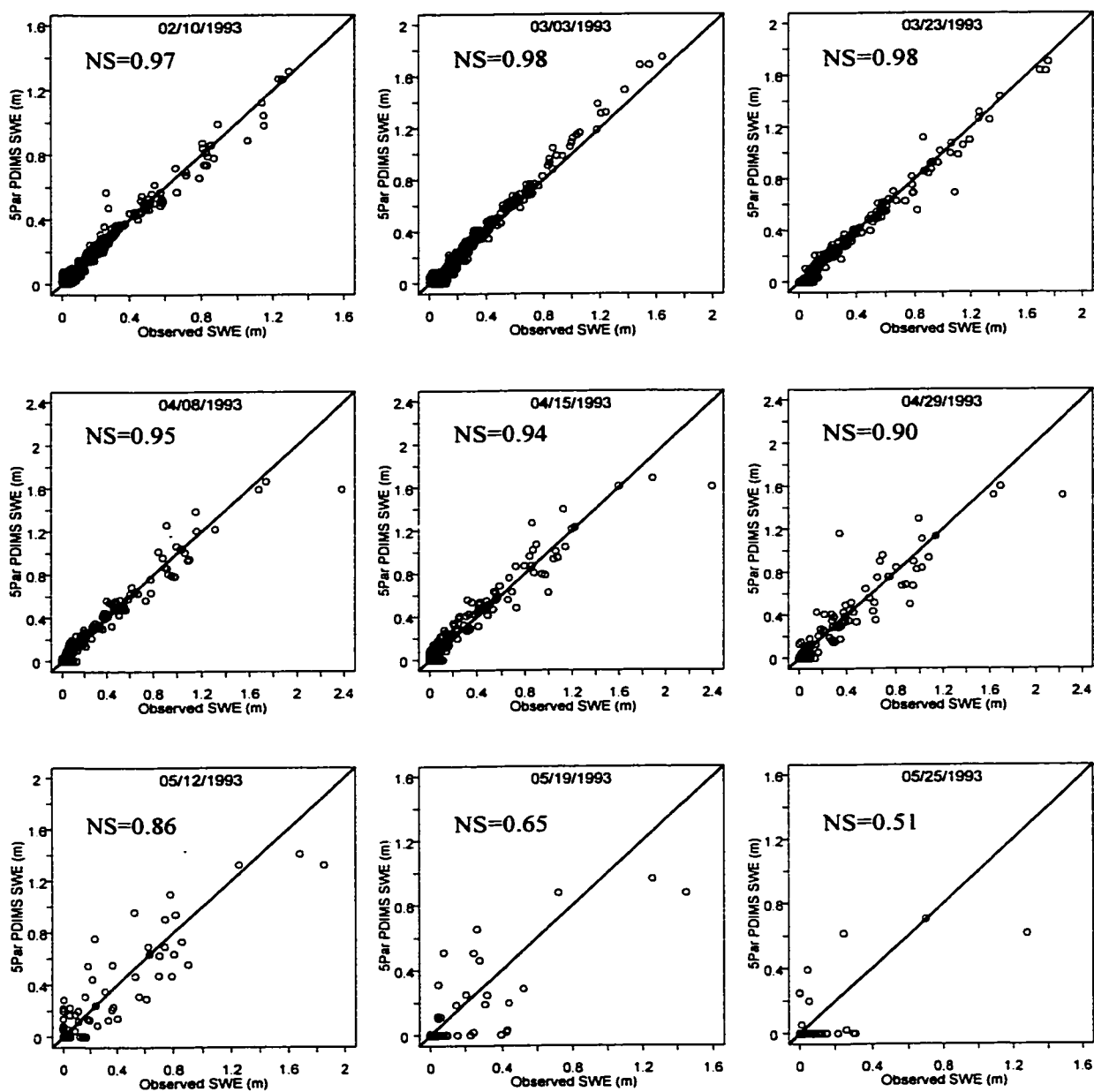


Figure 2-7. Comparison between 5 Par PDIMS modeled and observed SWE at USC. NS refers to the Nash-Sutcliffe goodness-of-fit measure.

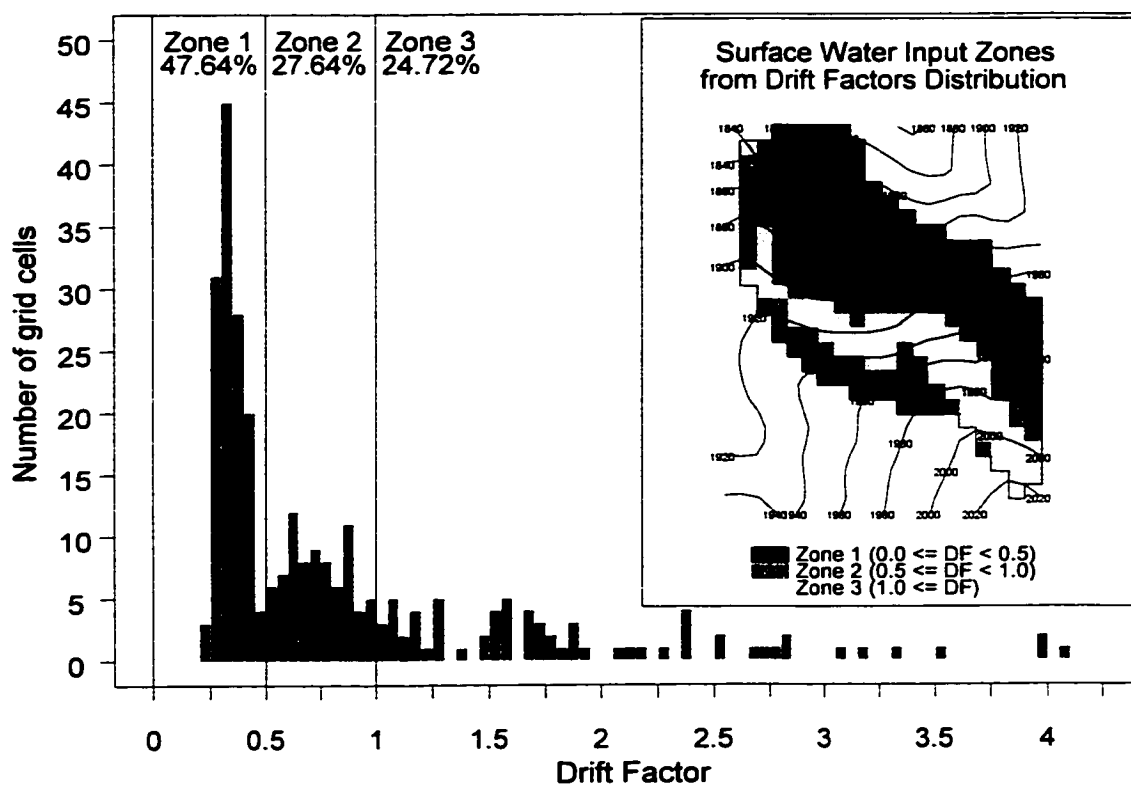


Figure 2-8. Distribution of drift factors at Upper Sheep Creek. There are 275 grid cells in the watershed. Inset: Three zones of Upper Sheep Creek based on drift factor distribution. Zone 1: $0.0 \leq DF < 0.5$ (47.64% of total area of USC), Zone 2: $0.5 \leq DF < 1.0$ (27.64%) and Zone 3: $1.0 \leq DF$ (24.72%).

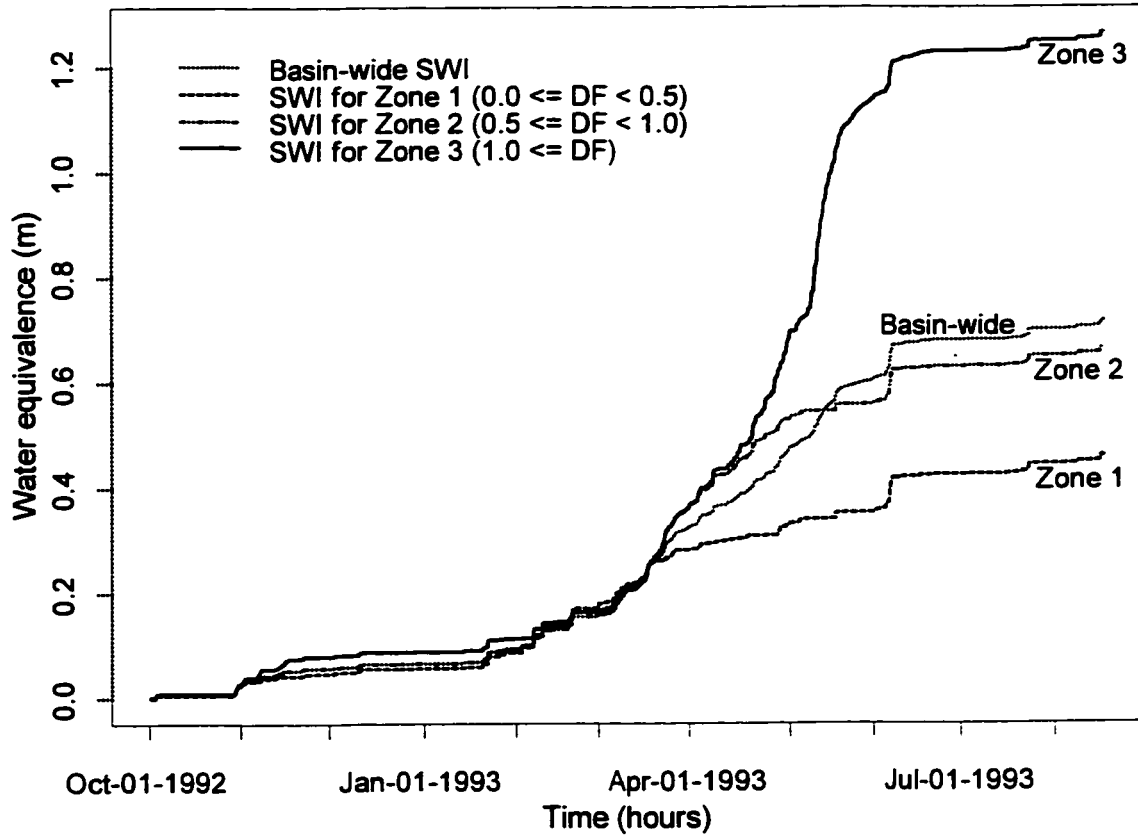


Figure 2-9. Time series of cumulative surface water input for the three zones at USC during 1992-93 as modeled by 5 Par PDIMS.

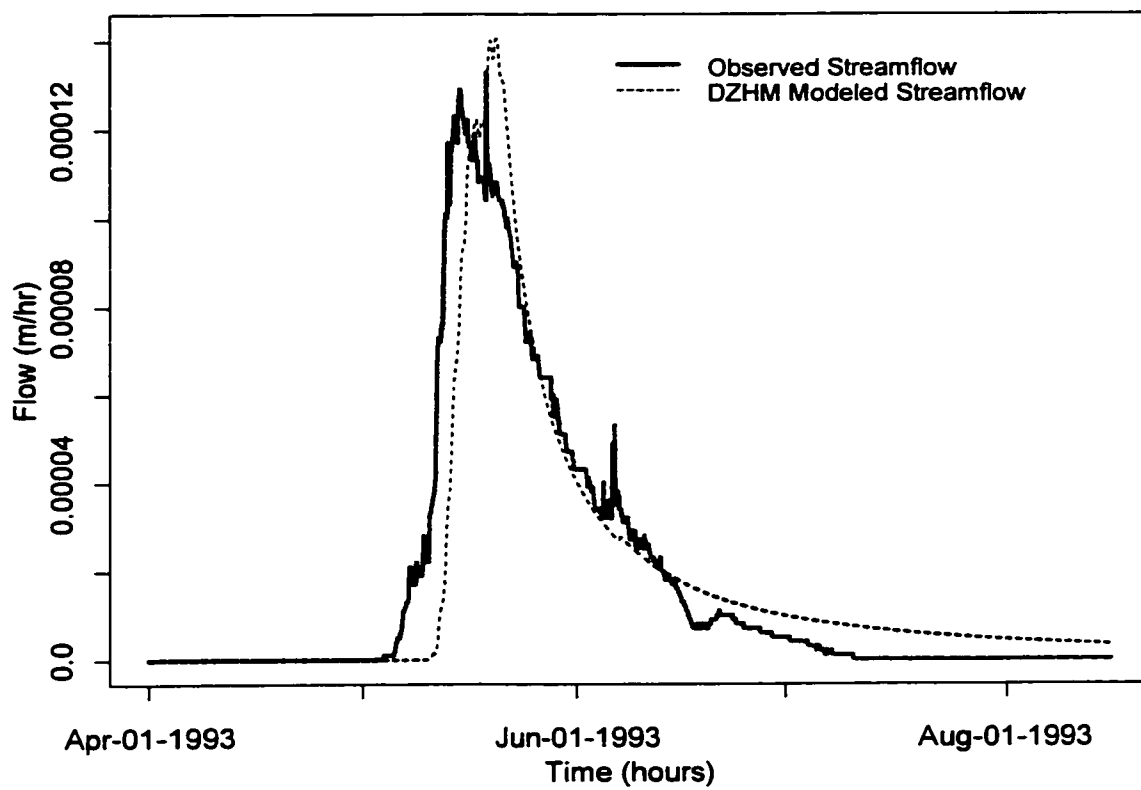


Figure 2-10. Observed and modeled outflow hydrographs at Upper Sheep Creek during 1992-93.

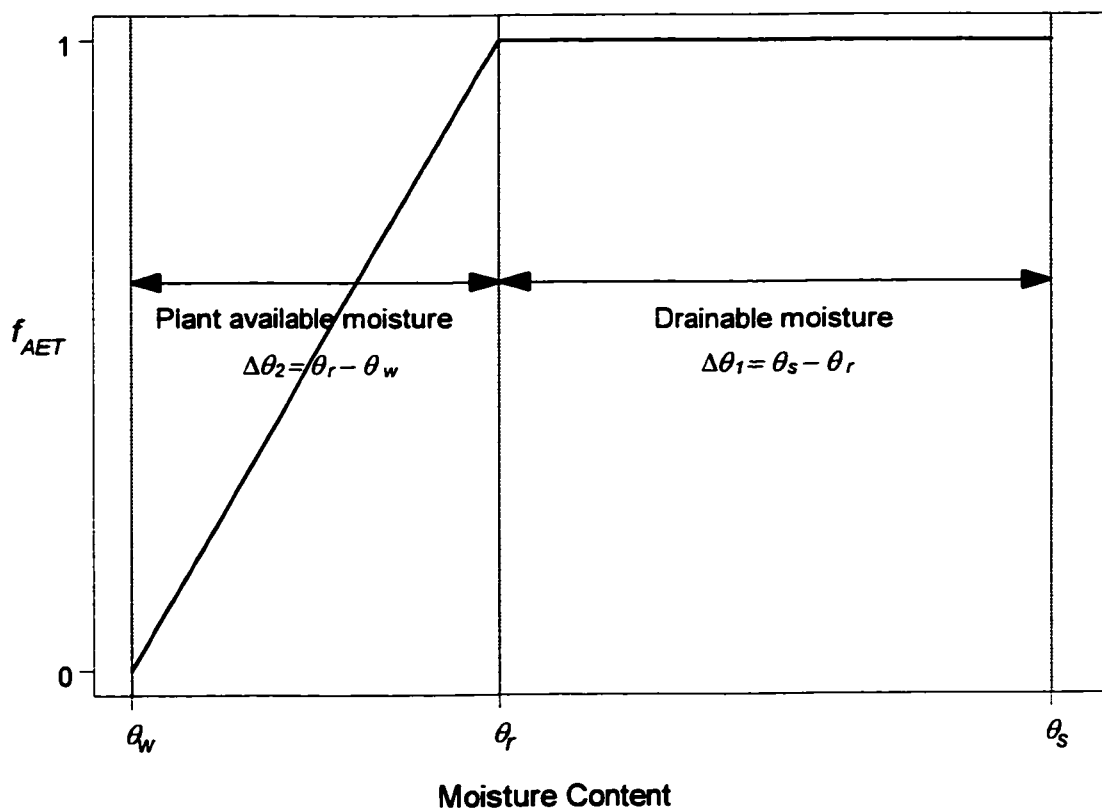


Figure 2-11. Moisture content-based reduction function for actual evapotranspiration. θ_s is saturation moisture content, θ_r is the field capacity or drainable moisture content and θ_w is permanent wilting point.

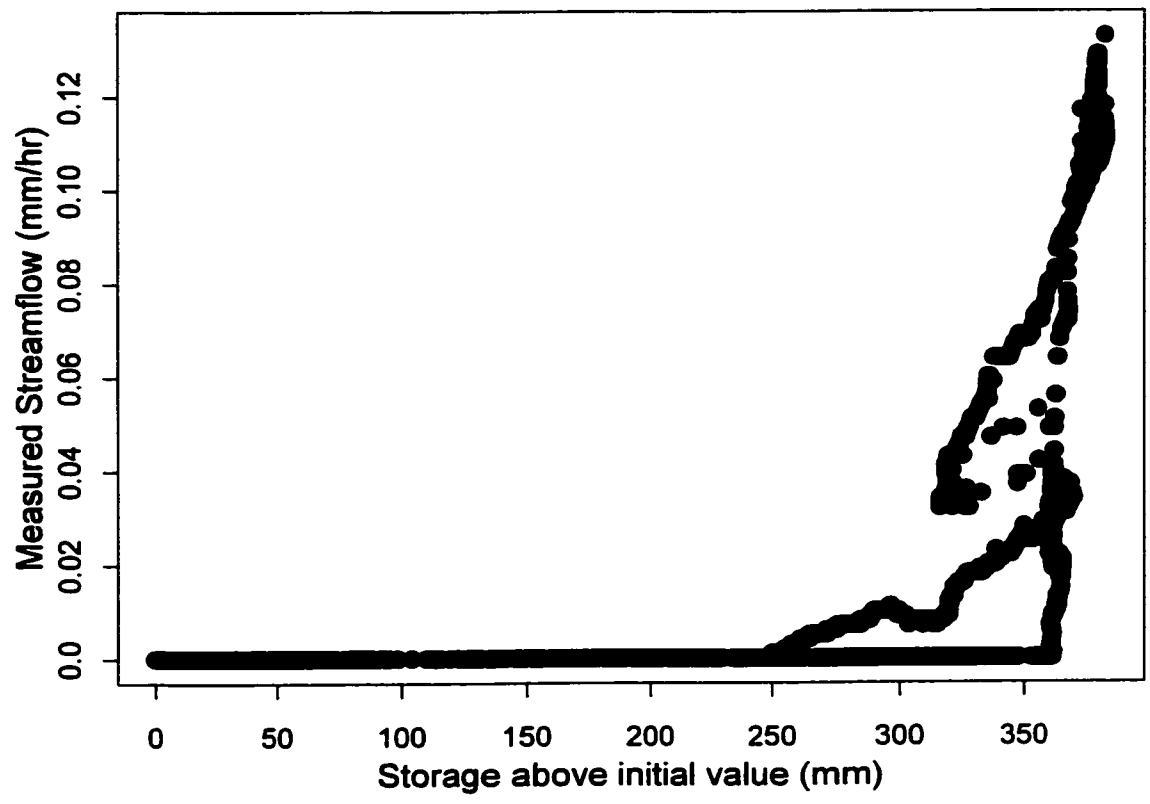


Figure 2-12. Measured streamflow versus inferred storage at USC during 1992-93.

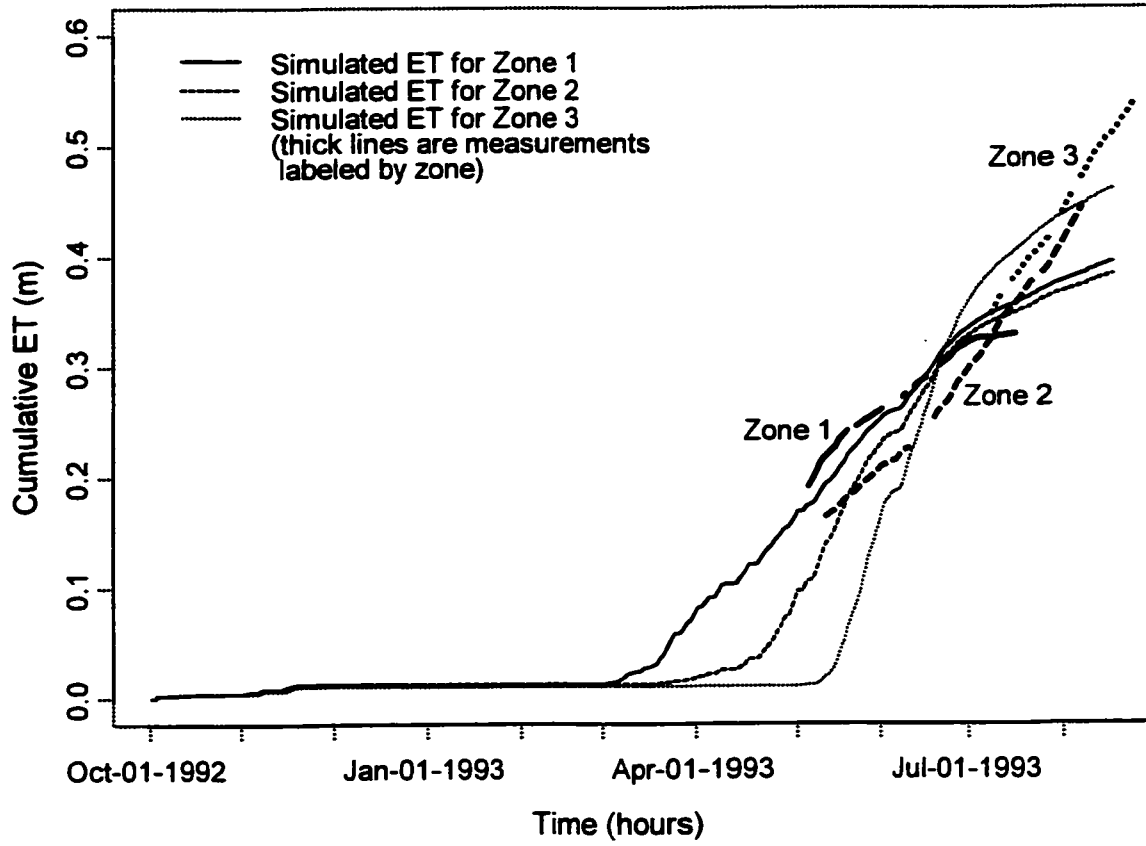


Figure 2-13. Modeled and measured cumulative evapotranspiration.

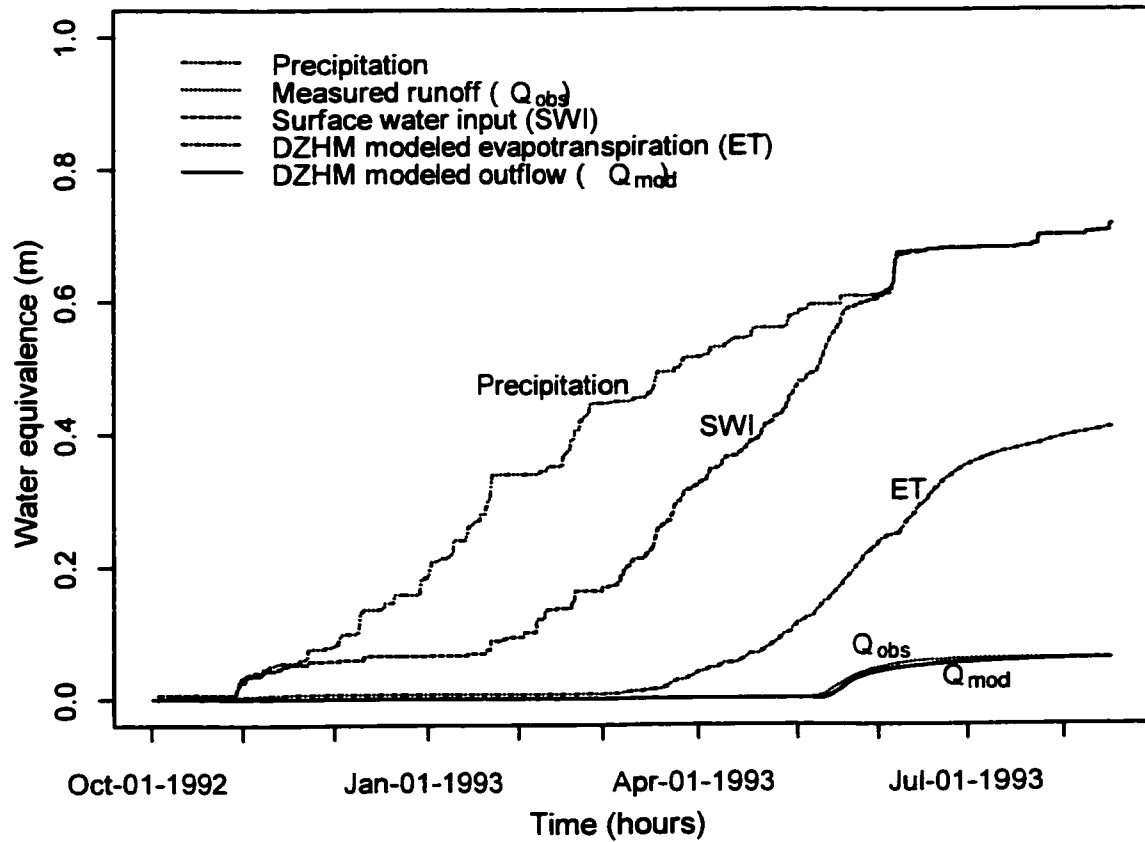


Figure 2-14. Cumulative basinwide mass balance plot for 1992-93. The difference between precipitation and surface water input is surface water storage as snowpack. The difference between the surface water input line and the evapotranspiration line is recharge, which is available for runoff.

CHAPTER 3
TESTING A BLOWING SNOW MODEL AGAINST DISTRIBUTED SNOW
MEASUREMENTS AT UPPER SHEEP CREEK, IDAHO,
UNITED STATES OF AMERICA¹

Abstract

In this paper a physically based snow transport model (SnowTran-3D) was used to simulate snow drifting over a 30-m grid, and was compared to detailed snow water equivalence (SWE) surveys on three dates within a small 0.25-km² subwatershed, Upper Sheep Creek. Two precipitation scenarios and two vegetation scenarios were used to carry out four snow transport model runs in order to: (1) evaluate the blowing snow model, (2) evaluate the sensitivity of the snow transport model to precipitation and vegetation inputs, and (3) evaluate the linearity of snow accumulation patterns and the utility of the drift factor concept in distributed snow modeling. Spatial comparison methods consisted of (1) pointwise comparisons of measured and modeled SWE, (2) visual comparisons of the spatial maps, (3) comparisons of the basinwide average SWE, (4) comparisons of zonal average SWE in accumulation and scour zones, and (5) comparisons of distribution functions. We found that the basin average modeled SWE was in reasonable agreement with observations, and that visually the spatial pattern of snow accumulation was well represented except for a pattern shift. Pointwise compari-

¹ Coauthored by Rajiv Prasad, David G. Tarboton, Glen E. Liston, Charles H. Luce and Mark S. Seyfried.

sons between the modeled and observed SWE maps displayed significant errors. The distribution functions of SnowTran-3D modeled drift factors from two precipitation scenarios on three dates were compared with the distribution function of observation-based drift factors obtained previously by calibration to evaluate the assumption of linearity. We found only a 14% reduction in explained variance in the distribution function of drift factors, for a 69% increase in precipitation, suggesting that the simplification provided by the use of drift factor distributions will result in errors that are tolerable in many cases.

1. Introduction

The hydrologic response from northwestern U.S. rangelands is strongly influenced by snowmelt. The importance of snow drifting in the magnitude and timing of snowmelt water inputs during the hydrologic response has been well documented [Cooley, 1988; Luce *et al.*, 1997; Luce *et al.*, 1998]. The spatial variability of surface water input from melting snowdrifts controls the magnitude and timing of runoff from these watersheds. One way of quantifying the spatial variability of snowpack is to conduct manual snow surveys throughout the winter. This is a costly endeavor, and can only be used to sample small areas. Since measurements are impractical at larger scales, some form of modeling is needed. Apart from some specialized blowing snow models [e.g., Pomeroy and Gray, 1995; Liston and Sturm, 1998], most physically based snow accumulation and melt models do not include a description of wind-driven drift; indeed, they are point models, and application of these models at the watershed scale needs to

account for lateral snow exchanges. One way to accommodate wind-driven snow drift is to use manually measured snow water equivalence (SWE) surveys in association with a snow accumulation and melt model to derive drift factors [Jackson, 1994; Tarboton *et al.*, 1995; Luce *et al.*, 1998]. The drift factor at a point is a factor by which gage snowfall must be multiplied to equate measured and modeled SWE on the ground. It is used to describe the tendency of a location to accumulate extra snow through drifting (drift factor > 1), or to lose snow due to scouring (drift factor < 1). These drift factors vary spatially over the domain and are multiplied with observed snowfall to model snowfall redistribution by wind.

The purpose of this paper is to apply a blowing snow model [Liston and Sturm, 1998] called SnowTran-3D, to portions of the Reynolds Creek Experimental Watershed (Figure 3-1) to estimate the spatial distribution of snowpack during the accumulation and drift period. This is a mass transport model which takes inputs of snowfall, air temperature, humidity, and wind speed and direction and models the effect of their interaction with topography and vegetation on the accumulation of wind blown snow. This study addressed the following questions:

- (1) how well does SnowTran-3D simulate the spatial patterns of snow accumulation due to drifting?
- (2) how sensitive is the modeled pattern of snow accumulation to vegetation?
- (3) how sensitive are the model-derived drift factors to precipitation?

The first question evaluates the performance of the blowing snow model. The second question is of interest because although topography is now readily available in the

form of digital elevation data, fine scale vegetation maps are less commonly available. It is thus useful to know how important fine scale vegetation information is in determining the spatial pattern of snow accumulation. The third question focuses on the validity and utility of the drift factor concept. The drift factor concept assumes linear scaling with amount of snowfall, so that with double the snowfall, accumulated snow amounts will be doubled while preserving the spatial pattern. We evaluate the validity of this assumption using SnowTran-3D model simulations.

2. Study Site and Available Data

Reynolds Creek Experimental Watershed (RCEW) is a semiarid mountainous watershed located in southwestern Idaho, USA, and has been the focus of intensive hydrologic instrumentation and investigation over the last three decades [*Hamon, 1973; Stephenson and Freeze, 1974; Winkelmaier, 1987; Hanson, 1989; Duffy et al., 1991; Stevens, 1991; Flerchinger et al., 1992*]. The watershed is maintained by the Northwest Watershed Research Center (NWRC), Boise, Idaho, a part of the Agricultural Research Service, U.S. Department of Agriculture. This study focused on the 54-km² Tollgate and 0.25-km² Upper Sheep Creek (USC) watersheds (Figure 3-1) located within RCEW. Elevations in the Tollgate watershed range from 1403 to 2239 m. Mean annual precipitation varies with elevation and ranges from approximately 450 to over 1200 mm. Mean annual precipitation in USC is about 508 mm. The watershed is almost entirely sagebrush rangeland (87%) with some stands of Douglas fir, aspen and alpine fir forest

(13%). The hydrology of the watershed is mainly snowmelt driven. Channel flow is sustained by groundwater recharged by infiltration of snowmelt.

Upper Sheep Creek was the location of intensive study of the distribution of snow over the period 1982 to 1996. A 30-m grid over the watershed defines 255 locations where snowpack was measured at roughly 2-week intervals during the winter [Cooley, 1988]. In particular, nine snow surveys were conducted during water year 1992-93, thereby establishing the spatio-temporal distribution of snow accumulation and melt at USC. Snow depth and SWE measurements were obtained using standard snow sampling techniques and the Rosen type snow sampler [Jones, 1983]. Each snow sample consisted of inserting the snow tube into the snow pack to the soil surface, recording the depth of the snow pack, removing the tube and recording the SWE as the residual of the weight of the tube and snow sample minus the weight of the empty tube. Manpower limitations were such that it required two storm-free days to fully sample the complete 30-m grid. Maps of SWE measured by the first three of the snow surveys are shown in Figure 3-2.

Point data used in this study consisted of observed time series of precipitation, radiation, wind speed and direction, air temperature, and relative humidity. A commercial, high-resolution, 10-m grid digital elevation model (DEM) was acquired from 1:24000 USGS quad sheets for Reynolds Creek Experimental Watershed. In this study, we used a 30-m DEM that was obtained by averaging the 10-m DEM to maintain consistency with the vegetation data which were available only at 30-m resolution. A LANDSAT 5 thematic mapper image acquired on August 1, 1993 was used to derive a plant community map using a maximum likelihood classification procedure. This vegeta-

tion map is shown in Figure 3-3. Hourly weather data including wind speed, global radiation, humidity, and air temperature were measured at three stations in RCEW during 1992-93. Wind direction, however, was available only at one station coinciding with PG7 (Figure 3-1). This study focused on the period October 1, 1992 to March 23, 1993, a single snow accumulation and drift season. Adjusted hourly precipitation data based on dual-gage system described by Hanson [1989] for 15 gages in RCEW for 1992-93 was provided by the NWRC. Measured precipitation can have significant uncertainty associated with it, especially in the context of estimation of spatial volume from a network of gages [see for example, *Hanson, 1989; Groisman and Legates, 1994; Morrissey et al., 1995; McCollum and Krajewski, 1998*].

Eight of the precipitation gages were located inside Tollgate. The cumulative precipitation and cumulative snowfall amounts for this period for the eight gages located inside Tollgate, PG7 (outside Tollgate, located inside Lower Sheep Creek) and PG8 (outside Tollgate, located inside USC) are given in Table 3-1. All of these 10 gages are located inside the rectangular study area that includes Tollgate and USC watersheds (Figure 3-1). Snowfall was estimated based on air temperature using the relationship given by *U.S. Army Corps of Engineers [1956]*. There is an increasing trend in precipitation with elevation as well as a decreasing southwest-to-northeast trend. Among the gages in Table 3-1, the lowest precipitation during the study period occurred at PG7 (254.8 mm) and the highest at PG12 (1067.3 mm). The amount of precipitation at USC (PG8), by comparison, was 555.8 mm during the same period. The simulation year 1992-

93 was above average in terms of precipitation (555.8 mm winter precipitation vs. 508 mm of mean annual precipitation).

3. The Snow Transport Model

A physically based snow transport model (SnowTran-3D) is described by *Liston and Sturm* [1998]. This is a three-dimensional mass-transport model, which includes processes related to snow captured by vegetation, topographic modification of wind speeds, snow-cover shear strength, wind induced surface shear stress, snow transport resulting from saltation and suspension, snow accumulation and erosion, and sublimation of blowing and drifting snow (Figure 3-4a). The model runs on a grid with variable vegetation cover, and is driven by air temperature, humidity, wind speed and direction, and precipitation. The model outputs the time-evolving snow depth distribution over the simulation domain.

The fundamental equation in the snow transport model is the mass balance equation

$$\frac{d\zeta}{dt} = \frac{1}{\rho_s} \left(\rho_w \cdot P - \left(\frac{dQ_s}{dx} + \frac{dQ_t}{dx} + \frac{dQ_s}{dy} + \frac{dQ_t}{dy} \right) - Q_v \right) \quad (3.1)$$

where t is time (s), x (m) and y (m) refer to the horizontal spatial coordinates in west-east and north-south directions, respectively, ρ_s (kg m^{-3}) and ρ_w (kg m^{-3}) are densities of snow and water, respectively, Q_s ($\text{kg m}^{-1} \text{s}^{-1}$) and Q_t ($\text{kg m}^{-1} \text{s}^{-1}$) are the horizontal mass trans-

port rates due to saltation and turbulent suspension, respectively, Q_v ($\text{kg m}^{-1} \text{s}^{-1}$) is the rate of sublimation of snow particles being transported, P (m s^{-1}) is precipitation in terms of water equivalence, and ζ (m) is the snow depth. This neglects (or implicitly includes in ζ) the mass storage in suspended and saltating snow particles. The schematic of this mass-balance accounting is shown in Figure 3-4b. Equation (3.1) is solved numerically over the simulation domain.

The shear stress that the wind exerts on the surface is used to parameterize snow transport by saltation and suspension. The shear stress is formulated in terms of the friction velocity u_* (m s^{-1}):

$$u_* = u_r \cdot \frac{\kappa}{\ln\left(\frac{z_r}{z_0}\right)} \quad (3.2)$$

where u_r (m s^{-1}) is the wind speed at the reference height z_r (m), z_0 (m) is the surface roughness length (dependent on vegetation height and whether snow completely covers the vegetation), and κ is von Karman's constant.

The availability of snow for transport is determined by a snow holding capacity parameter for each vegetation type. Only snow in excess of this capacity is available for wind transport.

The transport rate due to saltation is parameterized by

$$\begin{aligned} \frac{dQ_s(x^*)}{dx^*} &= \frac{\mu}{f} (Q_{s_max} - Q_s(x^*)) & \text{for } \frac{\partial u_*}{\partial x^*} \geq 0 \\ Q_s(x^*) &= \min[Q_s(x^* - \Delta x^*), Q_{s_max}(x^*)] & \text{for } \frac{\partial u_*}{\partial x^*} < 0 \end{aligned} \quad (3.3)$$

where x^* (m) is the horizontal coordinate in a reference frame defined by the direction of wind flow (increasing downwind), Δx^* (m) is the horizontal grid resolution, μ is a non-dimensional scaling constant, f (m) is the equilibrium fetch distance assumed to be somewhere between 300 m suggested by *Takeuchi* [1980] and 500 m adopted by *Pomeroy et al.* [1993], and Q_{s_max} ($\text{kg m}^{-1} \text{s}^{-1}$) is the saltation transport rate under equilibrium conditions [*Pomeroy and Gray*, 1990] given by

$$Q_{s_max} = \frac{0.68}{u_*} \cdot \left(\frac{\rho_a}{g} \right) \cdot u_{*t} \cdot (u_*^2 - u_{*t}^2) \quad (3.4)$$

where u_{*t} (m s^{-1}) is the threshold friction velocity, ρ_a (kg m^{-3}) is the density of air, and g (m s^{-2}) is the acceleration due to gravity.

The transport rate due to turbulent suspension is given by

$$Q_t(x^*) = \int_{h_s}^{z_t} \phi_t(x^*, z) \cdot u(x^*, z) dz \quad (3.5)$$

where z (m) is height above the snow surface, ϕ_t (kg m^{-3}) is the mass concentration of the particulate cloud, u (m s^{-1}) is the wind velocity, h_* (m) is the height at the top of the saltation layer, and z_t (m) is the height of the top of the turbulent-suspension layer, where the concentration is zero. The concentration of suspended snow ϕ_t is modeled using a particle settling velocity of 0.3 m s^{-1} [Schmidt, 1982] and the parameterization given by Kind [1992]. Liston and Sturm [1998] give full details.

During transport, snow particles are sublimated. The rate of sublimation during transport is much higher than that during non-transport conditions. The sublimation rate per unit area of snow cover is given by Q_v ($\text{kg m}^{-2} \text{ s}^{-1}$):

$$Q_v(x^*) = \int_0^{z_t} \psi(x^*, z) \cdot \phi(x^*, z) dz \quad (3.6)$$

where ψ (s^{-1}) is the sublimation loss rate coefficient and ϕ (kg m^{-3}) is the vertical mass concentration distribution. The detailed formulation for sublimation loss rate coefficient ψ is given by Liston and Sturm [1998].

The wind field which drives the snow transport can be generated by several methods, which include (1) using a physically based, full atmospheric model (e.g., the Regional Atmospheric Modeling System (RAMS), [Pielke *et al.*, 1992; Liston and Pielke, 2000]), or a boundary layer circulation model [e.g., Liston *et al.*, 1993; Liston, 1995] which satisfy relevant momentum and continuity equations, (2) using an atmospheric model in which only mass continuity is satisfied [e.g., Sherman, 1978; Ross *et al.*, 1988],

(3) interpolation using extensive (windward- and leeward-slope) wind speed and direction observations and (4) interpolation using wind speed and direction observations in conjunction with empirical wind-topography relationships [e.g., *Ryan, 1977*]. Input wind speeds in the domain are interpolated to the modeling grid, and then the wind speed field u_r is modified to account for topographic variations by multiplying by an empirical weighting factor W , given by

$$W = 1.0 + \gamma_s \cdot \Omega_s + \gamma_c \cdot \Omega_c \quad (3.7)$$

where Ω_s and Ω_c are topographic slope and curvature respectively, in the direction of the wind and γ_s and γ_c are positive constants which weight the relative influence of the topographic slope and curvature on modifying the wind speed. The slope and curvature are computed such that leeward and concave slopes produce Ω_s and Ω_c less than zero, and windward and convex slopes produce Ω_s and Ω_c greater than zero. Values of γ_s (= 11) and γ_c (= 360) reported to be consistent with wind-microtopographic relationships [*Yoshino, 1975*] were used. In this study the last method was used because only a single wind speed and direction were available for input. This spatially uniform wind field was modified using equation (3.7) to estimate grid wind speeds.

4. SnowTran-3D Results

SnowTran-3D simulations were carried out over the 165-km² rectangular area surrounding and including the Tollgate and USC watersheds (see Figures 3-1 and 3-3).

The buffer around the watershed accounts for snow sources and drift traps outside the watershed. This region was selected because our ultimate goal is to use the SnowTran-3D results to obtain drift factors for a hydrologic model over the Tollgate watershed. Detailed measurements are available only at Upper Sheep Creek so the focus of this paper is on comparison with the detailed USC data.

The SnowTran-3D simulations included two vegetation scenarios: (1) vegetation derived from classification of the LANDSAT image and (2) uniform vegetation assuming the parameters of Mountain big sagebrush, the most common vegetation class; and two precipitation scenarios: (1) precipitation obtained from Upper Sheep Creek precipitation gage (PG8) which was near the lower end of the range of precipitation in Tollgate and (2) precipitation obtained from PG12 which had the highest mean annual precipitation and highest measured precipitation during the study period within Tollgate. The combination of these scenarios necessitated four SnowTran-3D model runs. The vegetation properties estimated for each vegetation class and used as input to SnowTran-3D are given in Table 3-2. Height for each vegetation community identified in Figure 3-3 was assigned an average based on field observation. Snow-holding capacity for each vegetation community was assigned based on subjective evaluation of properties of these communities with respect to blowing snow.

SnowTran-3D models snow depths with an assumed snow density, here taken as 300 kg/m^3 . In the model, snow is available for transport only when the snow holding capacity of vegetation has been exceeded. SnowTran-3D does not include parameterization of snow morphology processes such as densification. *Liston and Sturm*

[1998] evaluated a simple densification parameterization within the model and did not find appreciable improvement in the accuracy of modeled snow cover and the increase in model complexity was not justified.

SnowTran-3D was run at hourly time steps for the study duration using wind speeds measured at USC (PG8) and wind directions measured at PG7. PG7 was the only location where wind directions were measured, so these were used over the entire grid despite questions as to how representative they may be of the overall wind direction field.

Results from the four model input scenarios were analyzed for sensitivity of the snow transport model with respect to vegetation conditions and precipitation volume by comparison with the observations at USC. We compared measured and modeled SWE on the three survey dates of February 10, March 3, and March 23, 1993, prior to the onset of substantial snowmelt. The results were similar for all three dates, so for brevity, only results from the date of peak accumulation (March 3, 1993) are shown. Figure 3-5a shows the SWE map as modeled by SnowTran-3D using vegetation derived from a LANDSAT image in and around Upper Sheep Creek, and Figure 3-5b shows the scatterplot of modeled versus observed SWE at each grid cell in Upper Sheep Creek.

In modeled versus observed comparisons such as Figure 3-5b, the goodness of fit was quantified using the coefficient of determination R^2 , from a linear regression of modeled versus observed SWE and the Nash-Sutcliffe measure [e.g., *Gupta et al.*, 1998]

$$NS = 1 - \frac{\sum_{i=1}^n (SWE'_{obs} - SWE'_{mod})^2}{\sum_{i=1}^n (SWE'_{obs} - \overline{SWE}_{obs})^2} \quad (3.8)$$

where SWE'_{obs} is the observed SWE at the i th location, SWE'_{mod} is the modeled SWE at corresponding location, \overline{SWE}_{obs} is the mean observed SWE, and n is the number of grid cells comprising USC. This latter measure is preferable because it accounts for systematic as well as unsystematic differences between modeled and observed quantities. R^2 (from linear regression) quantifies only the error due to unsystematic differences. NS is scaled by the observed variance so it may be interpreted as representing the fraction of variance explained by the model (which may be negative for a poor model).

The NS measure for the comparison in Figure 3-5b was -0.15 ($R^2 = 0.19$). Figure 3-6 is similar to Figure 3-5, except that the vegetation used in this case consisted of spatially uniform Mountain big sagebrush, the most common vegetation class at Tollgate. The NS measure for the comparison in Figure 3-6b was -0.25 ($R^2 = 0.17$). Figure 3-7 shows the SWE maps modeled by SnowTran-3D runs using PG12 precipitation.

There is a discernible pattern mismatch between the observed and modeled SWE maps (see Figures 3-2, 3-5, 3-6, and 3-7), mainly responsible for the large scatter in the scatterplots in Figures 3-5b and 3-6b, and the correspondingly poor goodness of fit values. The observed drift on the leeward slope of Upper Sheep Creek forms approximately 30-60 m away from the watershed ridge (Figure 3-2). The modeled snow drift formed right up to the ridge of the watershed. These results indicate that in terms of

pointwise comparisons the model performed poorly. We believe that the main reason for this discrepancy is that the model calculated wind speed based on a local estimate of terrain slope in the direction of the wind using the digital elevation data. This means that as soon as the computed slope is away from the wind (indicating a leeward slope), wind speed is reduced, leading to deposition of snow being carried by the wind. In reality, wind flowing over the terrain experiences flow separation, and deposition of snow occurs in the wake behind the ridges. A modeling approach that examines slope breaks rather than slope directly may be able to rectify some of these problems. Currently SnowTran-3D does not have this capability. The more advanced wind modeling options within SnowTran-3D may also be better at representing flow separation, but also require more input data. Another reason for some of the discrepancy may be differences between wind direction as modeled (based on the measured wind direction at Lower Sheep Creek, PG7, Figures 3-1 and 3-3) and the true wind direction at Upper Sheep Creek.

Although the pointwise comparisons between measured and modeled accumulations (Figures 3-5b and 3-6b) show significant differences, the spatial pattern looks similar, at a coarser scale. The patterns of accumulation with increased precipitation (Figure 3-7) also appear similar. In what follows, we test the performance of SnowTran-3D by comparisons of (1) the basin average SWE, (2) the scouring and accumulation on the erosion and deposition zones, respectively in relation to snowfall amount, and (3) the distribution functions of SWE and drift factors, rather than individual points.

These tests are important because we intend to use the drift factors obtained by SnowTran-3D simulations to parameterize the distribution function of drift factors within watersheds for a watershed-scale hydrologic model. The distribution function of drift factors is used to partition the watershed into surface water input zones (Chapter 2), which is shown to be necessary in order to reproduce the timing of runoff from USC. In order for the drift factors obtained from SnowTran-3D to be effective in the above-mentioned context, the distribution functions of the modeled and observation-based drift factors (described below) must show reasonable agreement.

4.1. Drift Factors

Drift factors are intended to capture in a dimensionless way the propensity of a location to accumulate or lose snow by wind redistribution. Drift factors vary spatially over the domain, but as applied practically are constant in time at each location. Drift factors are estimated by comparing either modeled or measured snow accumulation at each point to gage measured snowfall over the time period spanning snow accumulation.

When using measured snow accumulation, snowmelt during the accumulation and drift period, though relatively small, needed to be considered in the estimation of drift factors. Snowmelt was modeled at each grid cell using the Utah Energy Balance (UEB) snow accumulation and melt model, which is a physically based, energy balance model and operates on a one layer snowpack at a point [Tarboton *et al.*, 1995; Tarboton and Luce, 1996]. Calibration of drift factors was carried out against observed SWE maps on the first three dates of SWE measurements (February 10, March 3, and March 23, 1993).

The objective function used for each location during this calibration was the sum of signed differences between UEB modeled and observed SWE on the three dates. With this objective function definition, negative and positive differences retain their sign so when added can cancel. The objective function can therefore be positive or negative and is optimum at zero when negative and positive differences exactly cancel. Because the drift factor only affects snowfall inputs, increases in drift factor must result in increases in modeled SWE. The objective function is therefore monotonic with respect to drift factor, and this fact was used to compute drift factor at each location as the value that made the objective function equal to zero. Other parameters of UEB were fixed at their recommended values [Tarboton and Luce, 1996]. The resulting drift factors (Figure 3-8) are henceforth referred to as observation-based drift factors.

Cumulative winter snowmelt until the date of peak accumulation as modeled by UEB was 0.039 m as compared to the cumulative snowfall of 0.435 m measured at USC. Because this snowmelt is small, any snowmelt model errors have a small effect on drift factor estimates. The UEB snowmelt model, drift factor concept, and snow distribution at USC have been the subject of several previous studies [Jackson, 1994; Tarboton *et al.*, 1995; Luce *et al.*, 1998; Luce *et al.*, 1999]. The drift factors obtained from SnowTran-3D simulations are compared below with the observation-based drift factors.

Since SnowTran-3D does not model snowmelt, drift factors were obtained from the SnowTran-3D model simulations by normalizing modeled accumulated SWE for each grid cell in the computational domain by the amount of snowfall:

$$f_{drift}(\bar{x}) = \frac{SWE_{mod}(\bar{x})}{P_{snow}(\bar{x})} \quad (3.9)$$

where $SWE_{mod}(\bar{x})$ is the modeled SWE and $P_{snow}(\bar{x})$ is the cumulative snowfall at location \bar{x} over the simulation period.

4.2. Modeled Basin Average SWE

Figure 3-9 shows the basin average SWE from each SnowTran-3D simulation on the three dates (February 10, March 3, and March 23, 1993) and observed basin average SWE on these and following dates for USC. This figure also shows the UEB modeled basin average SWE computed using the observation-based drift factors. The SnowTran-3D simulations show more snow accumulation than observed (or modeled using UEB). This is because SnowTran-3D does not model snowmelt. To have comparable quantities it is necessary to estimate this melt. The UEB simulated cumulative melt was added to the observed SWE quantities (labeled as Observed SWE + UEB melt) to have a quantity that is comparable to SnowTran-3D simulations.

On March 3, the peak measured basin average accumulation was 0.277 m and the modeled basin average SWE from SnowTran-3D with LANDSAT vegetation was 0.328 m, almost exactly equal to the observed SWE plus UEB melt of 0.329 m. (This exact coincidence is fortuitous because we have already seen poor pointwise comparisons.) On March 3, the modeled basin average SWE from SnowTran-3D with uniform vegetation was 0.362 m, about 10% more than the observed SWE plus UEB melt. The basin

average SWE modeled by SnowTran-3D is greater for uniform vegetation as compared to the LANDSAT vegetation. This is due to the fact that the uniform vegetation used was mountain big sagebrush, assigned a height of 0.8 m and a snow holding capacity of 0.3 m snow depth (0.09 m SWE). At Upper Sheep Creek, the dominant vegetation in the scour zones is low sagebrush, assigned a height of 0.3 m and a snow holding capacity of 0.1 m snow depth (0.03 m SWE). The difference between the two runs thus was almost entirely due to the difference between the holding capacity of low sagebrush (LANDSAT vegetation scenario) and that of mountain big sagebrush (uniform vegetation scenario). Mountain big sagebrush held more snow, thereby reducing scouring on the erosion zone compared to the LANDSAT vegetation scenario, resulting in greater basin average SWE. These differences are indicative of the sensitivity of the modeled basinwide SWE to information on vegetation.

SnowTran-3D modeled a net loss of snow from USC for all scenarios. Total snowfall until the date of peak accumulation was 0.435 m for PG8 (USC) precipitation scenario. Of this amount, 0.333 m was the amount of modeled SWE in USC, and 0.05 m was modeled as lost due to sublimation for the LANDSAT vegetation scenario resulting in a net transport of 0.052 m out of the watershed. The modeled basin average SWE on the date of peak accumulation for the uniform vegetation scenario was 0.367 m and the modeled sublimation was 0.047 m, resulting in a net transport of 0.021 m out of the watershed. Since the vegetation holding capacity for uniform vegetation was greater than that for the LANDSAT vegetation scenario, it resulted in greater accumulation, and less sublimation and less net transport loss. For the PG12 precipitation scenario, total amount

of snowfall until the date of peak accumulation was 0.736 m. For the LANDSAT vegetation scenario, SnowTran-3D modeled basin average SWE at USC was 0.618 m, and the modeled sublimation was 0.066 m, resulting in a net transport of 0.052 m out of the watershed. For the uniform vegetation scenario, basin average SWE was 0.638 m, and the modeled sublimation was 0.065 m, resulting in a net transport of 0.033 m out of the watershed.

The comparisons of measured versus modeled SWE presented here need to be viewed considering the uncertainty associated with precipitation inputs, which could be as large as the differences due to the vegetation scenarios compared. Although based on a comparison of only three dates, the general agreement of SnowTran-3D modeled basin average SWE with the measured basin average SWE supports the adequacy of SnowTran-3D for modeling basin average SWE at USC.

4.3. Scouring and Accumulation Modeled by SnowTran-3D

In this section we examine the scouring on the erosion zone and the accumulation on the deposition zone of USC as observed and as modeled by SnowTran-3D. The erosion zone is defined as the set of grid cells where the drift factor (equation (3.8), Figure 3-8) is less than 1. The deposition zone is defined as the set of grid cells where drift factor was greater than or equal to 1. The erosion and deposition zones observed and modeled for each scenario are slightly different due to the pointwise differences between observed and modeled accumulation patterns. Table 3-1 gives the cumulative precipitation and cumulative snowfall at USC during the drift and accumulation period

for USC precipitation gage (PG8) and PG12 precipitation gage. Cumulative snowfall for the modeling period until peak accumulation (October 1, 1992 – March 3, 1993) at PG12 was 1.69 times that at PG8. Mean snow holding capacities of vegetation on the observed erosion and deposition zones were 0.071 m and 0.093 m, respectively, with the LANDSAT vegetation. With uniform vegetation, mean snow holding capacity was 0.09 m. The snow holding capacities are expressed in terms of SWE. Snow is transported away from a location by SnowTran-3D only when accumulation exceeds the snow holding capacity. Table 3-3 shows some statistics of the SWE on erosion and deposition zones at USC. Mean measured SWE on the erosion zone grew to its maximum of 0.129 m on the date of peak measured snow accumulation. Mean measured SWE on the deposition zone attained its maximum of 0.71 m on the day of peak measured accumulation.

The mean modeled SWE on the erosion zone for USC precipitation was greater (by about 23%) for the uniform vegetation compared to LANDSAT vegetation because of the greater snow-holding capacity of uniform vegetation. The corresponding increase in mean modeled SWE on the erosion zone for PG12 precipitation was about 5.5%. The mean modeled SWE on the deposition zone for USC precipitation was also greater (by about 3%) for the uniform vegetation compared to the LANDSAT vegetation. The corresponding increase in mean modeled SWE on the deposition zone for PG12 precipitation was about 1%.

Table 3-4 shows the amount of snow scoured away from the erosion zone and the accumulation on the deposition zone. Amount of snow scoured away is computed by

subtracting the SnowTran-3D modeled mean SWE on the erosion zone from the cumulative snowfall. Amount of accumulation is computed by subtracting the cumulative snowfall from the SnowTran-3D modeled average SWE on the deposition zone. The reduced scour for uniform vegetation on the erosion zone was due to the greater snow-holding capacity of the uniform vegetation as compared to that of LANDSAT vegetation. Note that when a larger quantity of precipitation was input, the modeled fraction that was scoured away reduced from around 60% to about 50%, while the modeled amount of scour in terms of SWE increased by about 25%. This analysis suggests that the quantity of snow redistributed is a function of both the available wind energy to transport snow (which was the same for both precipitation scenarios), and the amount of snow available to be transported. If available wind were the only limiting factor, we might have seen the same quantity of snow transported for both precipitation scenarios, and if available snow was the only limiting factor, we might have seen snow scoured down to the vegetation snow holding capacity for both scenarios with correspondingly higher scour fraction for the higher precipitation input scenario.

In the deposition zone, although the modeled relative accumulation for LANDSAT vegetation scenario reduced from about 64% for USC precipitation to about 42% for PG12 precipitation, the modeled amount of snow accumulation in terms of SWE on the deposition zone increased by about 13%. This again suggests that the quantity of redistribution is a function of both available wind energy and available amount of snow. If wind were the only limiting factor, we would have seen the same amount of snow accumulation in terms of SWE for both precipitation scenarios.

4.4. Distribution Function Comparisons

In this section we evaluate the distribution functions of SWE and drift factors obtained from SnowTran-3D as compared to observations. Figures 3-5b and 3-6b above gave pointwise comparisons, which were disappointing due to the spatial mismatch. Estimation of a large scale surface water input (e.g., at the watershed scale) may not require precise pointwise agreement. Adequate results may be obtained if the distribution function of snow is well parameterized and used with the depletion curve concept as a subgrid parameterization [Liston, 1999; Luce *et al.*, 1999]. This section seeks to evaluate the extent to which the SnowTran-3D simulations are usable despite poor pointwise comparisons.

Figure 3-10 shows the cumulative distribution functions (CDF) of the observed and SnowTran-3D modeled SWE for USC precipitation runs. The CDF from the LANDSAT vegetation scenario was closer to the observed than the CDF from the uniform vegetation scenario. The steps at the lower end of the CDF were due to the snow-holding capacities of low sagebrush (at 0.03 m) and taller sagebrush communities (0.09 m) on the windward slope. The CDF for uniform vegetation scenario showed only one step at around 0.09 m corresponding to the snow-holding capacity of uniform vegetation. Since SnowTran-3D does not model melt, the CDF for all scenarios started at values greater than 0. If snowmelt were modeled concurrently with snow transport, the CDF of modeled SWE would shift to the left, possibly resulting in better agreement with observed distribution function. Figure 3-11 shows the CDF of SWE modeled by SnowTran-3D at USC when precipitation from PG12 was used. Not surprisingly, the

comparison with observed SWE distribution function was poor since the total amount of snowfall was different for the modeled distribution functions as compared to the observations.

To properly account for the spatially variable melting that occurred during the snow accumulation and drift period, and to do this comparison in a dimensionless way, we compared the distribution functions of observation-based drift factors and SnowTran-3D modeled drift factors. The use of drift factors also allows us to estimate the sensitivity of SnowTran-3D distribution functions to precipitation inputs. The SnowTran-3D drift factors were computed for USC using equation (3.9) for all four scenarios. Figures 3-12 and 3-13 show the comparison between the CDF of drift factors at USC obtained from SnowTran-3D simulations with the CDF of observation-based drift factors. The agreement is generally quite good for both precipitation scenarios, indicating that the assumption of linearity as applied to the distribution function of drift factors with precipitation may not be bad. This observation was also suggested by *Liston* [1999]. Note, however, that the distribution functions do degrade for PG12 precipitation, and a measure of the degradation is desirable.

In order to compare the distribution function of modeled and observed SWE, we plotted sorted modeled SWE against sorted observed SWE (Figure 3-14). A one-to-one line on these plots would indicate a perfect match between the distribution functions of modeled and observed SWE. For the data in Figure 3-14, we computed the *NS* goodness of fit measure (equation (3.8)). A value of 1 for *NS* would indicate a perfect match between the distribution functions of modeled and observed SWE. The distribution

function of SWE obtained by the SnowTran-3D simulation which used USC precipitation and LANDSAT vegetation was quite good ($NS = 0.90$). The distribution function obtained from uniform vegetation scenario was slightly degraded, but still quite good ($NS = 0.83$). Some of these differences may be due to uncertainty in precipitation inputs. Distribution functions of SWE obtained from PG12 precipitation runs had negative values for NS , which indicated that the sum of squares of errors was greater than the variance of observed SWE, and that the modeled SWE was not comparable to observations, which is not surprising. The NS values were also computed for the drift factors by substituting observation-based UEB drift factors for observed SWE and SnowTran-3D modeled drift factors for modeled SWE in equation (3.8). The agreement between the distribution functions of SnowTran-3D modeled drift factors and observation-based drift factors was quite good when USC precipitation was used. The agreement worsens when precipitation from PG12 was used, but not much (from about 0.89 for USC precipitation to about 0.75 for PG12 precipitation). This was also indicated by the closeness of the sorted drift factors plots in Figure 3-14b, where drift factors from all SnowTran-3D runs were close to each other.

Analysis of Figure 3-14 provides an answer to our third question, namely, how sensitive the drift factors were to amount of precipitation, in the context of the distribution function of drift factors. Our test of the drift factor concept used the precipitation from USC (PG8) and PG12 to compare the distribution functions of modeled drift factors for each of these cases to the distribution function of observation-based drift factors. The precipitation at PG12 was 69% more than that at USC (PG8).

The significance of using PG12 as input was as a convenient and representative increased precipitation input (lacking a year of data at USC with significantly increased precipitation to simulate) rather than its geographic distance. There was also the question of the need for spatial precipitation interpolation, and by using the maximum (most different) value as a uniform input we could evaluate the possible error due to inaccuracy in precipitation input due to interpolation and other errors and uncertainties.

The distribution functions of drift factors obtained from the SnowTran-3D simulations using USC precipitation were in good agreement with the observation-based drift factors for both vegetation scenarios. With the observed precipitation, SnowTran-3D modeled drift factors explain 89% of the variance in the distribution function of observation-based drift factors. The fraction of explained variance reduced to 75% when precipitation from PG12 was used, resulting in a 14% reduction in explained variance of the distribution function of drift factors obtained from SnowTran-3D simulations for a precipitation increase of 69%. With the original (USC/PG8) precipitation there was 11% error (unexplained variance) so the error (unexplained variance) is only increased to 25% with the additional 69% precipitation.

Though the agreement with the distribution function of observation-based UEB drift factors is not perfect (indicated by the nonlinearity of the sorted drift factors plots on Figure 3-14), it is deemed reasonably good. Some of the discrepancies may be due to factors discussed earlier in this paper, notably the pattern mismatch, wind flow separation problems and the lack of melt estimation as part of the snow transport modeling.

5. Conclusions

The first question addressed in this study asked how well the spatial patterns of snow accumulation due to drifting was represented by the blowing snow model. Basin average SWE was in reasonably good agreement with observed SWE plus estimated melt (see Figure 3-9). The pattern of SWE modeled by the snow transport model was similar to measured SWE maps (see Figures 3-2, 3-5a, 3-6a, and 3-7), but pointwise comparisons showed significant errors (see Figures 3-5b and 3-6b), which could be attributed to the spatial mismatch and limitations of wind flow separation modeling. The analysis of scouring and accumulation on the scouring and deposition zones (Tables 3-3 and 3-4) showed that available wind as well as available snow played a role in limiting the amount of redistribution of snow.

The second question addressed by this study asked how sensitive the modeled pattern of snow accumulation was to vegetation. The snow held on the erosion zone was more sensitive to vegetation snow-holding capacity than that held on the deposition zone. As the amount of precipitation increased, this effect became relatively smaller. However, overall, in terms of drift factor distributions the differences between LANDSAT and uniform vegetation scenarios were insignificant. This suggests that, in this watershed at least, topography plays a more dominant role than vegetation in the determination of drift distributions and that efforts to map vegetation for the purposes of quantifying snow drift distributions are not critical. In other regions of the world (or in other landscapes), vegetation distributions can play a stronger role than topography in defining snow drift distributions [*Hiemstra, 1999; Liston et al., 2001; Sturm et al., 2001*].

The third question asked how sensitive the drift factors were to amount of precipitation. The drift factor concept is analogous to an assumption of linearity. It assumes that if snowfall is increased, the amount of accumulated SWE will be increased while the spatial pattern due to drifting will be the same. If this approximation were reasonable, it would allow a separation between the modeling of snow drifting and that of snowmelt and surface water input. This is a significant simplification in model structure, especially when large watersheds must be modeled. Our test of this concept used the precipitation from USC (PG8) and PG12 to compare the distribution functions of modeled drift factors for each of these cases to the distribution function of observation-based drift factors. There was only a 14% reduction in the amount of explained variance for a 69% increase in precipitation. This error is small and in our opinion probably comparable to or less than many of the other errors, such as uncertainty in precipitation, that hydrologic modelers need to deal with. Thus the simplifications provided by the use of distribution functions of drift factors will be appropriate in many cases. These results have significant implications for hydrologic models that operate at the watershed scale, and do not need precise pointwise agreement for parameterization of wind-induced drift (e.g., see Chapter 2).

In the context of upscaling of hydrologic models, we need to upscale the description of snow accumulation and melt processes. There are practical difficulties associated with running point snowmelt models at the grid scale, even if we can adequately approximate the wind redistribution of snow using the drift factors concept. Recent attempts to describe the process of snow accumulation and melt using a depletion

curve concept is a promising approach [Liston, 1999; Luce *et al.*, 1999]. Future work will involve modeling of hydrology at Tollgate using surface water input derived from (1) UEB run at the grid scale with SnowTran-3D drift factors and (2) depletion curve method applied to first order subwatersheds of Tollgate. This surface water input will be used to drive a three-zone hydrologic model (Chapter 2) to simulate annual water balance at Tollgate.

References

- Cooley, K. R., Snowpack variability on western rangelands, paper presented at Western Snow Conference, Kalispell, Montana, April 18–20, 1988.
- Duffy, C. J., K. R. Cooley, N. Mock, and D. Lee, Self-affine scaling and subsurface response to snowmelt in steep terrain, *J. Hydrol.*, 123, 395–414, 1991.
- Flerchinger, G. N., K. R. Cooley, and D. R. Ralston, Groundwater response to snowmelt in a mountainous watershed, *J. Hydrol.*, 133, 293–311, 1992.
- Groisman, P. Y., and D. R. Legates, The accuracy of United States precipitation data, *Bull. Am. Meteorol. Soc.*, 75, 215–227, 1994.
- Gupta, H. V., S. Sorooshian, and P. O. Yapo, Toward improved calibration of hydrologic models: Multiple and noncommensurable measures of information, *Water Resour. Res.*, 34(4), 751–763, 1998.
- Hamon, W. R., Computing actual precipitation, in *Proceedings of WMO-IDHS Symposium, Distribution of Precipitation in Mountainous Areas, Geilo, Norway, Rep. 326*, pp. 159–174, World Meteorol. Organ., Geneva, 1973.
- Hanson, C. L., Precipitation catch measured by the Wyoming shield and the dual-gage system, *Water Resour. Bull.*, 25, 159–164, 1989.
- Hiemstra, C. A., Wind redistribution of snow at treeline, Medicine Bow Mountains, Wyoming., M.S. thesis, 163 pp., Univ. of Wyo., Laramie, 1999.

- Jackson, T. H. R., A spatially distributed snowmelt-driven hydrologic model applied to the Upper Sheep Creek watershed, Ph.D. dissertation, 323 pp., Utah State Univ., Logan, 1994.
- Jones, E. B., Snowpack ground-truth manual, *Rep. CR 170584*, NASA Goddard Space Flight Cent., Greenbelt, Md., 1983.
- Kind, R. J., One-dimensional aeolian suspension above beds of loose particles - A new concentration-profile equation, *Atmos. Environ.*, *26A*(5), 927–931, 1992.
- Liston, G. E., Local advection of momentum, heat, and moisture during the melt of patchy snow covers, *J. Appl. Meteorol.*, *34*, 1705–1715, 1995.
- Liston, G. E., Interrelationships among snow distribution, snowmelt, and snow cover depletion: Implications for atmospheric, hydrologic, and ecologic modeling, *J. Appl. Meteorol.*, *38*, 1474–1487, 1999.
- Liston, G. E., and R. A. Pielke, Sr., A climate version of the regional atmospheric modeling system, *Theor. Appl. Climatol.*, *66*, 29–47, 2000.
- Liston, G. E., and M. Sturm, A snow-transport model for complex terrain, *J. Glaciol.*, *44*(148), 498–516, 1998.
- Liston, G. E., R. L. Brown, and J. Dent, Application of the $E - \epsilon$ turbulence closure model to separated atmospheric surface layer flows, *Boundary Layer Meteorol.*, *66*, 281–301, 1993.
- Liston, G. E., J. P. McFadden, R. A. Pielke, Sr., and M. Sturm, Sensitivity of snowcover, energy, and moisture interactions to increased Arctic shrubs, *Global Change Biol.*, in press, 2001.
- Luce, C. H., D. G. Tarboton, and K. R. Cooley, Spatially integrated snowmelt modeling of a semi-arid mountain watershed, *Eos Trans. AGU*, Fall Meet. Suppl., *78*(46), Abstract H11G-07, 1997.
- Luce, C. H., D. G. Tarboton, and K. R. Cooley, The influence of the spatial distribution of snow on basin-averaged snowmelt, *Hydrol. Processes*, *12*(10–11), 1671–1683, 1998.
- Luce, C. H., D. G. Tarboton, and K. R. Cooley, Subgrid parameterization of snow distribution for an energy and mass balance snow cover model, *Hydrol. Processes*, *12*(10–11), 1671–1683, 1999.

- McCollum, J. R., and W. F. Krajewski, Uncertainty of monthly rainfall estimates from rain gauges in the Global Precipitation Climatology Project, *Water Resour. Res.*, *34*(10), 2647–2654, 1998.
- Morrissey, M. L., J. A. Maliekal, J. S. Greene, and J. Wang, The uncertainty in simple spatial averages using rain gauge networks, *Water Resour. Res.*, *31*(8), 2011–2017, 1995.
- Pielke, R. A., W. R. Cotton, R. L. Walko, C. J. Tremback, W. A. Lyons, L. D. Grasso, M. E. Nicholls, M. D. Moran, D. A. Wesley, T. J. Lee, and J. H. Copeland, A comprehensive meteorological modeling system—RAMS, *Meteorol. Atmos. Phys.*, *49*(69–91), 1992.
- Pomeroy, J. W., and D. M. Gray, Saltation of snow, *Water Resour. Res.*, *26*(7), 1583–1594, 1990.
- Pomeroy, J. W., and D. M. Gray, Snowcover: Accumulation, relocation and management, *Sci. Rep. 7*, 144 pp., Natl. Hydrol. Res. Inst., Saskatoon, Sask., Canada, 1995.
- Pomeroy, J. W., D. M. Gray, and P. G. Landine, The prairie blowing snow model: Characteristics, validation, operation, *J. Hydrol.*, *144*, 165–192, 1993.
- Ross, D. G., I. N. Smith, P. C. Manins, and D. G. Fox, Diagnostic wind field modeling for complex terrain: Model development and testing, *J. Appl. Meteorol.*, *27*, 785–796, 1988.
- Ryan, B. C., A mathematical model for diagnosis and prediction of surface winds in mountainous terrain, *J. Appl. Meteorol.*, *16*, 571–584, 1977.
- Schmidt, R. A., Vertical profiles of wind speed, snow concentration, and humidity in blowing snow, *Boundary Layer Meteorol.*, *34*, 213–241, 1982.
- Sherman, C. A., A mass-consistent model for wind fields over complex terrain, *J. Appl. Meteorol.*, *17*, 312–319, 1978.
- Stephenson, G. R., and R. A. Freeze, Mathematical simulation of subsurface flow contributions to snowmelt runoff, Reynolds Creek Watershed, Idaho, *Water Resour. Res.*, *10*(2), 284–294, 1974.
- Stevens, G. R., A geophysical investigation of the Upper Sheep drainage, Reynolds Creek Experimental Watershed, Owyhee County, Idaho, M.S. thesis, 119 pp., Univ. of Idaho, Moscow, 1991.

- Sturm, M., J. P. McFadden, G. E. Liston, F. S. Chapin III, C. H. Racine, and J. Holmgren, Snow-shrub interactions in Arctic tundra: A hypothesis with climatic implications, *J. Clim.*, 14(3), 336–344, 2001.
- Takeuchi, M., Vertical profiles and horizontal increases of drift snow transport, *J. Glaciol.*, 26(94), 481–492, 1980.
- Tarboton, D. G., and C. H. Luce, *Utah Energy Balance Snow Accumulation and Melt Model (UEB), Computer Model Technical Description and Users Guide*, Utah Water Res. Lab., Logan, 1996.
- Tarboton, D. G., T. G. Chowdhury, and T. H. Jackson, A spatially distributed energy balance snowmelt model, in *Biogeochemistry of Seasonally Snow-Covered Catchments*, edited by K. A. Tonnessen et al., *IAHS Publ. 228*, pp. 141–155, 1995.
- U.S. Army Corps of Engineers, *Snow Hydrology, Summary Report of the Snow Investigations*, 437 pp., N. Pac. Div., Portland, Oreg., 1956.
- Winkelmaier, J. R., Ground-water flow characteristics in fractured basalt in a zero-order basin, M.S. thesis, 128 pp., Univ. of Idaho, Moscow, 1987.
- Yoshino, M. M., *Climate in a Small Area*, 549 pp., Univ. of Tokyo Press, Tokyo, 1975.

Table 3-1. Cumulative Precipitation Volume in and Around Tollgate

Precipitation Station	Cumulative Precipitation during October 1, 1992 – March 3, 1993 (mm)*	Cumulative Snowfall during October 1, 1992 – March 3, 1993 (mm)*
PG6 (Tollgate)	258.8 (332.2)	208.9 (237.9)
PG7 (Lower Sheep Creek)	206.2 (254.8)	163.1 (183.2)
PG8 (Upper Sheep Creek)	504.9 (555.8)	435.4 (450.3)
PG9 (Tollgate)	527.1 (693.4)	411.8 (459.9)
PG10 (Tollgate)	317.5 (387.6)	264.8 (289.6)
PG11 (Tollgate)	389.4 (522.0)	312.1 (353.7)
PG12 (Tollgate)	876.3 (1067.3)	735.8 (801.6)
PG13 (Tollgate)	598.4 (712.0)	510.2 (545.1)
PG14 (Tollgate)	649.7 (792.5)	545.5 (589.4)
PG15 (Tollgate)	744.5 (894.6)	634.3 (682.8)

* the numbers in parentheses are cumulative precipitation values for October 1, 1992 – March 23, 1993.

Table 3-2. Vegetation Properties for Study Area Defined in Figure 3-1

Description	Height (m)	Holding Capacity (m)		Area Covered (%)
		Depth	SWE	
Low Sagebrush	0.3	0.1	0.03	28.5
Wyoming Big Sagebrush	0.8	0.3	0.09	8.2
Big Sagebrush/Bitterbrush	0.8	0.3	0.09	13.9
Mountain Big Sagebrush	0.8	0.3	0.09	36.2
Aspen	4.0	1.0	0.3	7.3
Conifer	8.0	4.0	1.2	5.8

Table 3-3. SWE on Erosion and Deposition Zones at USC

Source of SWE	Measure	SWE on erosion zone on March 3, 1993	SWE on deposition zone on March 3, 1993
Observed	Range (m)	0.004 - 0.417	0.317 - 1.645
	Mean (m)	0.129	0.71
	Std Dev (m)	0.102	0.311
SnowTran3D ¹	Range (m)	0.044 - 0.434	0.451 - 1.439
	Mean (m)	0.169	0.718
	Std Dev (m)	0.115	0.197
SnowTran3D ²	Range (m)	0.104 - 0.666	0.458 - 1.265
	Mean (m)	0.208	0.740
	Std Dev (m)	0.124	0.191
SnowTran3D ³	Range (m)	0.060 - 1.498	0.681 - 1.765
	Mean (m)	0.421	1.083
	Std Dev (m)	0.305	0.216
SnowTran3D ⁴	Range (m)	0.120 - 1.510	0.724 - 1.677
	Mean (m)	0.444	1.093
	Std Dev (m)	0.295	0.217

Erosion zone is defined as the group of grid cells where measured or modeled SWE was less than snowfall, and the deposition zone is defined as the group of grid cells where measured or modeled SWE was greater than or equal to snowfall.

¹USC precipitation, LANDSAT vegetation.

²USC precipitation, uniform vegetation.

³PG12 precipitation, LANDSAT vegetation.

⁴PG12 precipitation, uniform vegetation.

Table 3-4. Scouring and Accumulation on the Respective Zones at USC

Source of SWE	Mass components of SWE redistribution	Amount of snow scoured or accumulated until March 3, 1993
Observed	Scour (m)	0.307
	Accumulation (m)	0.267
SnowTran3D ¹	Scour (m)	0.268 (62%)
	Accumulation (m)	0.277 (64%)
SnowTran3D ²	Scour (m)	0.250 (58%)
	Accumulation (m)	0.273 (63%)
SnowTran3D ³	Scour (m)	0.395 (54%)
	Accumulation (m)	0.312 (42%)
SnowTran3D ⁴	Scour (m)	0.379 (51%)
	Accumulation (m)	0.316 (43%)

Scour is defined as ($P_{\text{snow}} - \text{mean SWE}$) on the erosion zone and accumulation is defined as ($\text{mean SWE} - P_{\text{snow}}$) on the deposition zone. P_{snow} is cumulative snowfall.

¹USC precipitation, LANDSAT vegetation.

²USC precipitation, uniform vegetation.

³PG12 precipitation, LANDSAT vegetation.

⁴PG12 precipitation, uniform vegetation.

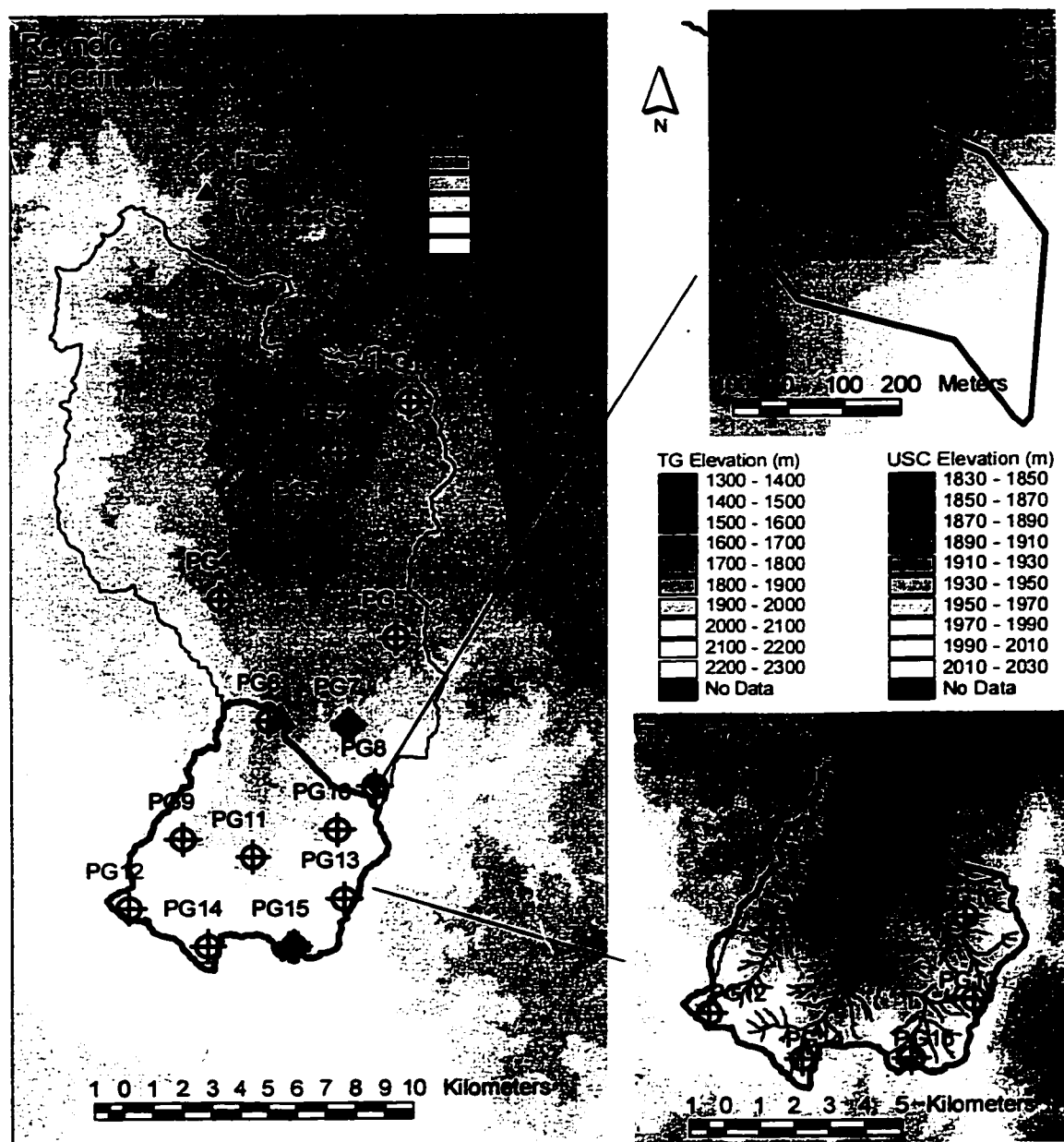


Figure 3-1. Reynolds Creek Experimental Watershed. Upper Sheep Creek is a 0.25-km² first-order subwatershed. Tollgate watershed is 54 km² in size. The underlying DEM is the 10-m resolution commercial DEM created from 1:24000 USGS quad sheets.

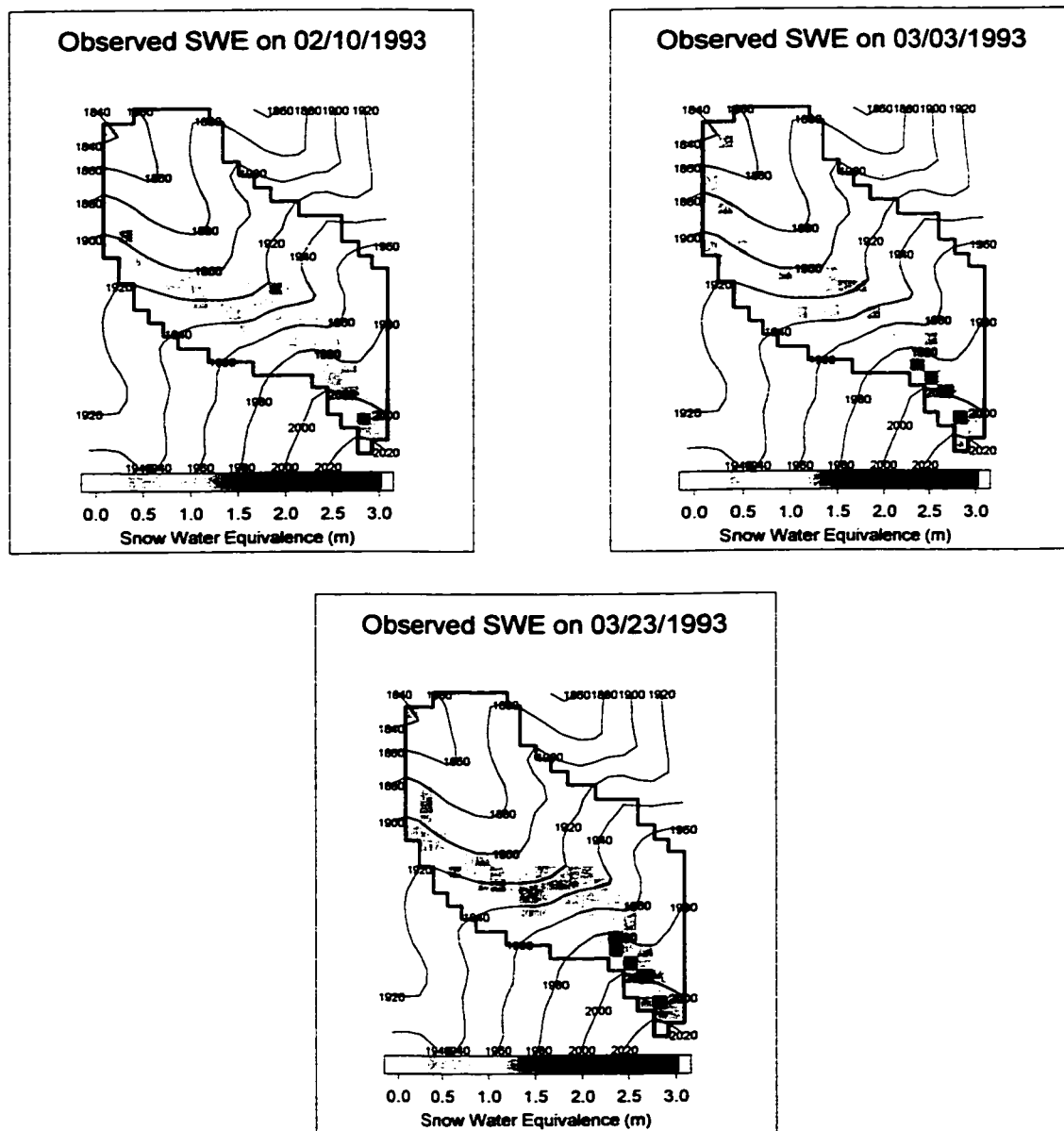


Figure 3-2. SWE measurements carried out on a 30.48 m grid approximately aligned with the long axis of Upper Sheep Creek watershed. The maps were produced by interpolation of measured data on to the USGS 30 m north-aligned DEM grid. Thin lines denote elevation contours.

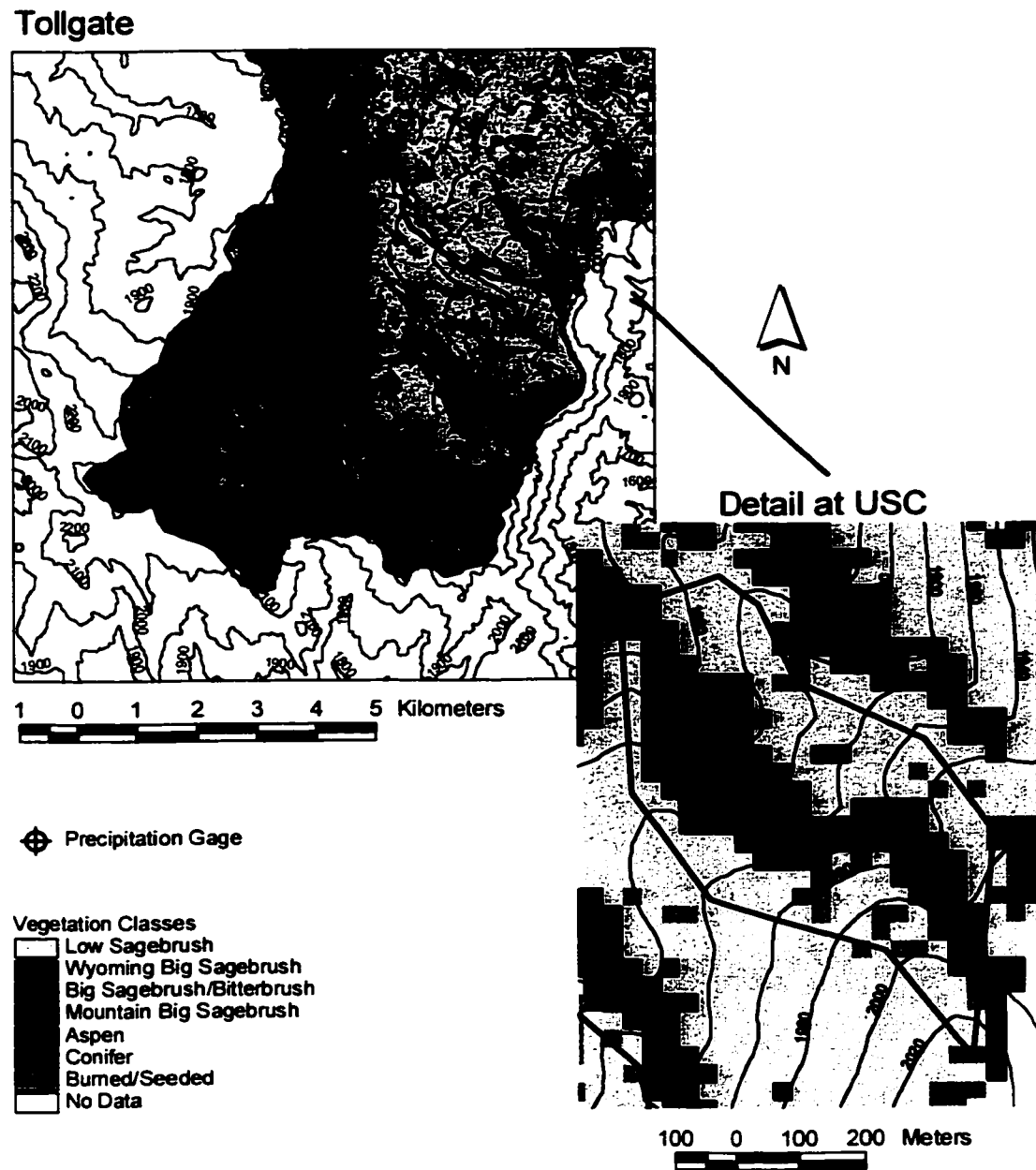
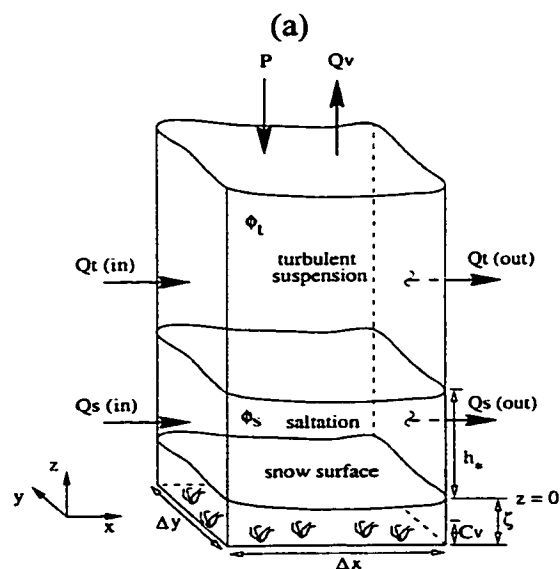
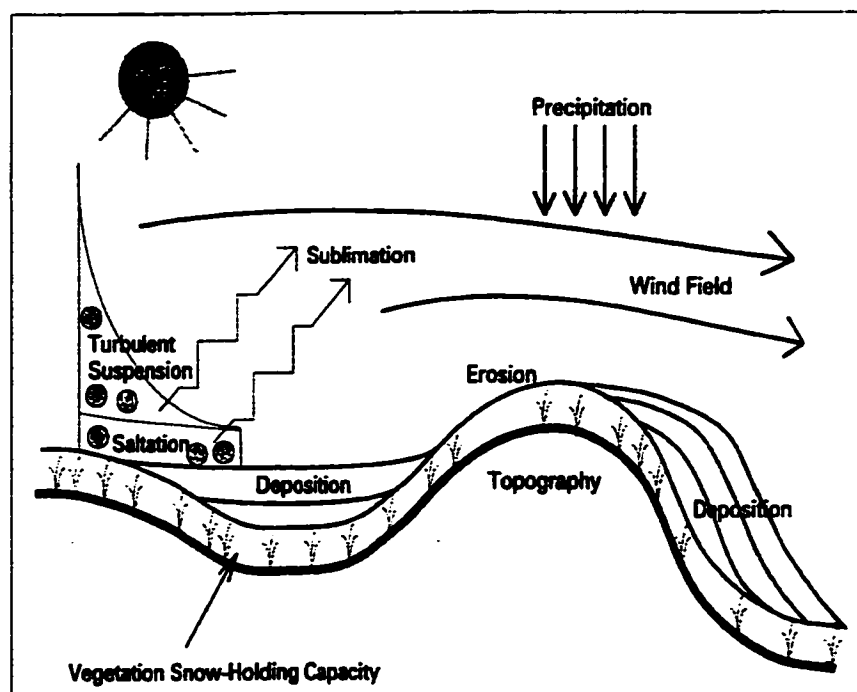
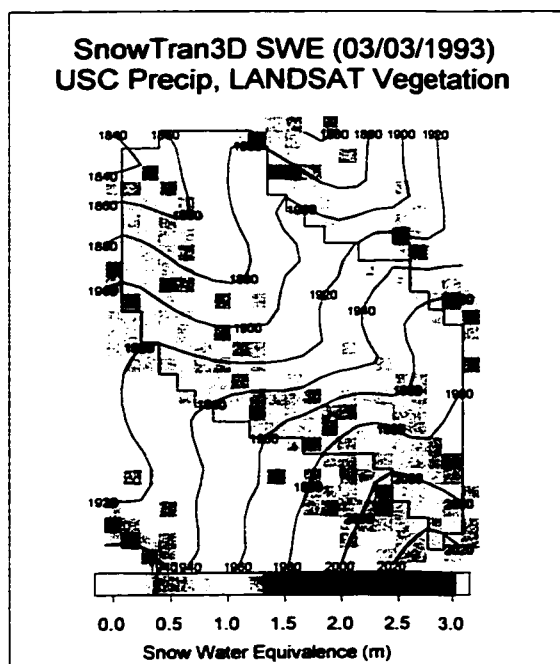


Figure 3-3. Vegetation map derived from LANDSAT 5 thematic mapper data for August 1, 1993, using a maximum likelihood classification. Note that the area outside the Reynolds Creek Experimental Watershed was masked out. For the model simulations, we assumed that this area was covered by the most prevalent vegetation class, which for entire Reynolds Creek was Wyoming big sagebrush.

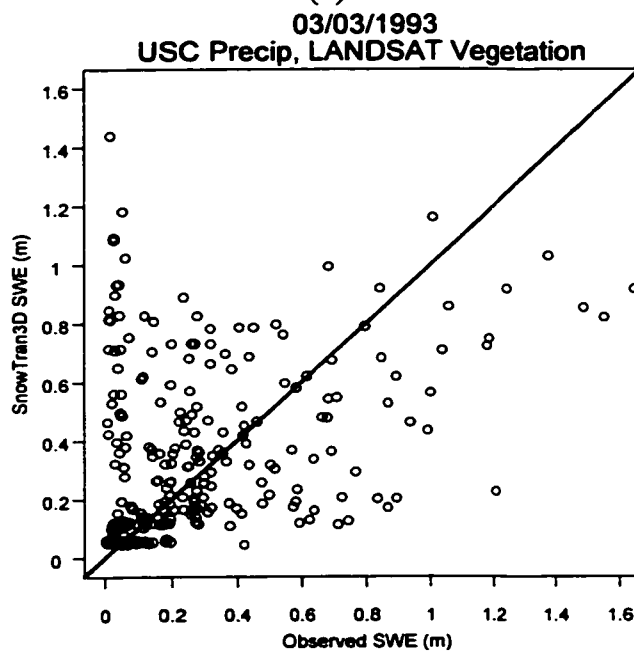


(b)

Figure 3-4. (a) Key features of the snow-transport model SnowTran-3D [Liston and Sturm, 1998] as applied to topographically variable terrain. (b) Schematic of mass-balance accounting in SnowTran-3D.

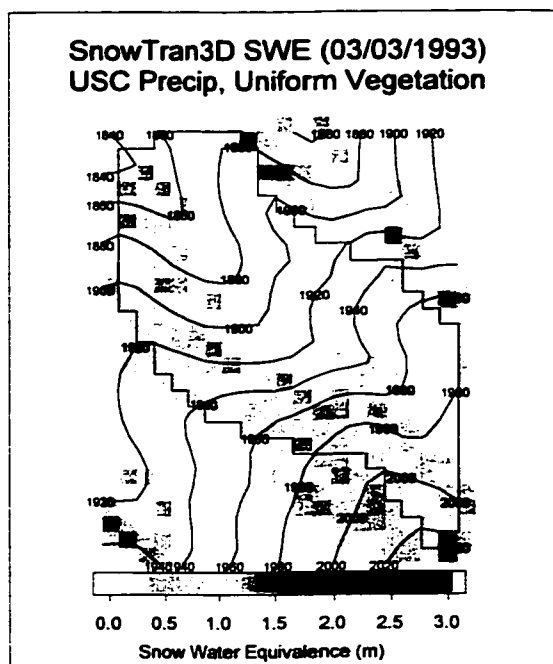


(a)

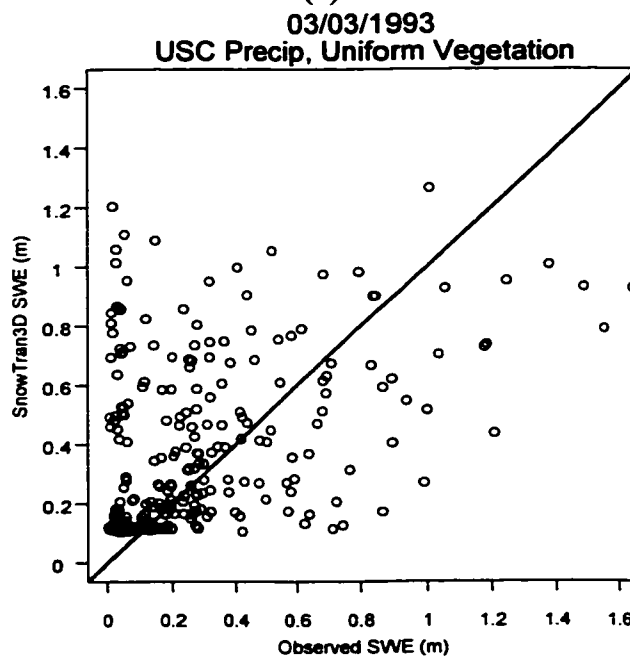


(b)

Figure 3-5. (a) SnowTran-3D-modeled snow water equivalence map. Thin lines denote elevation contours. Vegetation was obtained by classifying a LANDSAT image. (b) Pointwise comparison of modeled against observed SWE.



(a)



(b)

Figure 3-6. (a) SnowTran-3D-modeled snow water equivalence map. Thin lines denote elevation contours. Wyoming big sagebrush was used as uniform vegetation. (b) Pointwise comparison of modeled against observed SWE.

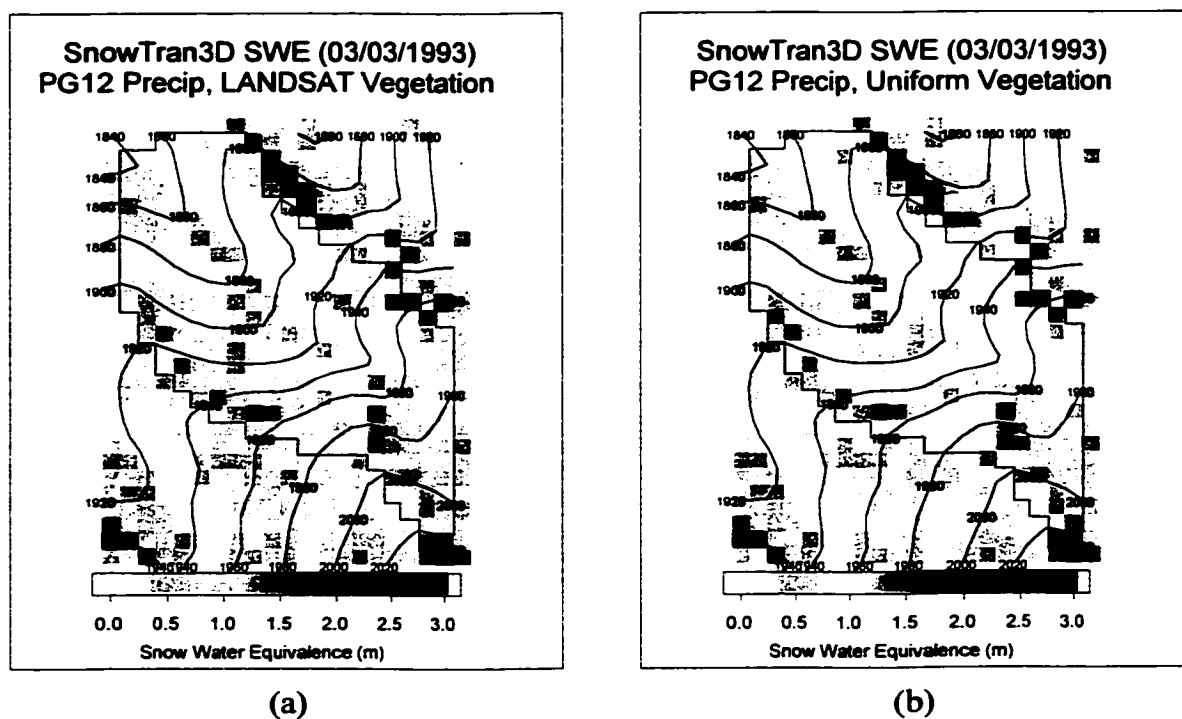


Figure 3-7. SnowTran-3D-modeled snow water equivalence maps at USC using PG12 precipitation. (a) LANDSAT vegetation scenario. (b) Uniform vegetation scenario. Thin lines denote elevation contours.

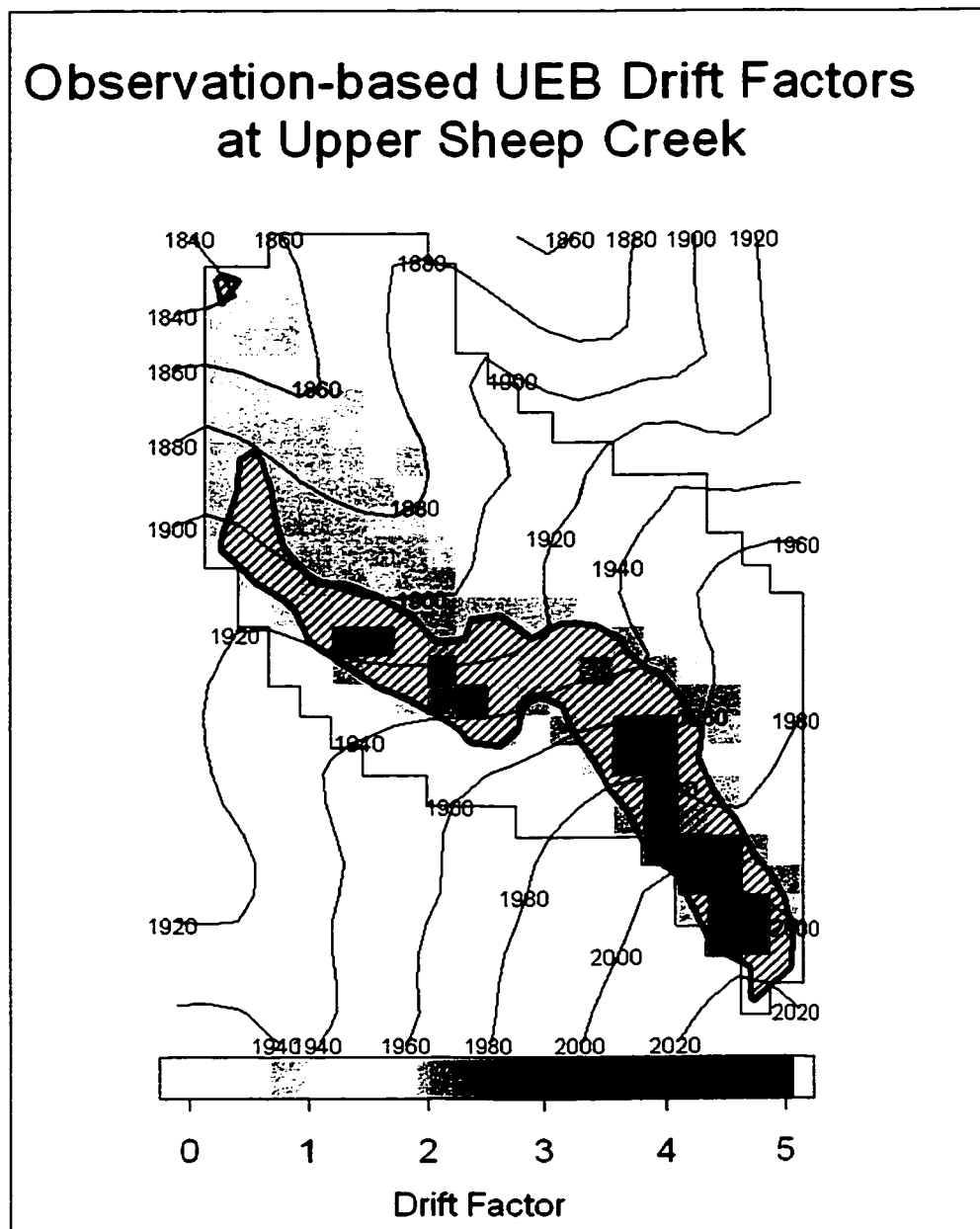


Figure 3-8. USC drift factors obtained by calibration. The hatched area is the observed deposition zone (drift factor ≥ 1) and the rest of the watershed is the erosion zone (drift factor < 1). Thin lines denote elevation contours.

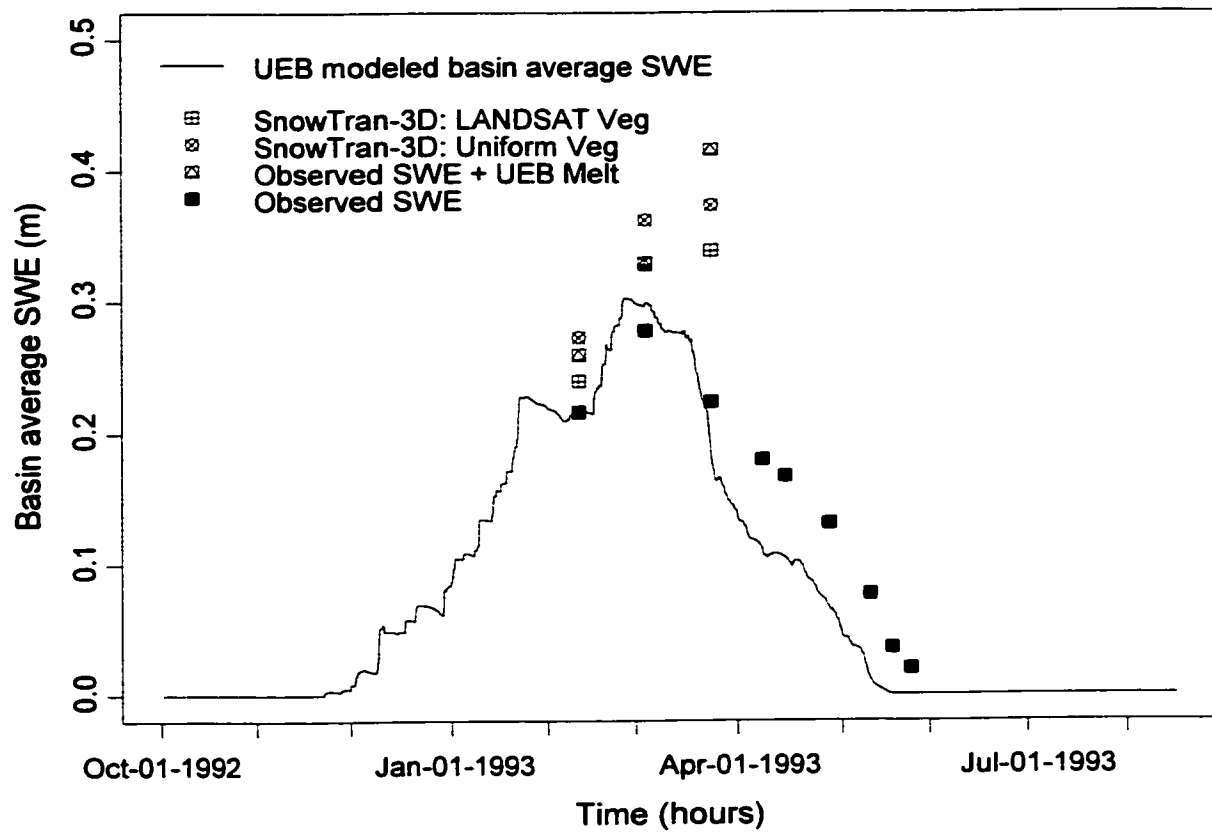


Figure 3-9. Comparison between SnowTran-3D predictions with observed snow water equivalence plus UEB modeled melt at Upper Sheep Creek. SnowTran-3D used USC precipitation.

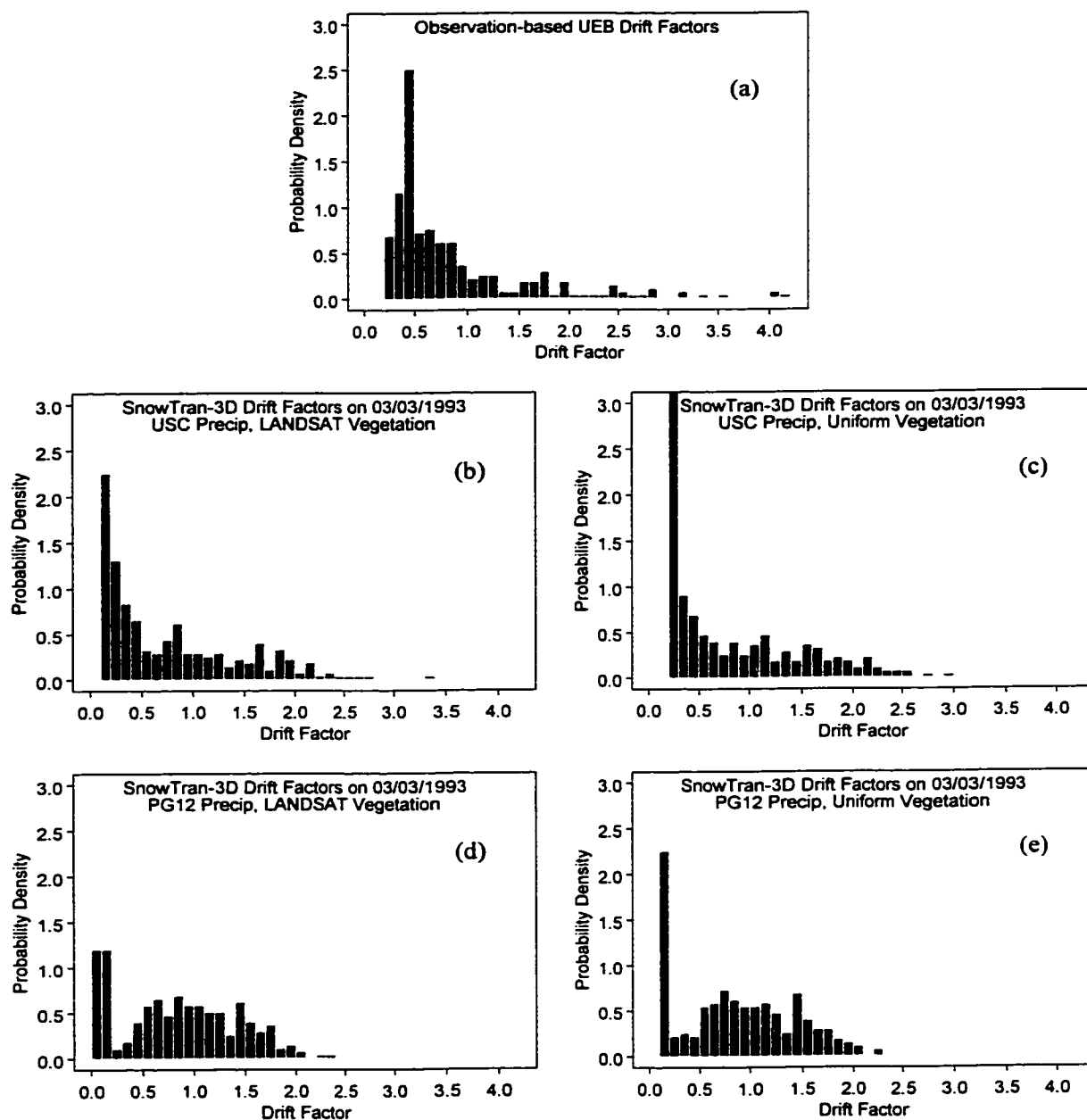


Figure 3-10. Distribution of drift factors at Upper Sheep Creek. (a) Observation-based UEB drift factors and SnowTran-3D-modeled drift factors using: (b) USC precipitation and LANDSAT vegetation, (c) USC precipitation and uniform vegetation, (d) PG12 precipitation and LANDSAT vegetation, and (e) PG12 precipitation and uniform vegetation, respectively.

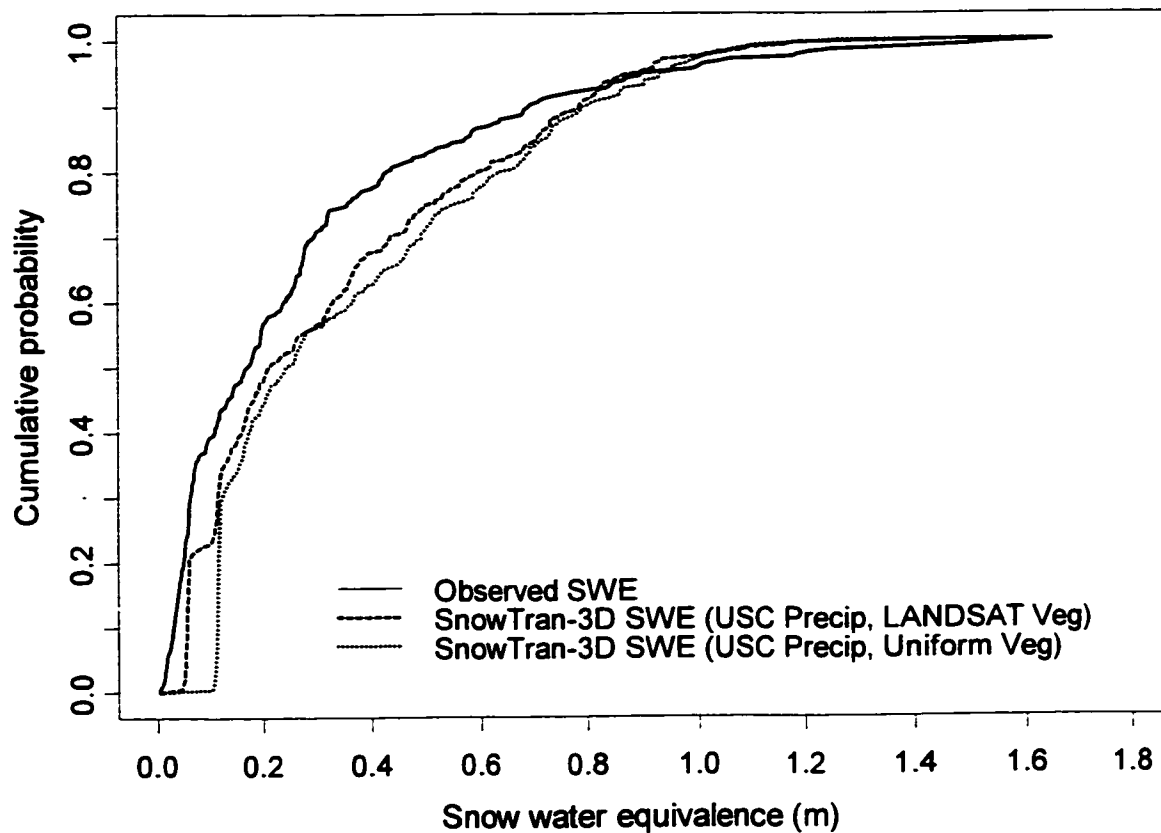


Figure 3-11. Comparison between cumulative distribution functions of observed and SnowTran-3D-modeled SWE at USC. SnowTran-3D used USC precipitation.

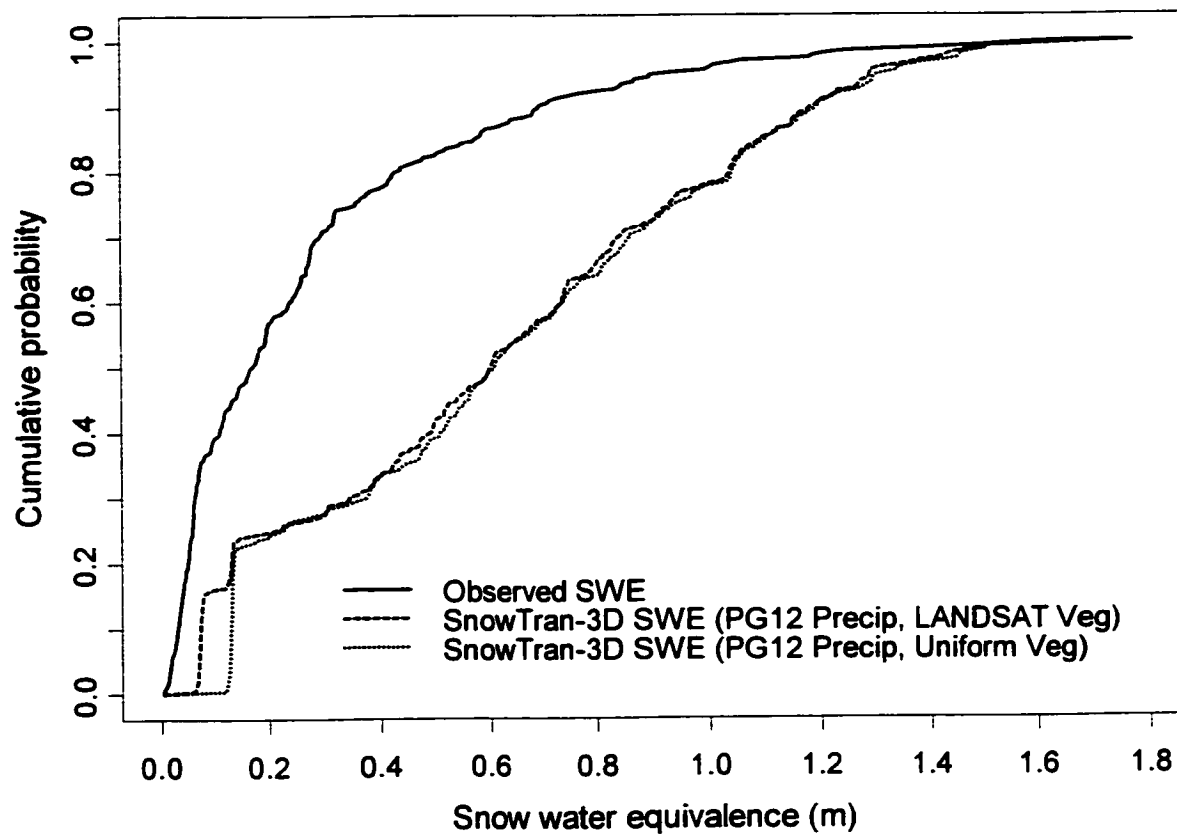


Figure 3-12. Comparison between cumulative distribution functions of observed and SnowTran-3D-modeled SWE at USC. SnowTran-3D used PG12 precipitation.

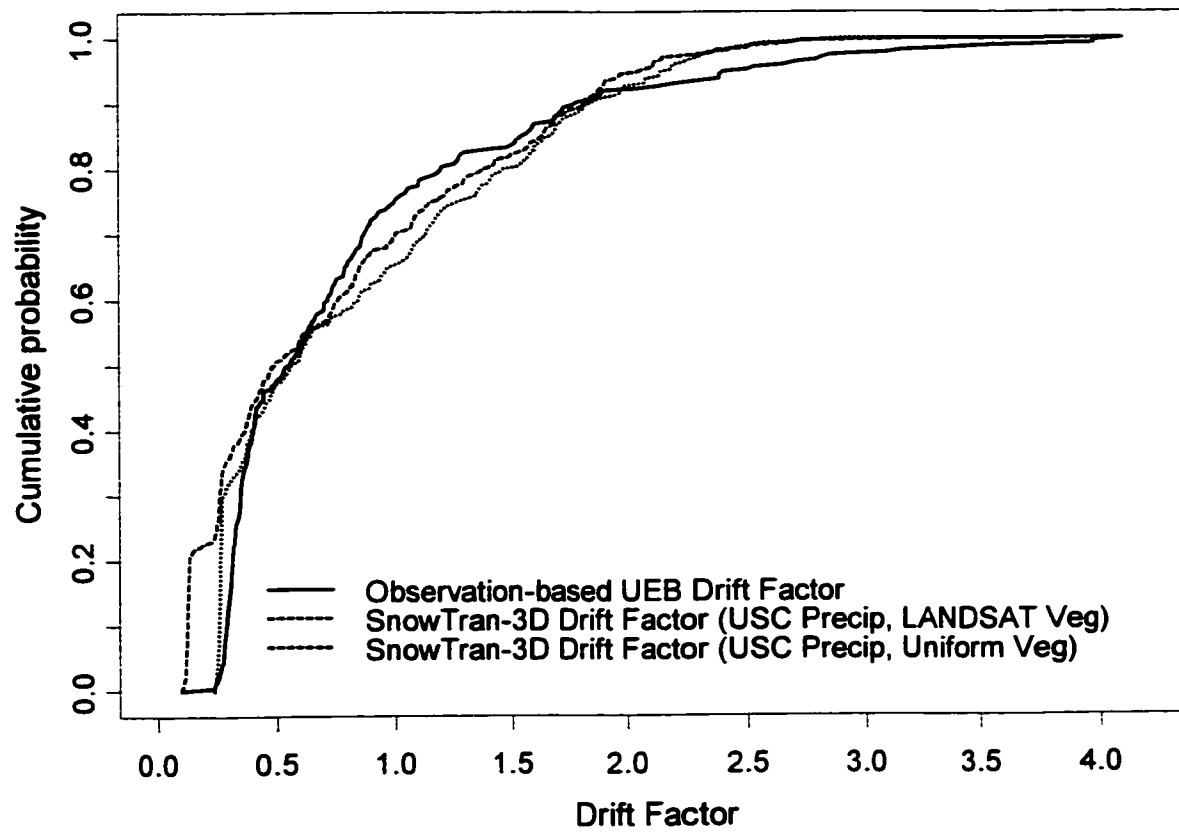


Figure 3-13. Comparison between cumulative distribution functions of observation-based and SnowTran-3D-modeled drift factors at USC. SnowTran-3D used USC precipitation.

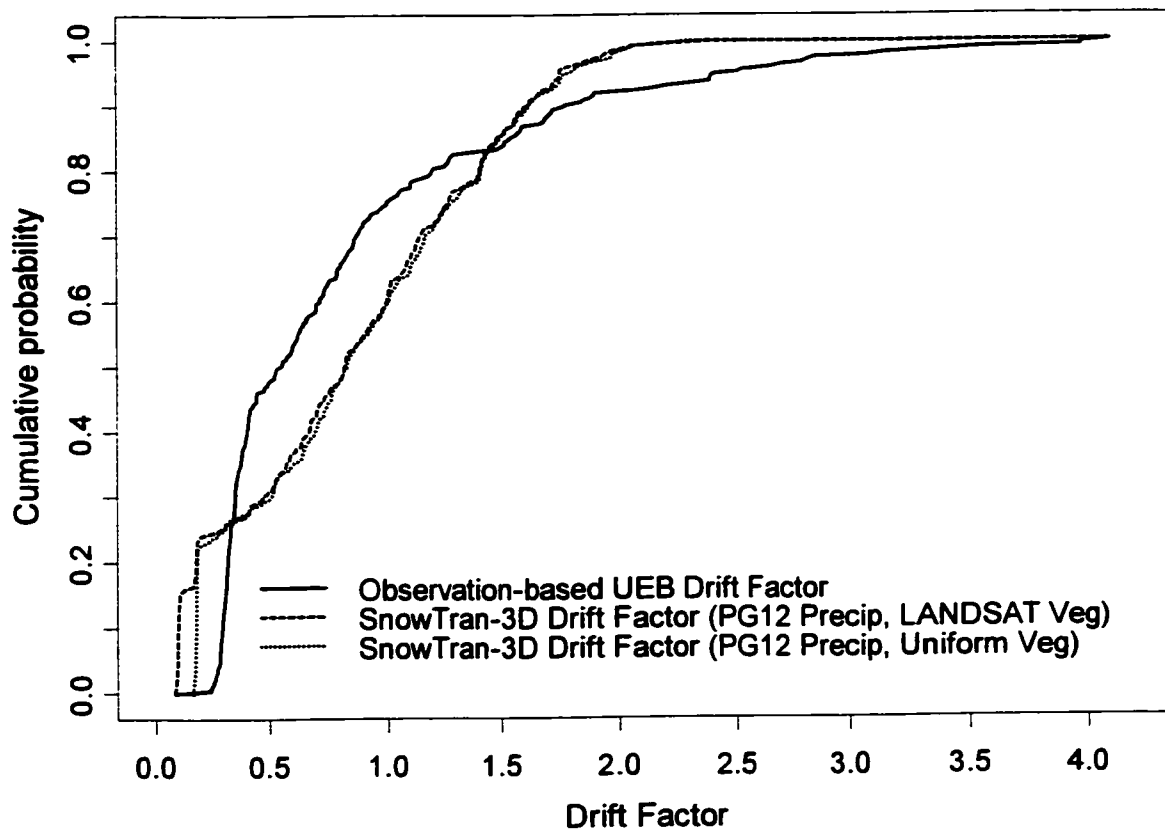


Figure 3-14. Comparison between cumulative distribution functions of observation-based and SnowTran-3D-modeled drift factors at USC. SnowTran-3D used PG12 precipitation.

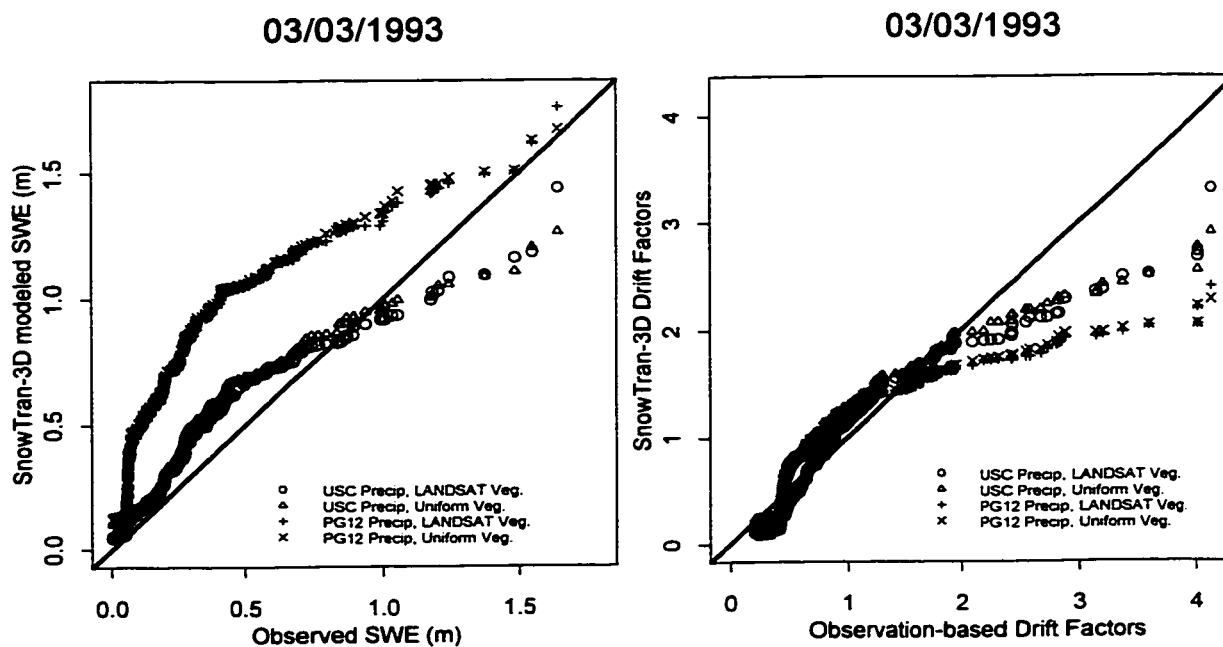


Figure 3-15. (a) Comparison between distributions of observed and SnowTran-3D-modeled SWE. Sorted modeled SWE is plotted against sorted observed SWE. The 1:1 line indicates perfect agreement between modeled and observed distributions of SWE. It can be seen that the SWE modeled using USC precipitation agrees better than that modeled using PG12 precipitation. (b) Comparison between distributions of observation-based drift factors and SnowTran-3D modeled drift factors. The plots are constructed in the same manner as in Figure 3-15a. It can be seen that the sensitivity of the distribution of drift factors to the amount of precipitation is less compared with the sensitivity of the distributions of SWE.

CHAPTER 4
HYDROLOGIC BEHAVIOR OF A FOURTH-ORDER WATERSHED IN
IN REYNOLDS CREEK, IDAHO, UNITED STATES OF AMERICA¹

Abstract

This focus of this study was to examine whether our understanding of the behavior of annual-scale hydrologic mass-balance was transferable from a small, intensively monitored first-order watershed to a larger, fourth-order watershed in a semi-arid mountainous region. The largest source of spatial variability in this watershed is due to surface water input, resulting from wind-induced redistribution of snow. A physically based numerical snow transport model was used to simulate snow drift, which provided the spatial pattern of snow accumulation at the fourth-order watershed. Parameters of a simple index-based snowmelt model, calibrated previously at the first-order watershed, were shown transferable to the fourth-order watershed. This snowmelt model was used to estimate surface water input at the fourth-order watershed over the 30-m USGS DEM grid. The subwatersheds of the fourth-order watershed were divided into three surface water input zones, based on a scheme used before at the first-order watershed. Aggregated surface water input for the three zones for each subwatershed was computed and used to drive a simple hydrologic mass-balance model to partition into hydrologic fluxes. Parameters of the hydrologic mass-balance model calibrated previously at the first-order watershed were shown to capture most of the variability in annual streamflow

¹ Coauthored by Rajiv Prasad, David G. Tarboton, and Charles H. Luce

from the fourth-order watershed. The study also analyzed the sensitivity of the annual hydrologic mass-balance to parameters of the model and the initial conditions. The mass-balance was found sensitive to two model parameters (vegetation factor for evapotranspiration computation and threshold parameter for saturated zone) as well as two initial conditions (initial soil moisture content and initial depth to the water table). Further avenues for research in this watershed are suggested based on these findings.

1. Introduction

Hydrologic response in western U. S. rangeland watersheds is strongly influenced by the spatial variability of snowpack [Cooley, 1988; Luce *et al.*, 1997; Luce *et al.*, 1998]. Surface water input into the subsurface determines the magnitude and timing of subsurface response from these watersheds [Chapter 2]. Spatial variability of snow accumulation and melt is identified as the dominant hydrologic process in these watersheds, and it has been shown that first-order watersheds can be adequately parameterized by subdividing into zones based on surface water input classes [Chapter 2]. The spatial distribution of snowpack can be determined by terrain-related drift factors, estimated by a wind blowing snow transport model [Chapter 3]. In this paper, we apply our understanding of small-scale hydrology and the spatial distribution of snowpack obtained from the snow transport model simulation to build a relatively simple model to describe hydrologic behavior at a 54.8-km², fourth-order watershed. This watershed is first subdivided into subwatersheds, which are then further divided into surface water input zones based on the distribution of snow drift factors, similar to Prasad

et al. [Chapter 2]. Each of these zones is modeled in the same way as at the first-order watershed. The stream network, which drains the fourth-order watershed, is used to route flow to the outlet of the watershed, where it is compared with observed outflow.

The questions that we address in this study are:

- (1) Is our understanding of the hydrologic behavior from the intensively monitored first-order watershed transferable to the subwatersheds of a fourth-order watershed in the same region?
- (2) As the hydrologic modeling is scaled up from a first-order watershed to a fourth-order watershed, which additional hydrologic processes need to be explicitly parameterized or modified?
- (3) What is the relative importance of the hydrologic processes as the modeling is scaled up?

Answering the first question is important because of several reasons. One of the expectations of process-based models is that they are generally applicable, at least for similar hydrologic conditions. Applying our existing understanding to the fourth-order watershed gives us an excellent opportunity to test the generality of the approach developed at the small scale.

As the spatial extent of the modeling domain increases, the spatial variability of processes as well as inputs increases. Some of these processes may become more important at larger scales, thus requiring explicit parameterization. For example, at the first-order watershed, channel routing was neglected, without affecting the volume and timing of outflow [Chapter 2]. At the scale of a fourth-order watershed, channel routing

may need to be considered to adequately model the timing of aggregate outflow. There are additional sources of spatial variability like precipitation distribution and vegetation and soil types across the fourth-order watershed, which may also affect the annual water balance significantly. The second question addresses these issues.

The third question focuses on evaluation of the relative importance of hydrologic processes at the modeling scale. It is important to know which processes contribute to most of the variability in observed hydrologic fluxes. This knowledge helps focus modeling efforts where gains from investments are significant. This knowledge also helps in allocating limited resources in monitoring processes, which play a more important role in the determination of overall hydrologic behavior.

In addition to answering the above questions, we also evaluate the sensitivity of the modeled annual scale mass-balance to several factors including (a) soil and vegetation parameters; (b) saturated zone storage-discharge parameters, and (c) initial conditions.

2. Study Site

Reynolds Creek Experimental Watershed (RCEW) is a 233.5-km² semiarid mountainous watershed located in southwestern Idaho (see Figure 3-1) and has been the focus of intensive hydrometeorologic instrumentation over the past 35 years. The watershed is maintained by the Northwest Watershed Research Center, Boise, Idaho, a part of the Agricultural Research Service, U. S. Department of Agriculture. Elevations in the watershed range from 1097 to 2237 m. Mean annual precipitation varies with elevation and ranges from 229 to 1107 mm. The watershed is almost entirely sagebrush

rangeland. Approximately 2% of the area is covered by small stands of scattered Douglas fir, aspen, and alpine fir. The main waterway of Reynolds Creek has a length of 25.1 km and overall slope of 4%. The hydrology of the watershed is mainly snowmelt driven. Channel flow is sustained by groundwater recharged by infiltration of snowmelt.

The focus of this study is Tollgate, a 54.8-km² subwatershed within RCEW (Figure 3-1). The Tollgate watershed is drained by a fourth-order stream network shown in Figure 3-1. The subwatersheds of Tollgate are shown in Figure 4-1. These subwatersheds were extracted using digital terrain analysis [Tarboton *et al.*, 1991; Tarboton, 1997; Tarboton and Shankar, 1998], and consist of areas draining to each channel link of the fourth-order drainage network. There are 15 precipitation gages and three weather stations in RCEW (see Figure 3-1). In this study, we used precipitation gages 4 through 15 to input spatially distributed precipitation field to the surface water input model described below. The precipitation field was interpolated using linear basis functions defined over the Delaunay triangulation of the precipitation gages weighted by an annual precipitation surface (Figure 4-2), as described below.

The first-order watershed referred to above is Upper Sheep Creek (USC), a 0.25-km² watershed shown in Figure 3-1.

3. Drift Factors and Surface Water Input Zones for Tollgate

Wind-induced snow drifting leads to a highly variable spatial distribution of snow in Reynolds Creek Experimental Watershed [Cooley, 1988]. Prasad *et al.* [Chapter 2] showed that spatial variability of snowpack strongly influences the timing of snowmelt,

and is the primary control on the timing of streamflow from USC (Figure 3-1), a small first-order watershed in RCEW. They obtained drift factors by calibration using measured snow water equivalence maps. The drift factor was defined as a factor by which gage measured snowfall input to a snowmelt model, must be multiplied to equate measured and modeled snow water equivalence at each point within the watershed. Assuming that the snowmelt model is correct in other respects, the drift factor describes the propensity of a location to accumulate extra snow through drifting (drift factor > 1), or to lose snow due to scouring (drift factor < 1). This approach approximates drifting which follows snowfall as occurring concurrently with snowfall. This approach also amounts to an assumption of linearity in the spatial pattern of snow accumulation, because snow accumulation at each point is linearly proportional to snowfall at a gage or reference location. Since field measurement of snow water equivalence maps is only possible at small scales, different approaches such as modeling physically based snow transport for simulation of wind-induced snow drifting must be considered at larger scales. Prasad et al. [Chapter 3] found that the distribution of drift factors is reasonably well modeled using SnowTran-3D, which is a physically based snow transport model [Liston and Sturm, 1998]. The linearity assumption was tested at USC [Chapter 3]. The simulated pattern of spatial snow accumulation was found to be reasonably independent of the amount of snowfall within the range of measured precipitation in and around Tollgate. In this paper, we will use the drift factor map obtained from the SnowTran-3D simulations for all of Tollgate. This drift factor map is shown in Figure 4-3a.

Prasad et al. [Chapter 2] showed that the hydrologic behavior of a first-order watershed at the annual scale was dominated by the variability in surface water input, which was a direct consequence of the spatial pattern of snow accumulation. The volume and timing of spring runoff from this first-order watershed was adequately parameterized using a simple mass balance model with the watershed divided into three surface water input zones [Chapter 2]. Following the same approach, the subwatersheds of Tollgate were subdivided into surface water input zones. Zone 1 corresponded to drift factor values from 0.0 to 0.5, zone 2 to drift factor values from 0.5 to 1.0, and zone 3 to drift factor values greater than 1.0. These zones, as delineated for Tollgate are shown in Figure 4-3b.

4. Interpolation of Precipitation to Obtain Spatial Field

The spatial distribution of precipitation in RCEW is highly variable and depends on elevation, prevailing storm patterns and the location of the precipitation stations with respect to storm movement [Hanson, 1982]. During earlier years of research at RCEW there were more precipitation gages than currently operating. Precipitation data from 38 sites was used by Hanson [1982] to develop annual and monthly precipitation-elevation relationships for downwind and upwind gage sites separately. The record length at these sites varied from 11 to more than 30 years. There is a general southwest-to-northeast decreasing trend [Hanson, 1982] in annual precipitation (Figure 4-2). Six of the aforementioned gages, which have record length exceeding 30 years, showed a variation in mean annual precipitation from 231 mm (elevation 1184 m) to 1114 mm (elevation

2164 m), a factor of 4.8 over a distance of less than 18 km [*Hanson and Johnson, 1993*]. This variability becomes more pronounced because of elevation effects. About 20% of the annual precipitation falls as snow at lower elevations. The percentage changes to 76 at higher elevations. This variation results in a highly variable snowpack distribution within the watershed. Prevailing winds at RCEW also result in significant amount of wind-induced snow drifting, as described above. Variability of air temperature with elevation and the variability of solar radiation over the rugged terrain combined with the spatial variability of snowpack due to wind-induced drifting result in a complex spring snowmelt and streamflow response at RCEW.

The annual precipitation surface estimated by *Hanson* [1982] for Tollgate is shown in Figure 4-2. This annual precipitation surface is used in conjunction with the precipitation stations in and around Tollgate to obtain precipitation at each grid cell in the modeling domain. Hourly (instantaneous or any other short duration) measured precipitation values were normalized by the value of the annual surface at the measurement location or gage and then the normalized values were interpolated in space. The annual surface was then used to scale back the normalized interpolated hourly values at any (nonmeasurement) location. This approach allowed us to use the annual precipitation surface in order to approximate the spatial precipitation pattern from spatially sparse hourly measurements. The precipitation at a nonmeasurement location (grid cell) \bar{x} is given by:

$$P(\bar{x}) = A(\bar{x}) \cdot \sum_{i=1}^3 \left[\phi_i(\bar{x}) \cdot \frac{P_i}{A_i} \right] \quad (4.1)$$

The summation in equation (4.1) above is carried over the three measurement gages located at the vertices of a Delaunay triangle, which encompasses the nonmeasurement location \bar{x} . In the above equation, $A(\bar{x})$ is the annual surface value at a nonmeasurement location \bar{x} , P_i is the hourly precipitation at the measurement gage located on the i th vertex of the encompassing Delaunay triangle, A_i is the annual surface value at the same vertex and $\phi_i(\bar{x})$ is a weight or a basis function, which depends only on the relative position of the non-measurement location \bar{x} within the encompassing Delaunay triangle. Three basis functions were used for each triangle, one at each vertex. The basis function for each vertex of a Delaunay triangle is defined by a plane with weight 1 at its own vertex and weights 0 at the other two vertices. The Delaunay triangulation was carried out using a publicly available triangulation program [Shewchuk, 1996], and is shown in Figure 4-2. Two precipitation gages (PG4 and PG5) which were located outside the study region were also used in addition to the ten precipitation gages (PG6 through PG15) located within the study region for constructing the triangulation and subsequent interpolation to obtain hourly precipitation at each grid cell in the study domain. The Delaunay triangulation (denoted by thick lines in Figure 4-2) carried out on the 12 precipitation gages (PG4 through PG15) did not cover the study area completely. In order to interpolate precipitation at grid cells of Tollgate that fell outside the Delaunay triangulation, we added seven virtual gages at a large distance (compared to the size of

the study domain) located on the orthogonal bisector of each of the outer edges of the triangulation. This procedure resulted in a revised precipitation gage set of 19. This new set of points was triangulated again while preserving the initial triangulation. The extended Delaunay triangulation is shown by thin lines (Figure 4-2) extending from the precipitation gages on the edge of the initial triangulation. The extended Delaunay triangulation covered the whole study region. The weights associated with the virtual gages were set to zero, thereby using either one or two nearest precipitation gages for interpolation on grid cells located outside of the initial Delaunay triangulation.

5. Surface Water Input at Tollgate

Surface water input was computed over the 30-m USGS DEM grid for Tollgate. Air temperature was used to partition precipitation into snow and rain [*U.S. Army Corps of Engineers, 1956*]. The fraction of precipitation falling as snow on a grid cell is given by:

$$\begin{aligned}
 f_{snow} &= 1.0 & T_a < T_s \\
 &= \frac{T_r - T_a}{T_r - T_s} & T_s \leq T_a \leq T_r \\
 &= 0.0 & T_a > T_r
 \end{aligned} \tag{4.2}$$

where T_r ($= 1$ °C) is the air temperature above which all precipitation is assumed to fall as rain, and T_s ($= -3$ °C) is the air temperature below which all precipitation is assumed to fall as snow. Snowfall at the grid cell was adjusted for wind-induced drifting, using the drift factor f_{drift} , and is given as:

$$P_{snow} = f_{drift} \cdot f_{snow} \cdot P \quad (4.3)$$

where P is the interpolated precipitation (m) at the grid cell.

SWE for the grid cell at the end of a time step t was determined from the mass balance equation:

$$SWE_t = SWE_{t-1} + (P_{snow,t} - M_t) \cdot \Delta t \quad (4.4)$$

where SWE_t (m) is the SWE at the end of the time step, SWE_{t-1} (m) is the SWE at the beginning of the time step, $P_{snow,t}$ (m) is the snowfall during the time step, M_t (m) is the snowmelt outflow during the time step, and Δt (hour) is the length of the time step.

In this paper, we computed hourly surface water input (SWI) over all grid cells of Tollgate (see Figures 3-1 and Figures 4-1 through 4-2) using two snowmelt models: (1) Utah Energy Balance [UEB, *Tarboton and Luce*, 1996] model, which solved the energy balance of a single-layer snowpack and a thin layer of soil at a point, applied over the 30-m USGS DEM grid, and (2) Pseudo-Distributed Index-based Model for Snowmelt [PDIMS, Chapter 2], which computed snowmelt at a point using a multiplicative temperature-radiation empirical relationship, also applied over the 30-m USGS DEM grid. Surface water input computed by UEB was either rainfall (if the grid cell was bare of snow) or snowmelt (if the grid cell melted any accumulated snow) during the time step. UEB modeled the energy input due to rain on snow and possible refreezing and

included remainder that did not refreeze in snowmelt outflow. In PDIMS, any rainfall on snow was assumed to pass through the snowpack and was immediately available at the soil surface. SWI was computed as the sum of rainfall and snowmelt when PDIMS was used as the snowmelt model.

Parameters of PDIMS were calibrated previously at Upper Sheep Creek [Chapter 2], and were assumed to be applicable at Tollgate. Arguably UEB is a more general and physically realistic model, and we will compare the results based on SWI computed using the two models to determine whether the assumptions made while developing PDIMS at USC are also valid at Tollgate. UEB did not perform satisfactorily at the small scale [i.e., at USC, Chapter 2], melting snow too rapidly during spring, and these comparisons will indicate the sources of the discrepancy.

Figure 4-4 shows a series of snow cover maps derived from aerial photographs at Tollgate. Although these snow cover maps correspond to different years (water years 1969, 1971, and 1989), they were similar in terms of streamflow conditions during the simulation year used in this study (water year 1993). The 1969 water year was a little above average (estimated from 34 years of streamflow data). The previous water year, 1968, was very dry, with streamflow only about one-sixth of that in 1969. The same was true for water years 1989 and 1993: both were a little above average, and followed a dry water year. The water year 1971 was about 150% of the long-term mean. The water year 1970 was close to mean. The spatial pattern of snow accumulation and melt at Tollgate is remarkably consistent from year to year (see Figure 4-4). Below, we compared these

snow cover maps with modeled SWE maps to determine in a qualitative sense whether the snowmelt models performed adequately.

Figure 4-5 shows the time series of basin-average snow water equivalence at Tollgate for the two different SWI runs: (a) UEB and (b) PDIMS with melt factors calibrated previously at Upper Sheep Creek [Chapter 2]. UEB melted snow relatively rapidly throughout the season. PDIMS with calibrated melt factors was better in performance, retaining snow later in the season. This relative behavior between these snowmelt models was similar to that observed at USC previously [Chapter 2]. The UEB simulation ran out of snow as early as the middle of May. PDIMS with melt factors calibrated at USC simulated less melt compared to UEB, and snow was present in the watershed until the end of June. As was evident from Figure 4-4, snow cover at Tollgate was expected to persist as late as middle of June. Although the spatial coverage of snow in Figure 4-4 seems small in June, these were deep snowdrifts, which formed due to wind induced snow drifting [see Chapter 3] and held a lot of water.

Figure 4-6 shows snapshots of modeled SWE on May 11, 1993, May 23, 1993, and June 3, 1993, obtained from the PDIMS simulation. These dates were the same day of the year as the dates of the snow cover maps shown in Figure 4-4. The modeled SWE maps did not agree well with the snow cover maps in a pointwise comparison. This disagreement may be related to pattern mismatch between modeled and observed snowpack due to uncertainty in wind data and the wind flow parameterization used by SnowTran-3D simulations [Chapter 3]. Another reason may be that the snow cover

pattern during 1992-93 was different than that shown in Figure 4-4 due to inter-annual variations.

The good visual agreement between the observed and modeled snow cover maps in terms of area coverage however, suggested that PDIMS with melt factors calibrated at USC was close to being accurate at the scale of Tollgate. This result also suggested that our understanding of the way snow accumulates and melts in RCEW was transferable from USC to Tollgate. This result was very significant because it provided us a way to upscale surface water input, which was the largest source of spatial variability in this watershed, from the scale of a first-order subwatershed to the scale of a fourth-order subwatershed.

Hourly SWI was computed for three drift factor zones for each of the 153 subwatersheds of Tollgate by aggregating the SWI from all grid cells that comprise the given zone. These SWI time series were used for input to the hydrologic model for partitioning of water fluxes at Tollgate into its components.

6. Hydrologic Model for Tollgate

The transferability of surface water input from the first-order subwatershed to the fourth-order subwatershed was demonstrated above. This section addresses the question whether the hydrologic mass-balance model developed and calibrated at USC [see Chapter 2] could be used at the subwatersheds of Tollgate. Results in this section will provide answers for the first two questions listed above.

Each of the first-order subwatersheds of Tollgate was subdivided into surface water input zones based on the distribution of drift factors (Figure 4-3). These zones were used to implement a three-zone hydrologic mass balance model at each first-order subwatershed similar to Prasad et al. [Chapter 2].

The hydrologic model (the Dominant Zone Hydrologic Model, DZHM) consisted of an evapotranspiration (ET) component which extracted water from the soil; a soil zone component which served as a temporary store for infiltrated water before ET and saturated zone recharge deplete this store; and a saturated zone component which acted as a bucket-like store, spilling to produce baseflow when a storage threshold was exceeded.

Potential evapotranspiration (PET) demand was computed using the Priestley-Taylor equation with the coefficient α set to 1.74 for arid climate [Shuttleworth, 1993]. Modeled evapotranspiration (ET) was computed by reducing PET by multiplying it with f_{AET} , a factor that depends on the moisture content of the soil zone similar to Shuttleworth [1993 Fig 4.4.3, p. 4.46]. The ET component required a vegetation-specific parameter, K_{veg} , which was used as a multiplier to PET to compute ET.

$$ET = K_{veg} \cdot f_{AET} \cdot PET \quad (4.5)$$

The soil zone was characterized by a depth parameter z_r , which determines the capacity parameter, given the saturation moisture content θ_s . The soil properties were specified using two additional moisture contents: field capacity θ_r , and wilting point θ_w .

The active capacity of the soil was divided into drainable moisture $\Delta\theta_1 = \theta_s - \theta_r$, and plant available moisture $\Delta\theta_2 = \theta_r - \theta_w$. Potential rate of infiltration was computed using a Green-Ampt like formulation [Chapter 2]. Drainage to the saturated zone was allowed to occur only when moisture content in the soil zone exceeded the field capacity. Potential rate of drainage from the soil zone was computed as the hydraulic conductivity at the base of the soil zone, which effectively assumes unit hydraulic gradient at the base of the soil zone. Actual rate of drainage was reduced depending on the moisture content of the soil zone relative to the drainable capacity according to a pore disconnectedness parameter.

The saturated zone was implemented as a bucket-like store, which spilled when the storage exceeded a threshold. The storage-discharge function was a generic power-function. Details of implementation and calibration of parameters of DZHM is given by Prasad et al. [Chapter 2]. The parameters of DZHM calibrated earlier at Upper Sheep Creek [Chapter 2] were used here as baseline values for each of the subwatersheds of Tollgate.

DZHM was used to implement a three-zone hydrologic model at each of the subwatersheds of Tollgate. All parameters of DZHM were kept the same as in Prasad et al. [Chapter 2].

The initial condition describing the depth to groundwater table \bar{z} , was reduced from the baseline values of 1.825 m for all zones of USC to 1.380 m for zone 1, 1.360 for zone 2, and to 1.700 m for zone 3. These modifications were required to visually match the outflow hydrograph simulated by the model to the observed outflow hydrograph from

Tollgate as closely as possible without any additional calibration of model parameters (see Figure 4-7a). For comparison, Figure 4-7a also shows the modeled hydrograph when the initial condition for depth to the groundwater table was kept same as that at USC in Prasad et al. [Chapter 2]. All model parameters were kept uniform in a zonewise fashion, i.e., model parameters for corresponding zones of all subwatersheds of Tollgate were the same. This allowed us to focus on the importance of the spatio-temporal pattern of snowmelt in this watershed and at the same time to evaluate the applicability of the model parameters calibrated at USC to the subwatersheds of Tollgate.

At USC, the hydrologic modeling ignored any time delay internal to the first-order subwatershed, which may have been associated with surface and baseflow generated at each zone [Chapter 2]. This approach was supported by the observation that the timing of rapid surface water input and that of streamflow measured at the outlet of USC were in close synchronization. Similar behavior was also seen at Tollgate (Figure 4-7). The observed peaks in streamflow just after the event timelines marked 1, 2, and 3 (Figure 4-7a) were in close synchronization to surface water input events, which occurred just after these timelines (Figure 4-7d). This observation indicated that there was little if any time delay (both internal to the subwatersheds as well as that associated with channel travel time) in Tollgate, and we decided to ignore time delay.

There was some additional indication for ignoring the travel time in channels. The channel slopes at Tollgate, obtained from DEM analysis, varied between 0.01 and 0.3. Assuming wide rectangular channels flowing with a depth of 0.1 m, the channel flow velocity for gravelly channels (with Manning's roughness coefficient $n = 0.02$, see

Table 12.2.1, p. 12.15 in [Maidment, 1993]) works out between 1.0 m/s (for friction slope = ground slope = 0.01) and 5.9 m/s (for friction slope = ground slope = 0.3). The longest channel length from a subwatershed to the outlet of Tollgate is 10.4 km. These conditions indicated that the longest travel time in the channels was approximately of the order of 10,400 seconds or about 2.9 hours assuming constant depth and least steep slope. Even with smaller depth of flow and greater roughness, the channel travel time would not exceed a few tens of hours.

6.1. Performance of Baseline DZHM at Tollgate

DZHM was run for simulation period beginning October 1, 1992 through August 16, 1993 at hourly time steps for each of the 153 first-order subwatersheds of Tollgate. These runs provide the outflow hydrograph from each subwatershed at hourly time steps. The measured hydrograph at the outlet of Tollgate was compared to the modeled hydrograph obtained using “no-delay” routing. This comparison is shown in Figure 4-7a.

The modeled and observed hydrographs in Figure 4-7a had significant differences, and also significant similarities. The volume of runoff measured at Tollgate was 393 mm, and the modeled runoff with modified depths to groundwater table was 277 mm. The volume of runoff modeled without adjustment to depth to groundwater table (i.e., using values same as that at USC) was 89 mm. The observed hydrograph showed more abrupt rises and falls, as compared to the modeled hydrograph, where the rises were slower and recessions smoother. In addition, during the early part of the season, these differences were more pronounced than those later in the season. Part of the reason for

this behavior might be due to the soil parameters at Tollgate being different from their baseline values, which were being transferred from USC. It is also possible that the snow at lower elevations melted more rapidly than the snow at the higher elevations, which might result in more rapid surface water input leading to more steep rises in the modeled streamflow hydrograph. This observation might indicate a need for spatially varying melt factors at Tollgate. The first peak (just after event timeline 1 in Figure 4-7) in the observed hydrograph was not reproduced by DZHM simulation. We believe that this peak was due to a rain-on-snow event producing runoff from frozen soil patches. Mean air temperature during this observed streamflow peak was above freezing (Figure 4-7b), and there was significant precipitation (Figure 4-7c). Rain-on-snow was ignored by PDIMS in that all rain falling on snow was allowed to be available for infiltration into the soil. Since DZHM does not include any mechanism to simulate frozen soils, significant part of the rain falling on snow or frozen ground might infiltrate. In reality, there might have been runoff from frozen soil patches, which produced the observed peak. The last peak in the streamflow hydrograph was mostly due to rainfall, since almost all the snow had already melted by this time (Figure 4-5). The modeled peak was in reasonably good agreement with the timing of the observed peak, although the rise was slower and the recession smoother compared to observed streamflow. The larger observed peak could also be due to runoff produced from partially saturated areas in the watershed, a process not included in DZHM. The absence of representation of processes like runoff from frozen soil patches, rain-on-snow, and partially saturated areas might be responsible for the disagreement in the volumes of modeled and measured runoff.

It was encouraging, however, that the majority of secondary peaks was reasonably well represented in the modeled hydrograph, and was in close agreement in terms of timing. The hydrologic model DZHM, with only some modifications to initial conditions was able to simulate the outflow hydrograph reasonably well. Since all parameters in DZHM, as well as the initial conditions were spatially uniform, we concluded that most of the observed variability in the outflow hydrograph was explained by the spatially varying surface water input. It is possible that a better match to the streamflow hydrograph could be obtained if the uniformity assumption for some of the parameters were relaxed. However, there are two reasons we did not attempt to do this: (1) the main goal of this study was to address the question of transferability of our understanding from Upper Sheep Creek to Tollgate, not to build the best model we could at Tollgate, and (2) because there was little supporting data to justify such an exercise.

6.2. Internal Testing

In addition to testing the performance of DZHM against the outflow hydrograph for Tollgate, we also tested it for one internal first-order subwatershed. This subwatershed was Reynolds Mountain East (RME), numbered 35 on Figure 4-1. RME is 0.42 km² in area, located on the southeastern ridge of Tollgate. Measured streamflow for this watershed was available for 1992-93. Figure 4-8 shows the comparison between the DZHM modeled and measured streamflow at the outlet of RME. The volume of measured streamflow at RME was 695 mm and the volume of DZHM modeled streamflow was 662 mm. The behavior of DZHM was similar to that for Tollgate. The

simulated hydrograph rose slowly compared to more abrupt rises in the measured hydrograph. The recession was also smoother compared to measurements. These observations could be attributed to differences in model parameters between Upper Sheep Creek and Tollgate, and also to absence of some processes like runoff from frozen ground and partially saturated areas. Although there were differences, the DZHM simulation captured the overall behavior of RME. This observation pointed to the conclusion that annual-scale watershed mass balance at the subwatersheds of Tollgate was strongly influenced by the spatial variability of the snowpack and the timing of snowmelt. The hydrologic behavior of the subwatersheds of Tollgate was also very similar to that of USC, indicating that the understanding in terms of annual-scale mass-balance was mostly transferable from the first-order subwatershed to the fourth-order subwatershed.

7. Sensitivity Analysis

We have shown in the previous sections that surface water input computed from a spatially varying snowpack over Tollgate could be used to drive DZHM in a three-zone configuration to reproduce a large part of the variability in annual streamflow from Tollgate. It is, however, important to understand the sensitivity of this modeling approach to various model parameters and initial conditions in order to decide the relative importance of these parameters in the context of modeling and to justify resource allocation in measurement or determination of these parameters. We decided to limit the

sensitivity analysis to only those parameters that were calibrated at USC [see Chapter 2], and to the initial conditions, listed below:

- (1) the vegetation parameter K_{veg}
- (2) the surface saturated hydraulic conductivity, K_0
- (3) the decay parameter, f
- (4) the saturated zone threshold parameter, z_i
- (5) the saturated zone exponent parameter, η
- (6) the initial soil zone moisture content, θ_0 , and
- (7) the initial depth to the water table, \bar{z}_0 .

Since all of the above variables could potentially be spatially variable, it became rather difficult to assign specific spatial patterns in absence of supporting data. Instead, we decided to use multipliers to scale these parameter values while preserving zonewise spatial uniformity. We used multiplier values of 0.5 to 1.5 in steps of 0.1. The effects of changes in these variables on modeled basin average annual mass balance components (ET, change in soil zone storage, change in saturated zone storage and streamflow for the simulation period) for Tollgate are shown in Figures 4-9 through 4-12. We discuss the results below.

The modeled ET was insensitive to values of K_0 , f , η , z_i and \bar{z}_0 (Figure 4-9). All of these variables controlled the behavior of the soil zone and the saturated zone. In DZHM, ET was the first extraction demand satisfied by available surface water input, depending on the wetness of the soil and the vegetation type. Modeled ET was

thus sensitive only to the values of initial soil zone moisture content θ_0 and the vegetation parameter K_{veg} . The sensitivity of modeled ET to θ_0 was relatively small. The baseline value of θ_0 was set equal to the wilting point θ_w , which was the minimum allowable moisture content in the soil zone. Consequently, at θ_0 values less than θ_w , the modeled ET was the same, because DZHM reset the initial moisture content to θ_w . As the multiplier increased beyond 1.0, modeled ET increased in response to greater available moisture in the soil zone. At the maximum multiplier value of 1.5, modeled ET increased by 4.5% from the baseline value.

The modeled ET showed a lot more variation with respect to K_{veg} ; from a 37% decrease at multiplier value of 0.5 to a 19% increase at multiplier value of 1.5. It was thus important to accurately know this parameter for the study site. At Upper Sheep Creek, measured ET data was available to calibrate this parameter for the three zones. However, the vegetation properties at Tollgate might be different from that at Upper Sheep Creek, especially at higher elevations (Pine stands) and near streams (grasslands). There might be two possibilities for the determination of K_{veg} . ET measurements could be carried out at sites that are representative of different vegetation communities [e.g., *Artan et al.*, 1993]. The measured ET data could then be used to calibrate K_{veg} for each vegetation type. This approach however, is labor intensive and expensive. Another approach could be based on remotely sensed data. Reflectance values in appropriate spectral bands (e.g., near and thermal infrared) could be correlated to K_{veg} values calibrated at Upper Sheep Creek, and extended to Tollgate. There might be the need for

additional measured ET data for vegetation types at Tollgate that are not present at Upper Sheep Creek. These approaches might be venues for further research.

The modeled change in soil zone storage over the simulation period was insensitive to changes in values of K_0 , f , η , z_i and \bar{z}_0 (Figure 4-10). This was expected since there was no feedback from the saturated zone to the soil zone in DZHM. The modeled change in soil zone storage was more sensitive to changes in θ_0 and K_{veg} . The modeled change in soil zone storage increased 112% from baseline for multiplier value of 0.5 and decreased 112% from baseline for multiplier value of 1.5. The corresponding changes for K_{veg} resulted in a 102% increase and a 44% decrease in modeled change in soil zone storage from its baseline value. The multiplier value range 0.5 to 1.5 represented a large range of soil moisture conditions in the field. At the low end, it represented soil dried below wilting point, a condition expected only under sustained extremely dry conditions. At the high end, the soil would be very wet, possibly after an extremely wet summer. At the start of the 1992-93 water year used in this study, initial soil conditions were very dry following the lowest streamflow year (1991-92) on record, and the baseline value of θ_0 was set equal to θ_w . For other years, it might be possible to obtain a reasonable value of θ_0 based on the streamflow during the previous year. In general, soil moisture conditions are extremely difficult to obtain, especially for large areas.

The modeled change in saturated zone storage reduced slightly as K_{veg} increased (Figure 4-11), but was insignificant (an 8% increase for multiplier value of 0.5 and a 4%

decrease for multiplier value of 1.5). The modeled change in saturated zone storage was also insensitive to changes in θ_0 . As K_0 increased, saturated zone storage decreased, but only slightly (about 5.5%). Although there was more drainage from the soil zone because of higher K_0 , baseflow from the saturated zone was also higher, thus reducing the storage in the saturated zone. Similar behavior was observed for f . As f increased, hydraulic conductivity at the base of the soil zone decreased. This condition resulted in slightly reduced drainage to the saturated zone, but greater reduction in the modeled baseflow from the saturated zone, resulting in overall increase in modeled change in saturated zone storage. The modeled change in saturated zone storage was more sensitive to changes in η for the range used in sensitivity runs (a 23% decrease for multiplier value of 0.5 and a 47% increase for multiplier value of 1.5).

The modeled change in saturated zone storage was most sensitive to the threshold parameter z_i , and the initial depth to the water table \bar{z}_0 (Figure 4-11). The multiplier range used during sensitivity runs represented a large range of groundwater level variation, with lower end signifying initial water level above the threshold. DZHM used a bucket-like formulation for saturated zone baseflow component with z_i representing the threshold above which baseflow was generated. If the initial depth to the water table \bar{z}_0 were less than z_i , baseflow (and hence streamflow) would be generated at the start of the simulation, indicating very wet conditions. In the study watershed, streamflow was only observed during and a few weeks after spring snowmelt, indicating that a multiplier closer to 1.0 is more appropriate. The higher end of the multiplier would represent

sustained extremely dry conditions and groundwater depletion, which was also unexpected in the study region. It is, however, necessary to accurately know these variables for a simulation year. In general, it might be quite difficult to obtain this information, especially at the scale of Tollgate. In addition, since DZHM made several simplifying assumptions about the structure of the subsurface, it might be difficult to correlate observations such as piezometer levels (point measurements) to derive \bar{z}_0 .

The modeled total annual streamflow showed significant sensitivity to almost all of the variables analyzed (Figure 4-12). Relatively, sensitivity to initial soil moisture content θ_0 (+13% at multiplier value of 1.5), the hydraulic conductivity decay parameter f (+7% at multiplier value of 0.5, -13% at multiplier value of 1.5), and the saturated zone parameter η (+10% at multiplier value of 0.5, -21% at multiplier value of 1.5) seemed small. Modeled streamflow, however, was very sensitive to the initial depth to the water table \bar{z}_0 , and to the threshold parameter z_i . This sensitivity might in part be due to the large ranges of wetness conditions represented by the multiplier values used in the sensitivity runs, as explained above. However, it is important to accurately know the values of these variables at the start of the simulation since they significantly affect the annual mass balance.

According to the discussion above, the annual mass balance at Tollgate was affected significantly by the values of \bar{z}_0 , z_i , θ_0 and K_{veg} . Further research in this watershed should concentrate on accurately determining the values of these parameters and initial conditions at the start of the simulation year. Some pointers along these lines

have been discussed in this section. For some of the others (like \bar{z}_0 and θ_0) appropriate measurement techniques do not yet exist [see *Beven*, 1996] and we may need to find better approaches for estimating these quantities.

8. Summary and Conclusion

The hydrologic behavior of a first-order watershed in the study region was largely determined by the spatial variability of surface water input, which was a direct consequence of the spatial distribution of the snowpack in response to wind-blown snow drifting [Chapter 2]. The drift pattern for the fourth-order watershed was obtained from a snow transport model simulation carried out earlier [Chapter 3]. We subdivided the larger, fourth-order watershed into its subwatersheds, and assumed that these subwatersheds can be treated as basic computational elements. These subwatersheds were then further subdivided into snow drift zones similar to Prasad et al. [Chapter 2]. The overall response of the fourth-order watershed was determined by the aggregation of the hydrologic behavior of its constituent subwatersheds. The aggregation of the subwatershed responses took place through the channel network, which drained the fourth-order watershed.

We set out to answer some questions at the outset of this study. The first of these was to determine whether our understanding of the hydrologic behavior of USC was transferable to other watersheds in the same region. The following paragraphs address this question.

Since the hydrologic model was implemented in two distinct parts (an “above-surface” component, the surface water input model, and a “below-surface” component, the ET-soil zone-saturated zone model called DZHM), we tested each of these parts separately in terms of transferability from USC to the subwatersheds of Tollgate. We found that the characteristics of snowmelt at Tollgate were very similar to those at USC. The physically based snowmelt model UEB did not perform well at Tollgate, melting snow too rapidly throughout winter and spring, leading to all snow melting by the middle of May (Figure 4-5). Snow in Tollgate was expected to persist as late as second week of June at higher elevations (Figure 4-4). The index-based snowmelt model PDIMS performed better, retaining snow until the end of June, resulting in better agreement with the observed snow cover maps. We concluded that PDIMS, with melt factors calibrated at USC and driven by the spatial precipitation field interpolated using Delaunay triangulation weighted by annual surface values and the spatially varying radiation over rugged terrain, accurately represented the characteristics of snowmelt at Tollgate. This conclusion also indicated that our understanding of the surface water input processes was mostly transferable from USC to Tollgate.

DZHM was used to construct the below-surface mass balance for each of the 153 subwatersheds of Tollgate. The baseline model was driven with parameters calibrated previously at Upper Sheep Creek. It was necessary to adjust \bar{z}_0 , the initial depth to the water table for the three drift zones in order to visually match the streamflow hydrograph measured at Tollgate. With only these modifications, DZHM was able to reasonably reproduce the characteristics of the outflow hydrograph. However, there were significant

differences, probably attributable partially to local variations in model parameters and initial conditions, and partially to the absence of some processes (like runoff from frozen soil and partially saturated areas) from DZHM. Internal time delay and time delay corresponding to channel flow were insignificant at Tollgate. The below-surface component of the hydrologic model was thus mostly transferable from USC to Tollgate.

We concluded that our understanding of the annual-scale hydrologic mass-balance in RCEW was mostly transferable from a first-order watershed to a fourth-order watershed. Further research in regard to transferability would need to address the identification of spatial pattern of DZHM parameters and accurate determination of initial conditions.

The second question posed by this study was to identify additional processes that needed explicit parameterization. Internal time-delay and channel routing ignored at USC [Chapter 2] were shown to be insignificant at Tollgate also. There was some evidence, however, that runoff from frozen ground and partially saturated areas influenced streamflow peaks. It might be necessary to build these processes into DZHM in order to better simulate streamflow peaks during years when these two processes might be more important.

The third objective of this study was to determine the relative importance of the hydrologic processes at the scale of the fourth-order subwatershed. The most important hydrologic process at Tollgate was the spatial variability of surface water input, which was a consequence of wind-induced snow drifting during winter. Deep snow drifts that formed on the lee slopes sustained snowmelt and soil recharge late in the season. The

drift factor concept was shown to be reasonably good in terms of distribution of snowpack [Chapter 3] and could be used to adequately capture the spatial distribution of snowpack at the fourth-order watershed.

The annual-scale ET was sensitive to the vegetation-dependent parameter K_{veg} , and to a smaller extent on the initial soil moisture content θ_0 . Streamflow was sensitive to the threshold parameter z_i , and the initial depth to the water table \bar{z}_0 . Accurate determination of the initial conditions is expected to present significant challenges in the study watershed. Accurate determination of the spatial pattern of model parameters might also be necessary in order to match other internal state variables like streamflow at other locations within the watershed and soil moisture and snow cover patterns. ET is the primary moisture feedback to the atmosphere, and streamflow influences aspects of water resources planning and management. Further research in this watershed should thus focus on accurately determining these model parameters and initial conditions.

References

- Artan, G., C. M. U. Neale, C. Hanson, and J. R. Wight, Energy balance flux measurements in complex terrain for validation of hydrologic models, *Eos Trans. AGU*, 74(43), Fall Meet. Suppl., Abstract 318, 1993.
- Beven, K. J., A Discussion of distributed hydrological modelling, in *Distributed Hydrological Modelling*, edited by M. B. Abbott and J. C. Refsgaard, pp. 289–295, Kluwer Academic Publishers, Dordrecht, The Netherlands, 1996.
- Cooley, K. R., Snowpack variability on western rangelands, paper presented at Western Snow Conference, Kalispell, Mont., April 18–20, 1988.
- Hanson, C. L., Distribution and stochastic generation of annual and monthly precipitation on a mountainous watershed in southwest Idaho, *Water Resour. Bull.*, 18(5), 875–883, 1982.

- Hanson, C. L., and G. L. Johnson, Spatial and temporal precipitation characteristics in southwest Idaho, in *Proceedings ASCE Management of Irrigation and Drainage Systems: Integrated Perspectives*, edited by R. G. Allen and C. M. U. Neale, Park City, Utah, 1993.
- Liston, G. E., and M. Sturm, A snow-transport model for complex terrain, *J. of Glaciol.*, 44(148), 498–516, 1998.
- Luce, C. H., D. G. Tarboton, and K. R. Cooley, Spatially integrated snowmelt modeling of a semi-arid mountain watershed, *Eos Trans. AGU*, Fall Meet. Suppl., 78(46), Abstract H11G-07, 1997.
- Luce, C. H., D. G. Tarboton, and K. R. Cooley, The influence of the spatial distribution of snow on basin-averaged snowmelt, *Hydrol. Processes*, 12(10–11), 1671–1683, 1998.
- Maidment, D. R., ed., *Handbook of Hydrology*, 1424 pp., McGraw-Hill, New York, 1993.
- Shewchuk, J. R., Triangle. A two-dimensional quality mesh generator and Delaunay triangulator, Version 1.3, Sch. of Comp. Sci., Carnegie Mellon Univ., Pittsburgh, Pa., 1996.
- Shuttleworth, W. J., Evaporation, in *Handbook of Hydrology*, edited by D. R. Maidment, pp. 4.1–4.53, McGraw-Hill, New York, 1993.
- Tarboton, D. G., A new method for the determination of flow directions and contributing areas in grid digital elevation models, *Water Resour. Res.*, 33(2), 309–319, 1997.
- Tarboton, D. G., R. L. Bras, and I. Rodriguez-Iturbe, On the extraction of channel networks from digital elevation data, *Hydrol. Processes*, 5(1), 81–100, 1991.
- Tarboton, D. G., and C. H. Luce, *Utah Energy Balance Snow Accumulation and Melt Model (UEB), Computer Model Technical Description and Users Guide*, Utah Water Res. Lab., Logan, 1996.
- Tarboton, D. G., and U. Shankar, The identification and mapping of flow networks from digital elevation data, *Eos Trans. AGU*, Fall Meet. Suppl., 79(45), Abstract H71D-02, 1998.
- U.S. Army Corps of Engineers, *Snow Hydrology, Summary Report of the Snow Investigations*, 437 pp., N. Pac. Div., Portland, Oreg., 1956.

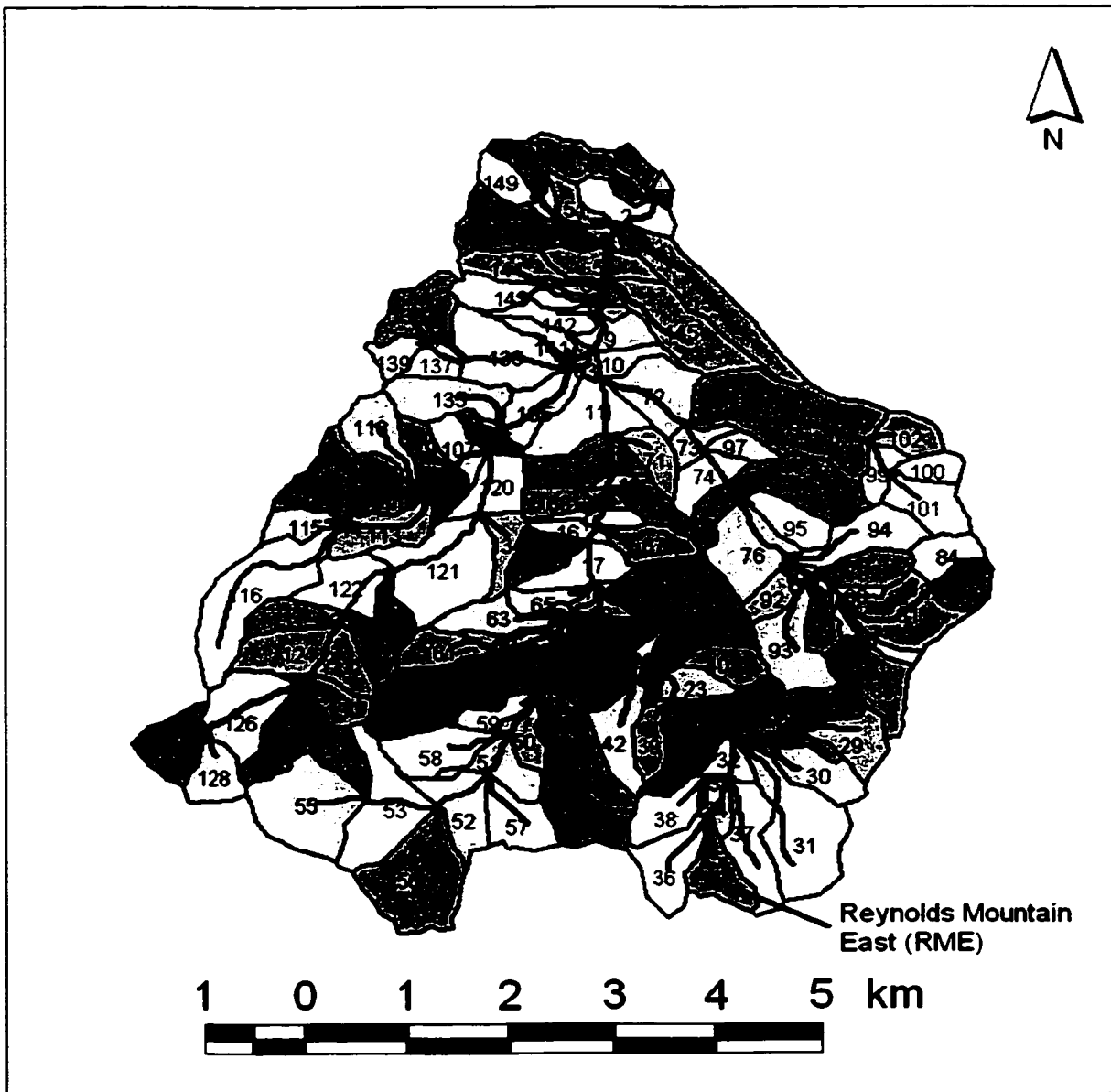


Figure 4-1. Subwatersheds of Tollgate. The corresponding stream network is shown by dark solid lines. The triangle denotes the location of the outlet streamflow gage. The rectangle marks the boundary inside which snow transport model simulation was performed to determine the snow drift factor map.

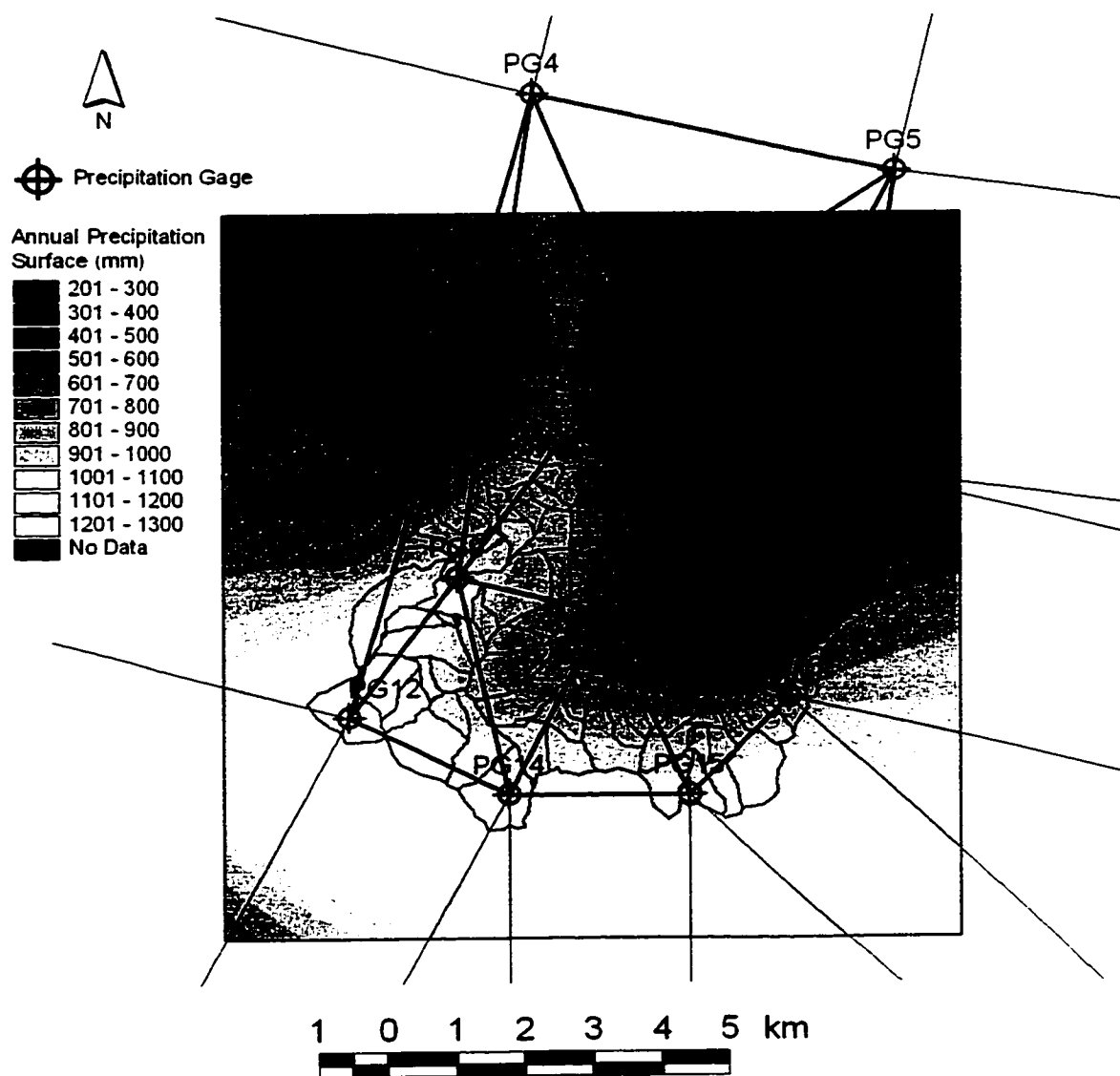
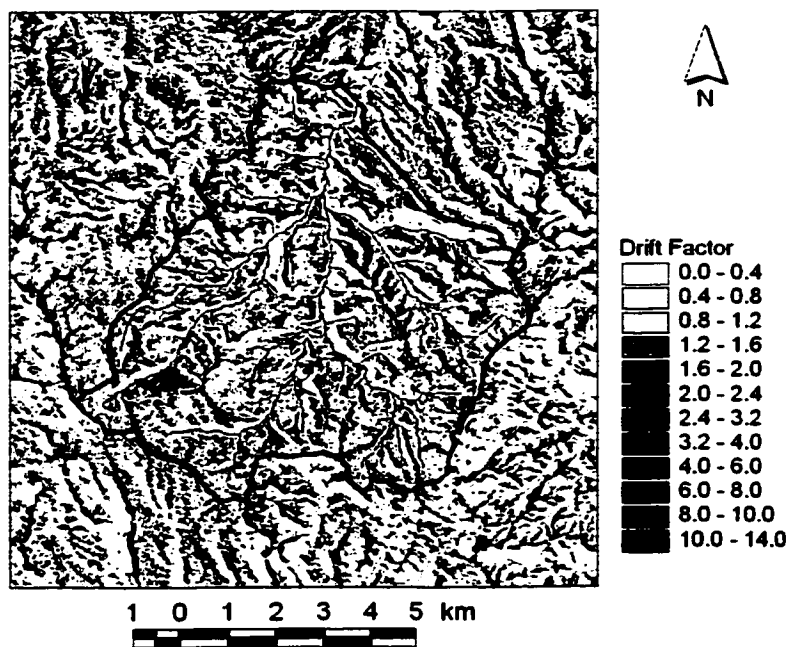


Figure 4-2. Annual precipitation surface from *Hanson* [1982], precipitation gages and extended Delaunay triangulation.



(a)



(b)

Figure 4-3. (a) Drift factor map simulated by the snow transport model. (b) Drift factor zones at Tollgate. White area is zone 1 ($0.0 \leq DF < 0.5$), green area is zone 2 ($0.5 \leq DF < 1.0$), and yellow area is zone 3 ($DF \geq 1.0$).

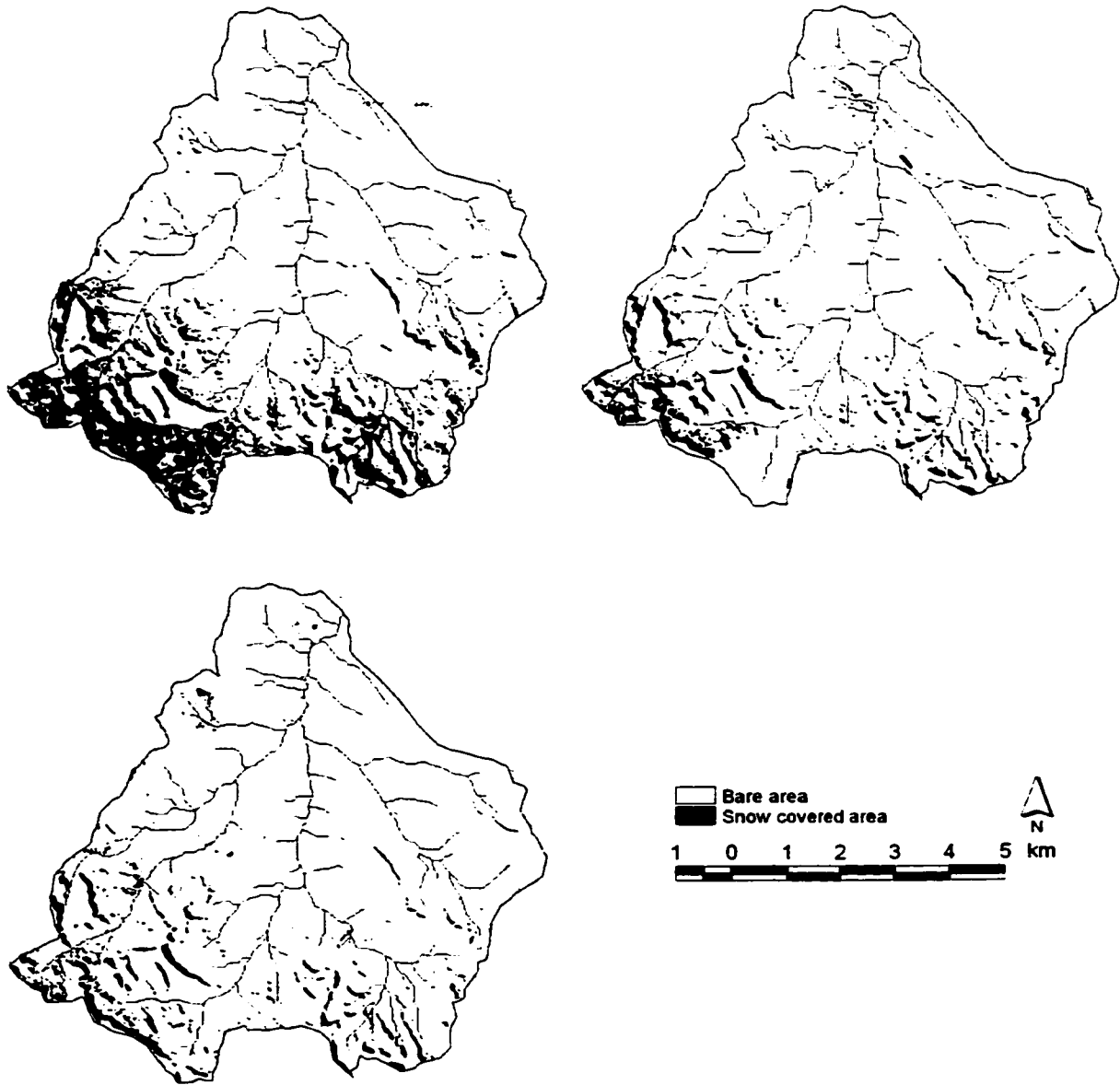


Figure 4-4. Snow-covered area at Tollgate obtained from classification of aerial photographs. Top left: May 11, 1971, top right: May 23, 1969, and bottom: June 3, 1989.

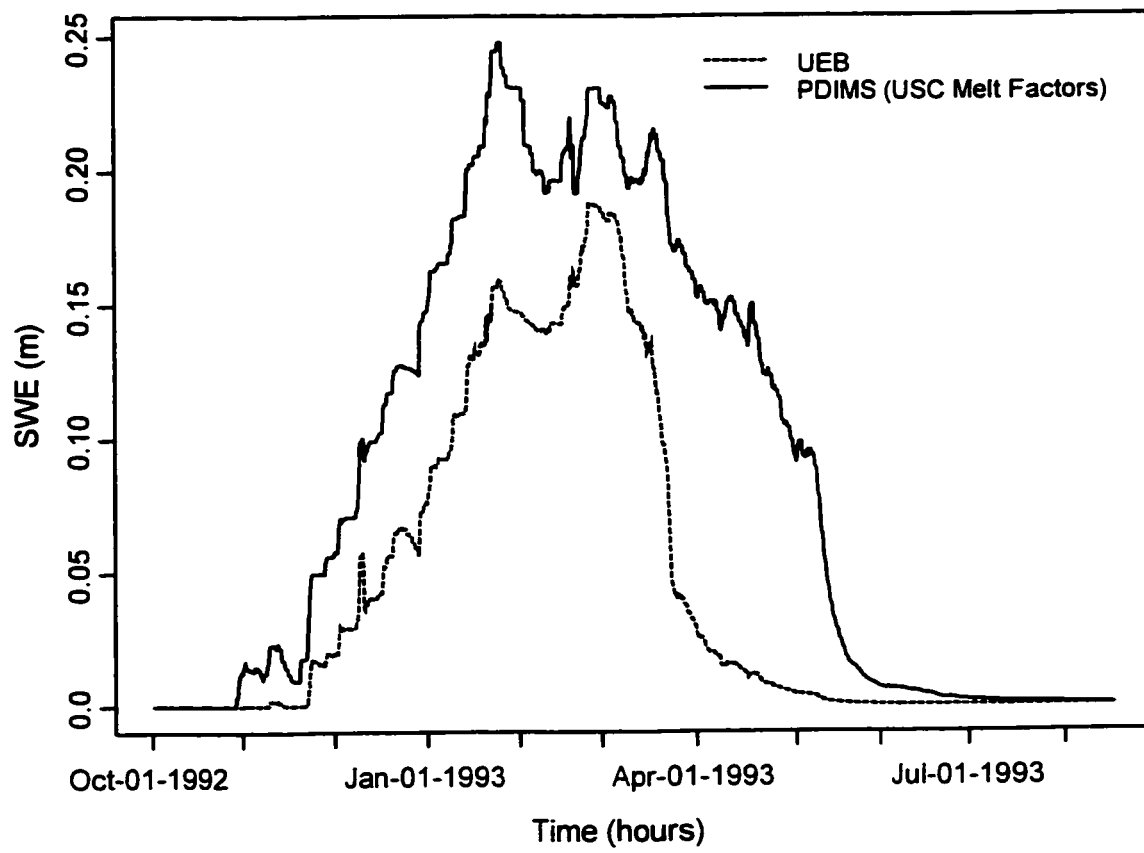


Figure 4-5. Time series of modeled basin average snow water equivalence at Tollgate during 1992-93.

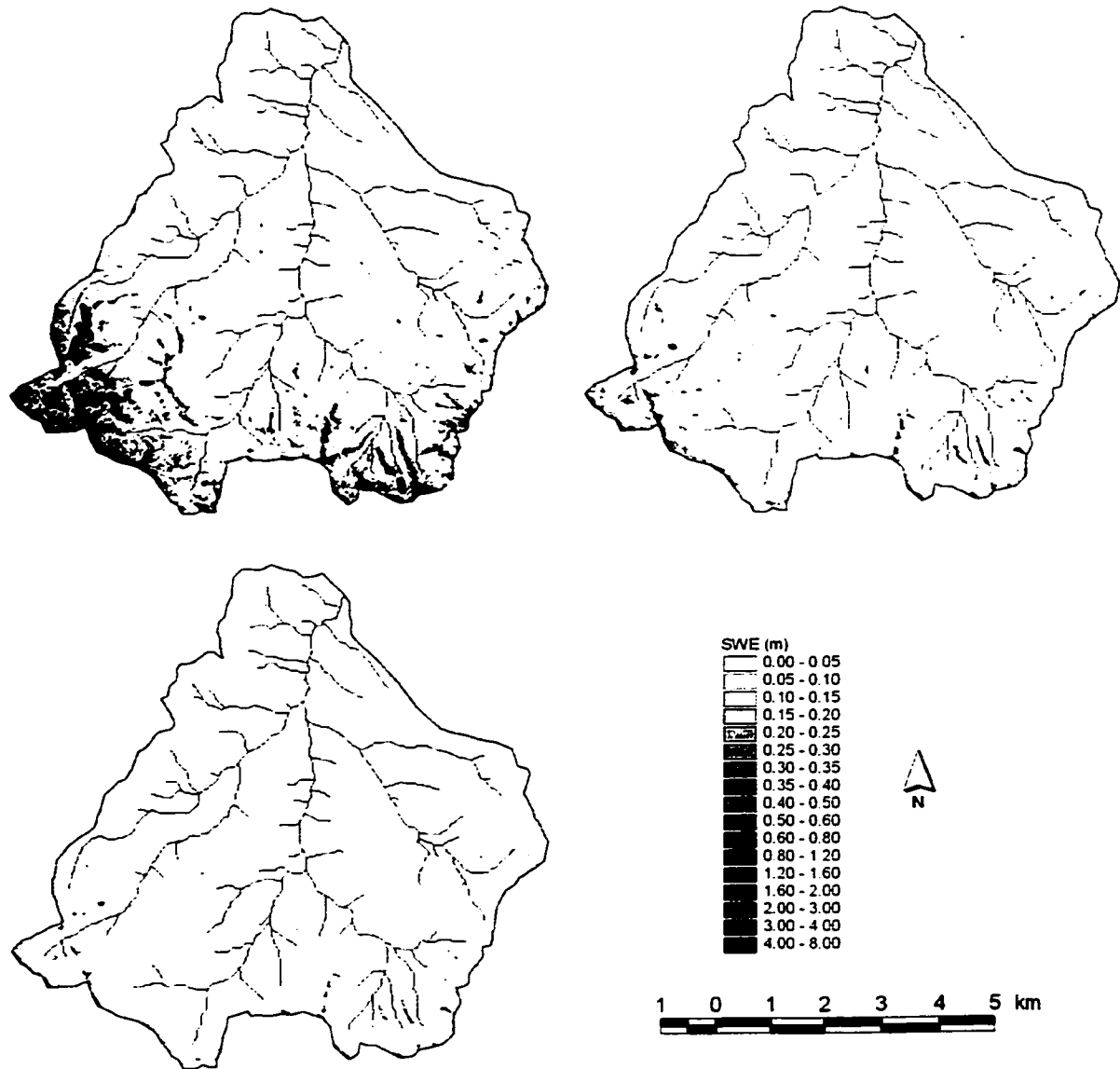
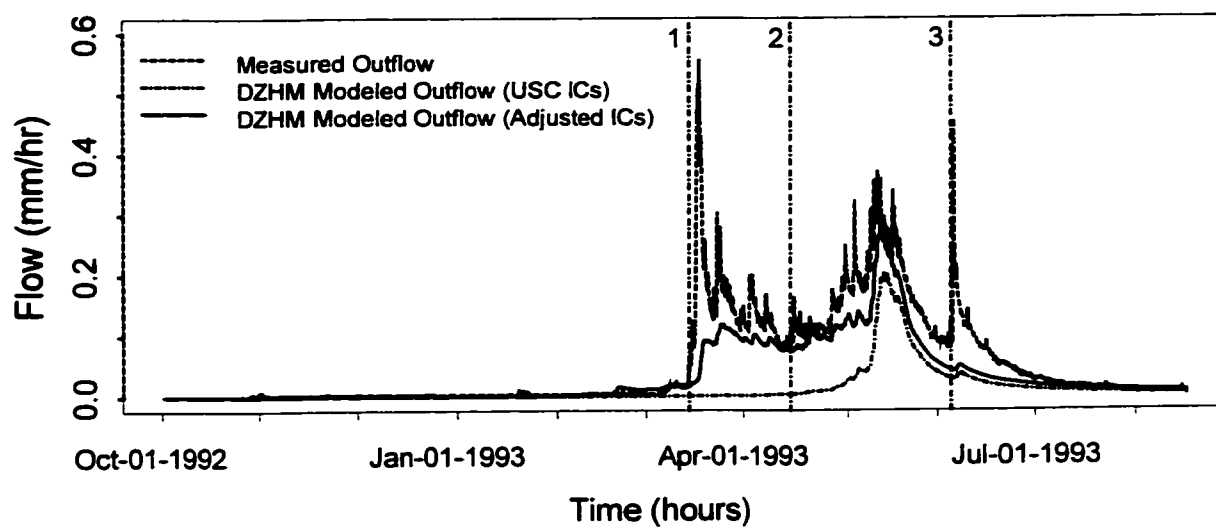
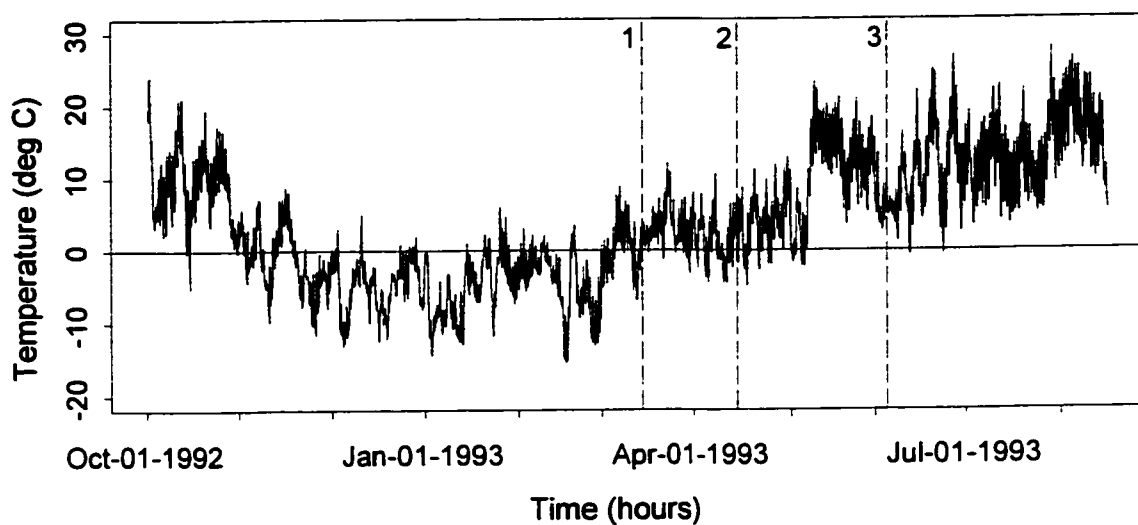


Figure 4-6. PDIMS modeled snow water equivalence maps at Tollgate. Top left: May 11, 1993, top right: May 23, 1993 and bottom: June 3, 1993.

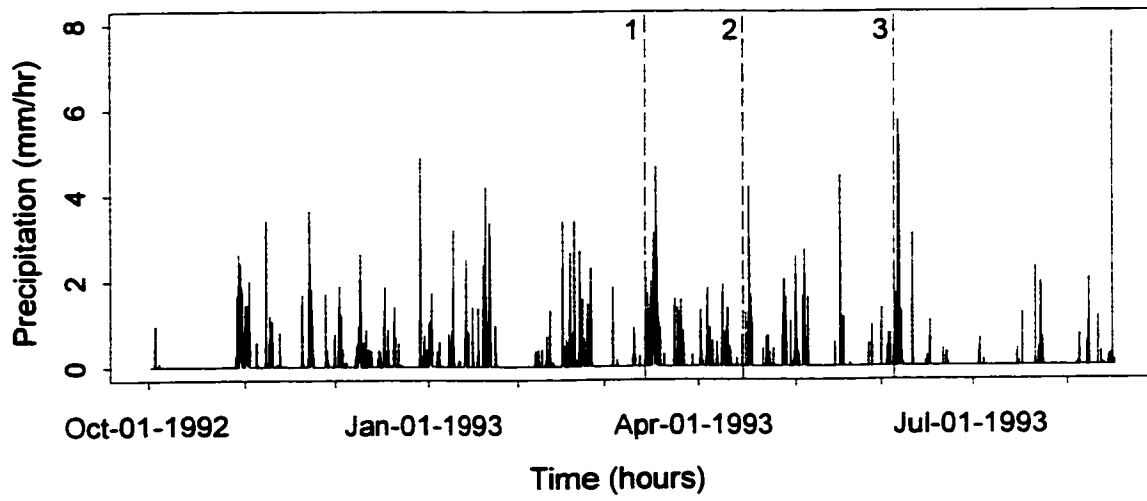


(a)

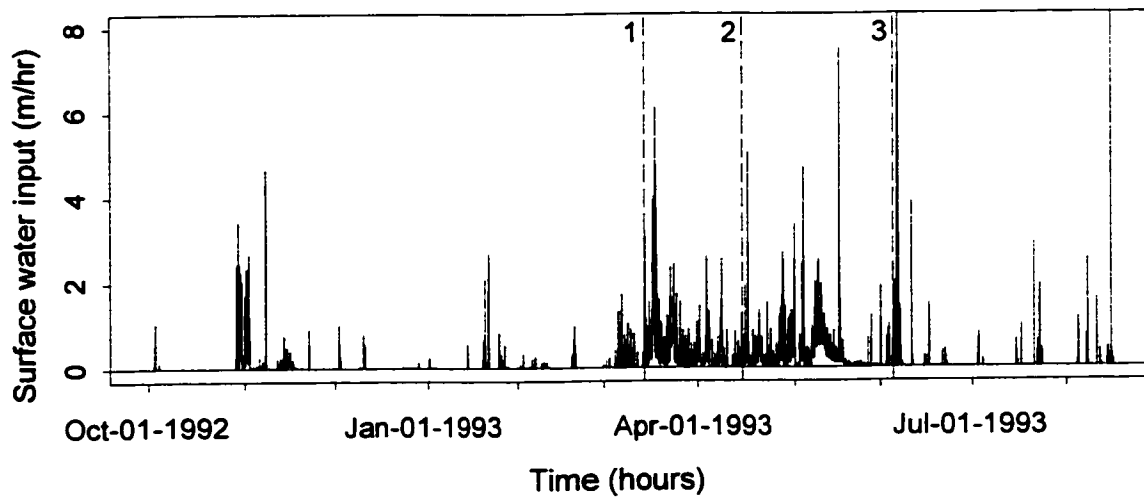


(b)

Figure 4-7. (a) Measured and DZHM modeled streamflow. (b) Mean air temperature. (c) Mean measured precipitation. (d) Basin average surface water input at Tollgate during 1992-93.



(c)



(d)

Figure 4-7. Continued.

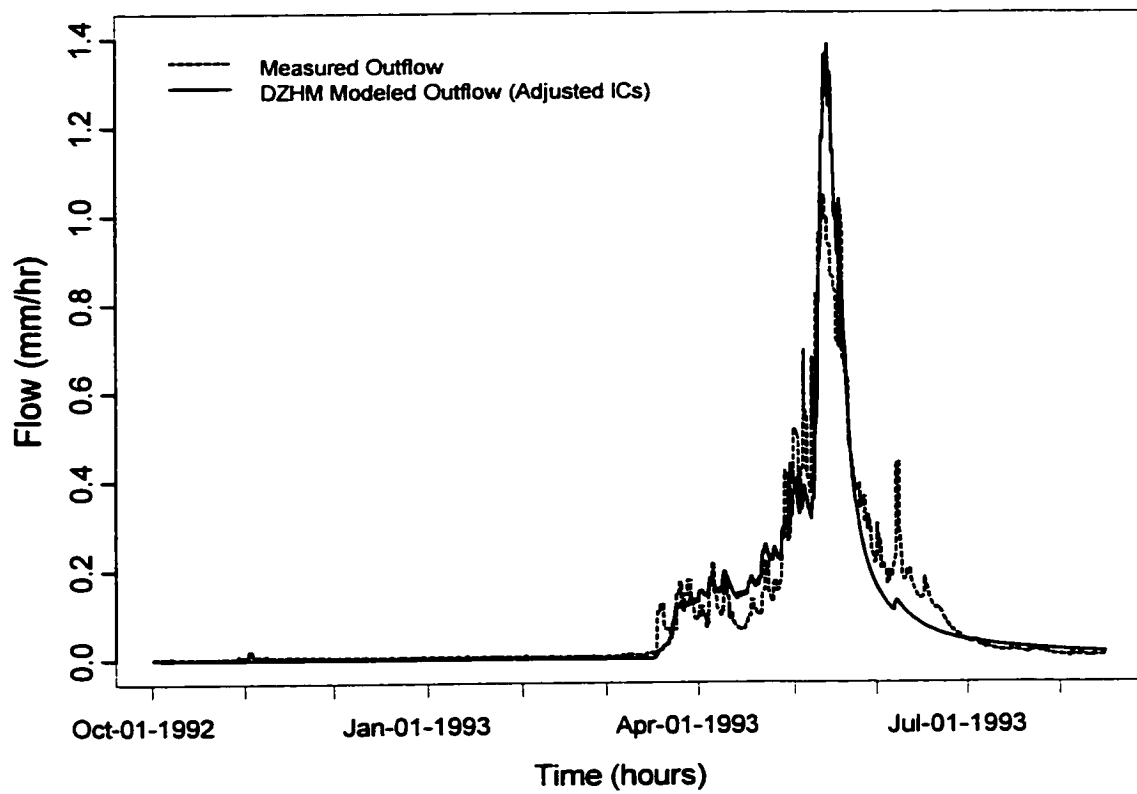


Figure 4-8. Internal check for DZHM: comparison between measured and DZHM-modeled streamflow at the outlet of Reynolds Mountain East (subwatershed #35 in Figure 4-1).

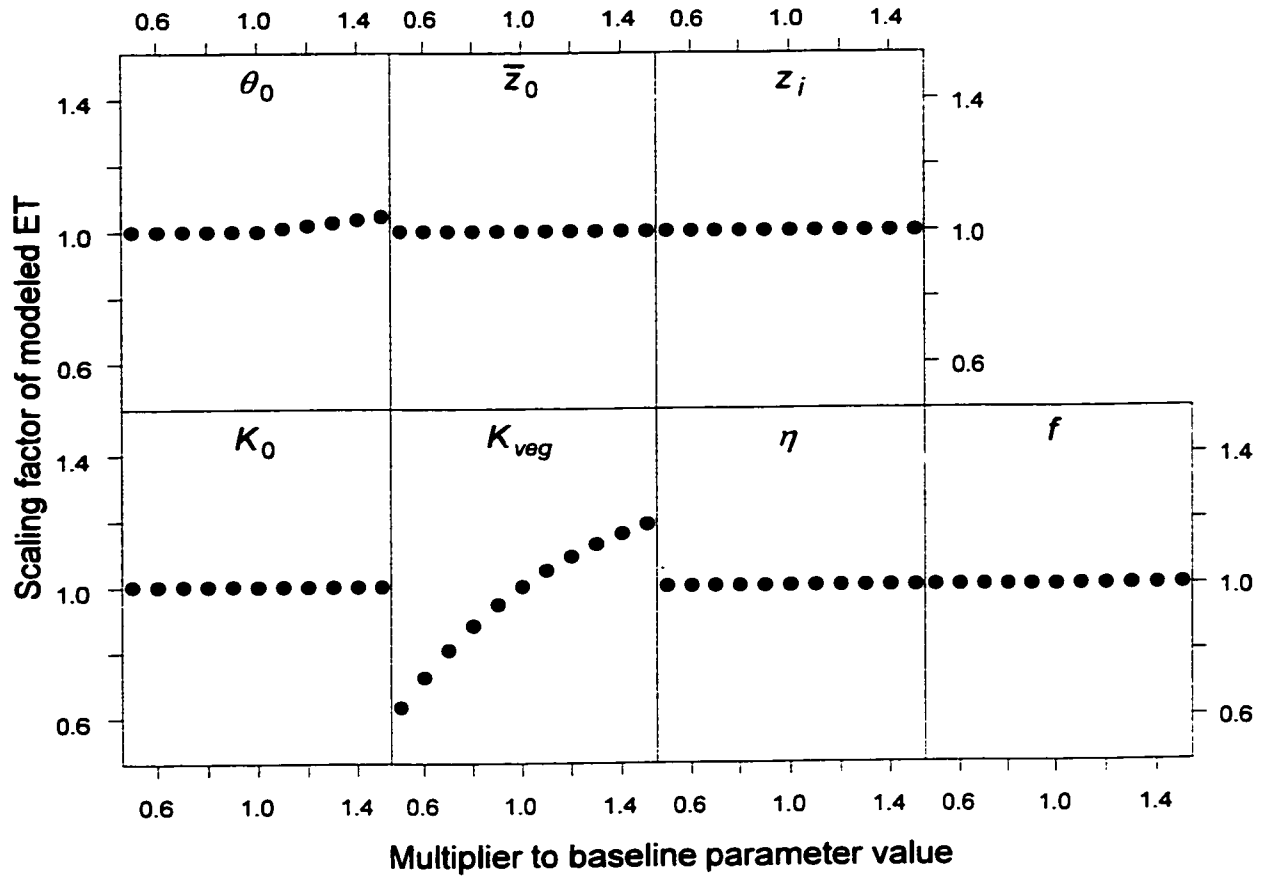


Figure 4-9. Sensitivity of modeled ET to DZHM parameters and initial conditions.

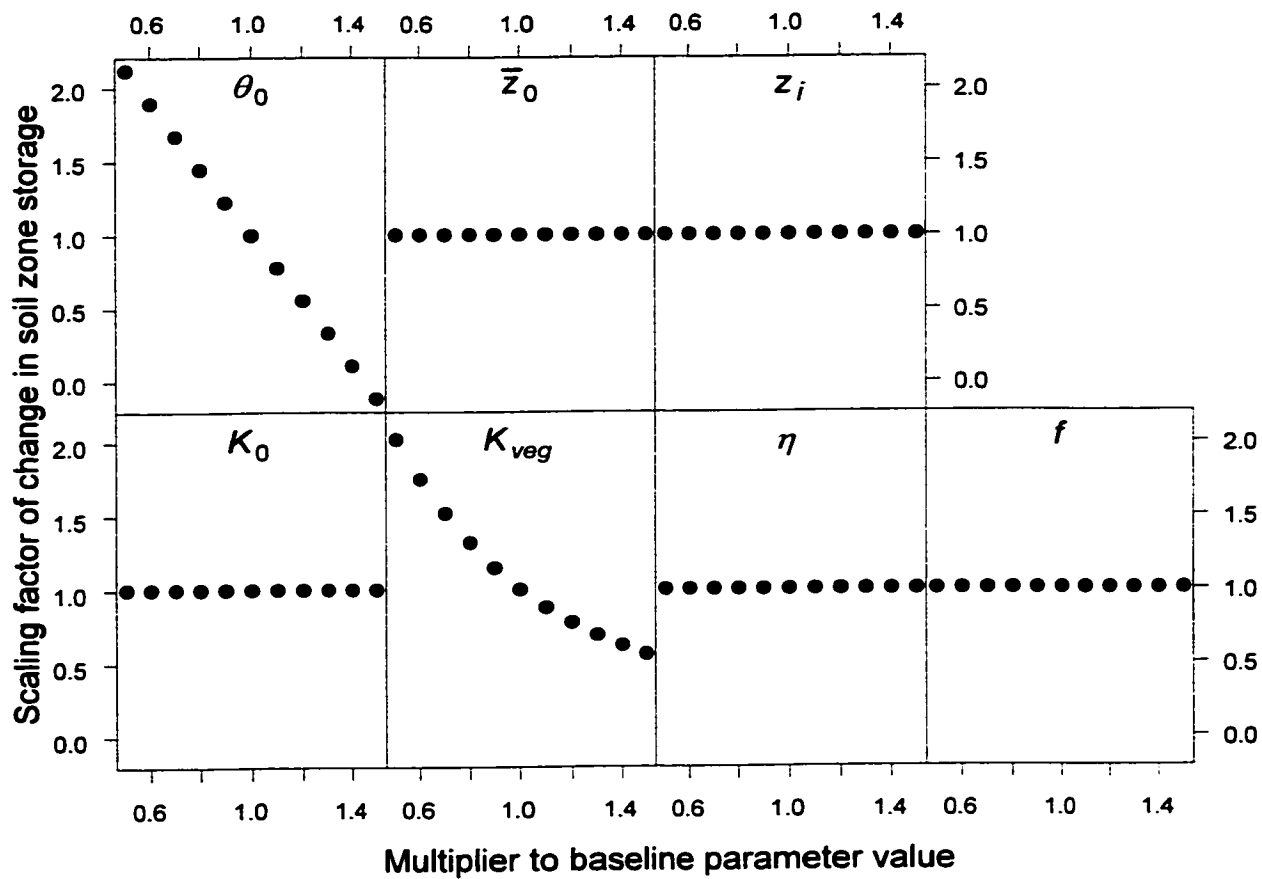


Figure 4-10. Sensitivity of modeled change in soil zone storage to DZHM parameters and initial conditions.

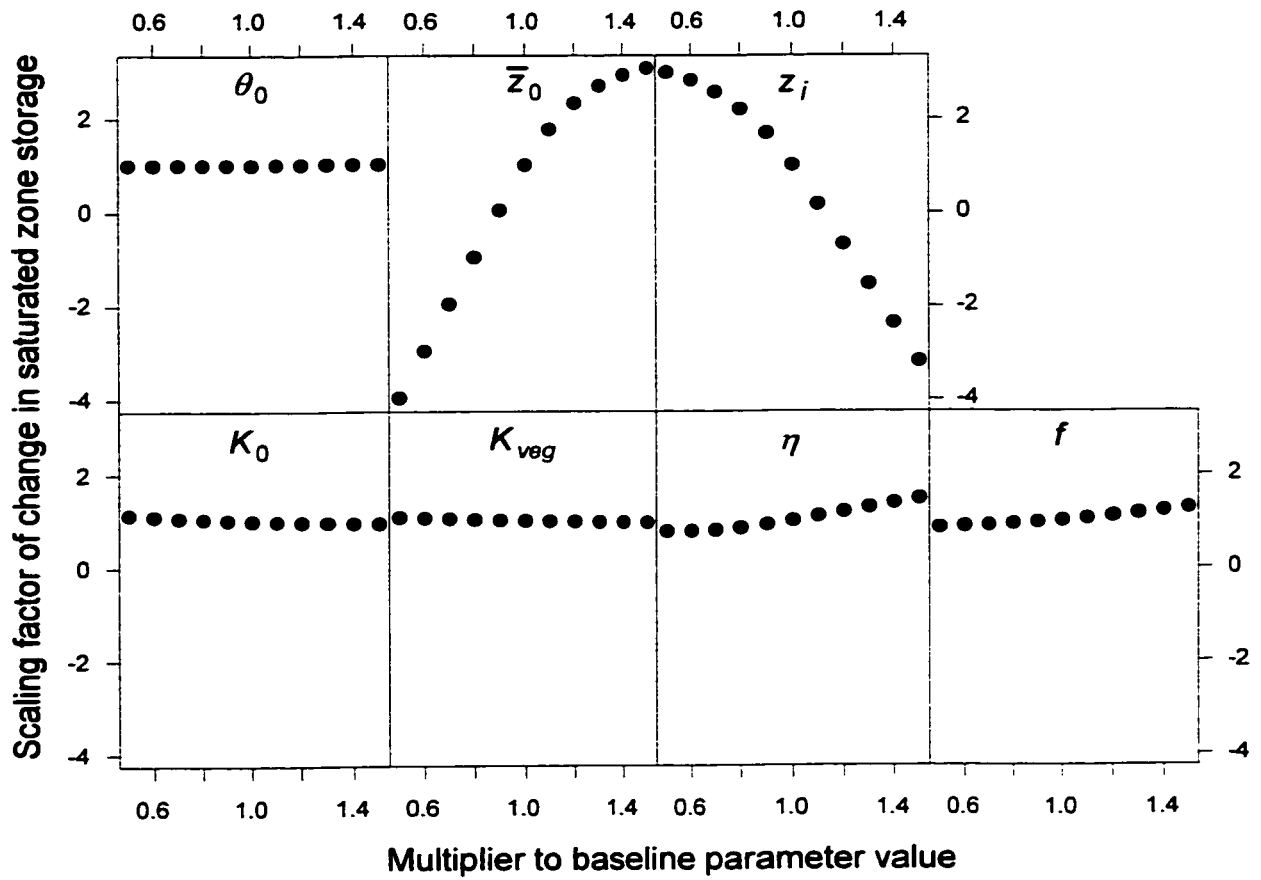


Figure 4-11. Sensitivity of modeled change in saturated zone storage to DZHM parameters and initial conditions.

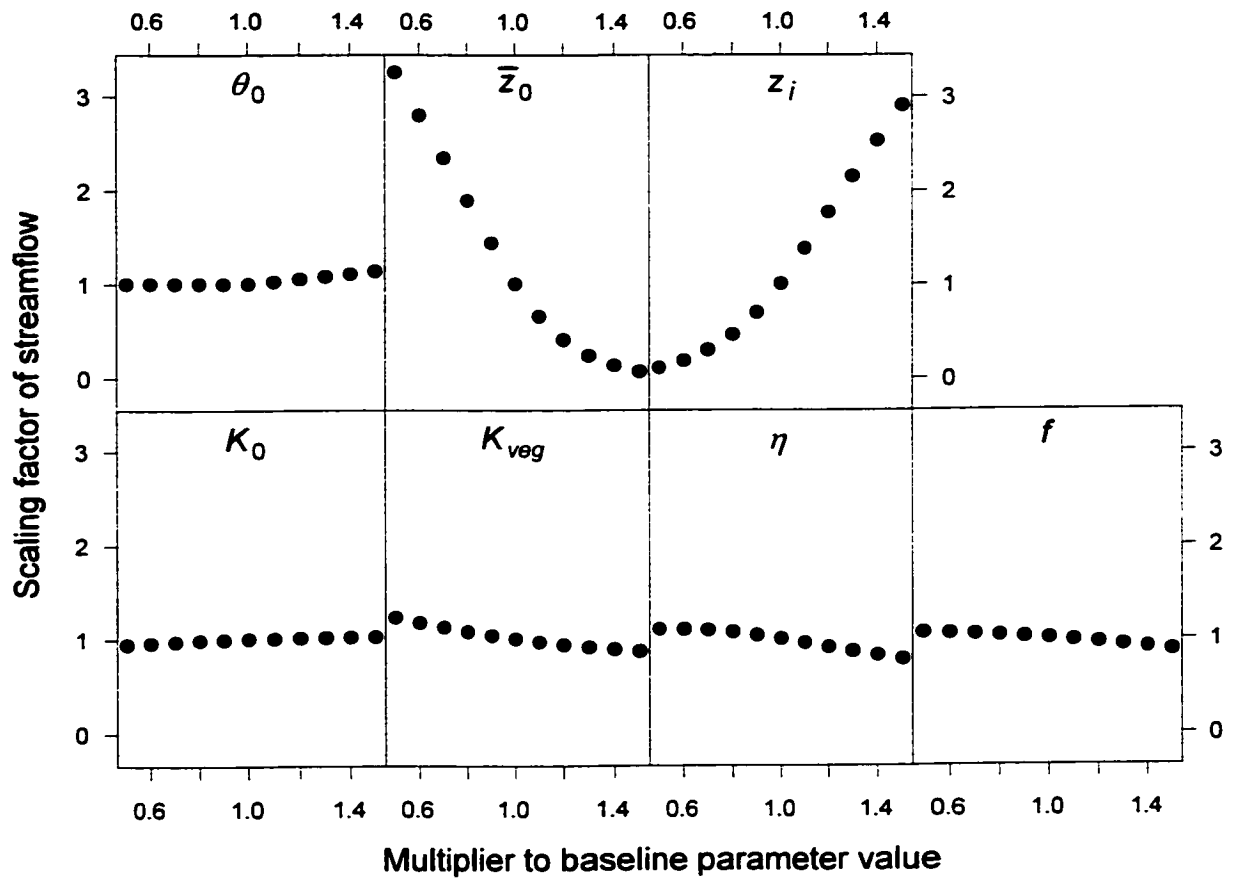


Figure 4-12. Sensitivity of modeled streamflow to DZHM parameters and initial conditions.

CHAPTER 5

SUMMARY, CONCLUSIONS, AND RECOMMENDATIONS

1. Summary

The objectives of the study described in this dissertation were to understand the hydrologic processes acting in Reynolds Creek Experimental Watershed (RCEW, see Figure 2-1) at a range of scales, to identify the dominant hydrologic processes at the watershed scale, and to further hydrologic understanding in order to provide a basis for building hydrologic models for RCEW. Results from hydrologic data analysis and modeling at RCEW, were presented in the preceding chapters. This chapter summarizes the findings of this study and recommends avenues for further research.

RCEW is a semiarid environment and is dominated by snow drifting during winter and snowmelt during spring. The precipitation in RCEW is highly variable in space due to prevalent southwesterly storm paths and elevation effects (Figure 4-2). Most of the winter precipitation falls as snow and is stored until it melts in the spring. The snowpack is redistributed in space in response to strong southwesterly winds, especially at higher elevations. This redistribution results in relatively thin net snow accumulation on hillslopes that are generally south-facing windward sides, and deep snow drifts on hillslopes that consist of generally north-facing leeward sides. This wind-induced redistribution of snow is of utmost importance in this watershed because snowmelt from the highly variable snowpack results in highly variable surface water input to the soil. This effect can be seen in preferential vegetation patterns and soil types,

which have developed over eons in this watershed. The south-facing windward slopes accumulate less snow, and so can only support shrubs on relatively thin soils. The north-facing slopes accumulate deep snowdrifts, which sustain water input into the soil much later into the spring, and can support more diverse vegetation types like Aspen and pines on deeper soils. Most of the pine stands in this watershed occur on the north-facing slopes on or directly below the deep snowdrift zones.

The first step during this study was to develop a parameterization for capturing the spatial pattern of snow drifting. During 1992-93, nine measured snow water equivalence (SWE) maps were available (Figure 2-2). The spatial pattern of snow accumulation, drifting and melt was reflected in these measurements. The drift factor concept was used (Chapter 2) to include snowdrift in the snow accumulation and melt modeling. During early winter, there was small but significant snowmelt. The Utah Energy Budget (UEB) snow accumulation and melt model, which is a physically based point model, was used to estimate early season melt. Drift factors were calibrated at each grid cell of USC (Figure 2-3) by minimizing the sum of unsigned errors in modeled SWE as compared to the first three of nine SWE measurements.

The nature of surface water input at the watershed scale was examined by analyzing the distribution of drift factors at USC (Figure 2-8). This analysis indicated that USC could be partitioned into three surface water input zones based on breaks in the distribution of drift factors at 0.5 and 1.0. The corresponding zones are shown in Figure 2-4, which agreed closely with watershed zones based on soil and vegetation types used previously in literature. The distribution of the drift factor thus provided a quantitative

basis for dividing USC into surface water input zones. Establishing this quantitative basis was one of the most important contributions of this work.

The time series of cumulative surface water input for the three SWI zones showed the importance of subdividing USC into these zones (Figures 2-9 and 2-10). The timing of measured streamflow at the outlet of USC was in close agreement to the timing of a rapid rise in the cumulative SWI on zone 3. During this time, zones 1 and 2 did not show appreciable increase in SWI. Also, as computed later, the cumulative potential evapotranspiration (ET) demand for the simulation period was greater than cumulative SWI for zones 1 and 2 in contrast to zone 3 where it was less than cumulative SWI (Table 2-4). This observation suggested that streamflow generation from zone 3 was more likely than that from zones 1 and 2. These observations led to the working hypothesis at USC: most of the streamflow was generated by the deep snowdrift on zone 3, which melted late into spring, whereas surface water input on zones 1 and 2 was used mainly to satisfy ET and soil storage demands.

In order to understand the behavior of other annual-scale hydrologic fluxes, it was necessary to simulate SWI into the three zones as accurately as possible. The SWI model was built using UEB to simulate snow accumulation and melt over a 30-m grid at USC for the period October 1, 1992 to August 16, 1993 at hourly time steps. The SWI model was driven by drift adjusted precipitation and radiation computed over the DEM (see Chapter 2 and Appendix A). It was found that UEB melted snow more rapidly than that observed during spring. An index-based model called the Pseudo-Distributed Index-based Model for Snowmelt (PDIMS) was developed and calibrated using the SWE

measurements at USC. The SWI model using PDIMS in place of UEB resulted in a more accurate simulation of SWI at USC (Figure 2-4).

A relatively simple hydrologic model called the Dominant Zone Hydrologic Model (DZHM) was built to test the working hypothesis described above. This model included lumped parameterizations of vegetation, soil and baseflow components for each SWI zone (Chapter 2). DZHM received aggregated surface water input for each zone from the SWI model, and partitioned it into ET, soil and saturated zone storage, and streamflow. Some of the parameters of this model were obtained based on other ancillary data, or set to reasonable value in absence of any other supporting information. The other parameters were calibrated using measured data at USC. The parameters and their prescribed or calibrated values are shown in Table 2-3. The annual mass balance components at USC (ET, change in soil and saturated zone storage and streamflow) were simulated satisfactorily (Figure 2-12 and Table 2-4).

It was concluded that the hydrologic behavior at the scale of a first-order watershed in RCEW was primarily controlled by the spatially varying surface water input, which was a direct consequence of the wind-induced redistribution of snow in the watershed. The variability of surface water input can be described by the distribution of drift factors (Figure 2-8), which also provided the quantitative basis for delineating the watershed into SWI zones.

It was possible to calibrate drift factors for USC at the grid scale since SWE measurements were available at this scale. It is impractical to obtain such measurements at scales larger than that of USC. Alternatives to measurements include physically based

blowing snow models, which can simulate redistribution of snow over larger domains. Chapter 3 described a study that evaluated the performance of SnowTran-3D, which is a three-dimensional snow transport model, at USC where measured SWE maps were available. The objective of this study was to evaluate the sensitivity of the model to precipitation and vegetation inputs, and to test the linearity assumption implicit in the drift factor concept. Four input scenarios were considered by combining two precipitation inputs and two vegetation patterns at USC. The precipitation inputs consisted of measured precipitation from two measurement gages in RCEW: PG8, which is located at USC, and PG12, which is located in the southwest corner of RCEW, and received the greatest amount of precipitation of all gages in RCEW. Precipitation input to SnowTran-3D was spatially uniform. The vegetation inputs consisted of a spatial pattern obtained from classification of a LANDSAT image, and a uniform vegetation pattern consisting of the most prevalent vegetation class at RCEW. SnowTran-3D was run at hourly time steps over the same 30-m grid used before in Chapter 2.

Results from SnowTran-3D runs were evaluated by (1) pointwise comparison of measured and modeled SWE, (2) visual comparison of spatial pattern of snow accumulation, (3) comparison of basinwide averages of measured and modeled SWE, (4) comparison of measured and modeled accumulation and scour in the corresponding zones, and (5) comparison of the distribution of measured and modeled drift factors. It was found that the modeled basin average SWE was in reasonably good agreement with measurements. The spatial patterns of snow accumulation were shifted with respect to observations. The fraction of explained variance of the distribution of observation-based

drift factors was close to 90% when precipitation from the same site (PG8) was used. The fraction of explained variance degraded to 75% when precipitation from PG12 was used. The precipitation at PG12 during the SnowTran-3D simulation period was 69% more than that at PG8. The reduction in explained variance of the distribution of drift factors was of the order of 15% (i.e., 90% – 75%), if precipitation other than the actual was used for a watershed. This observation indicated that drift factors provided by SnowTran-3D could be used to parameterize the distribution of drift factors with an error bound of about 25% in a watershed where the variability of precipitation between measurement sites was of the order of 70%. This was an important finding, because it allowed the use of drift factors obtained from a single SnowTran-3D simulation driven by spatially uniform precipitation, without coupling SnowTran-3D with the rest of the hydrologic model. It should also be noted here that if the drift factors from SnowTran-3D were used in a pointwise fashion, errors would be larger, since the pointwise comparison was poorer.

Chapter 4 described a study to examine whether the understanding of the behavior of annual-scale hydrologic mass-balance gained at small scale (USC) was transferable to a larger, fourth-order watershed, Tollgate, within RCEW. SnowTran-3D was used to obtain drift factors at Tollgate because no SWE measurements were available, nor are practicable at this scale. Digital terrain analysis was used to partition Tollgate into 153 subwatersheds, each of which consisted of an area draining to a channel link in the fourth-order stream network, which drains Tollgate. Since SWI was the largest source of

spatial variability in RCEW, each of the subwatersheds of Tollgate were divided into three SWI zones following the same scheme as in Chapter 2.

The transferability of hydrologic understanding was tested in two parts: (1) the above-surface component, which consists of the SWI model, was tested for transferability of PDIMS melt factors calibrated previously at USC (Chapter 2), and (2) the below-surface component, which consists of DZHM, was tested for transferability of DZHM parameters calibrated previously at USC (Chapter 2).

The SWI model, which used PDIMS with melt factors calibrated at USC, was used to compute snow accumulation and melt at each of the 153 subwatersheds of Tollgate over the 30-m USGS DEM grid. The only data available for testing the performance of PDIMS was a set of snow cover maps obtained from classification of aerial photographs of Tollgate (Figure 4-4). Although these maps corresponded to different years, these years were similar to the simulation year used in this study in terms of volume of annual streamflow during and one previous year based on 34 years of streamflow records (Chapter 4). Pointwise comparison between the modeled maps and the snow cover maps obtained from photographs was poor, which was a result of the poor pointwise match between SnowTran-3D simulations and observations reported in Chapter 3. The map of modeled SWE on the same days of the year when the snow cover photographs were taken, compared well visually in terms of snow-covered area, although the modeled maps showed less coverage compared to the photographs. This difference might be attributed to interannual variations between the simulation year (1992-93) and the years when the photographs were taken (1969, 1971, and 1989).

Hourly SWI was computed for each SWI zone using PDIMS with melt factors calibrated at USC by aggregating the SWI for all grid cells that constitute the required zone. These SWI series were used for input to DZHM. The initial condition corresponding to the depth to the water table needed to be modified from the values used at USC (Chapter 2) to visually match the streamflow hydrograph from Tollgate. All parameters were kept spatially uniform in a zonewise fashion. This allowed the analysis to focus on the importance of spatio-temporal pattern of SWI at Tollgate and the validity of the DZHM parameter transferred from USC to Tollgate. The general agreement of the timing of secondary peaks between the measured and modeled hydrograph suggested that most of the variability in annual-scale streamflow at Tollgate was due to the spatial variability of SWI. The comparison between measured and modeled hydrograph also suggested that runoff from frozen ground and partially saturated areas within Tollgate might be of importance. These processes were not included in DZHM, and might need to be parameterized in order to reproduce peak streamflow in the measured annual streamflow at Tollgate (Chapter 4).

A sensitivity analysis focussing on the parameters and initial conditions of DZHM revealed that the annual-scale hydrologic fluxes at Tollgate were most sensitive to the DZHM parameter for vegetation K_{veg} , DZHM parameter for saturated zone threshold z_i , the initial soil moisture θ_0 , and the initial depth to the water table \bar{z}_0 . It is important to know these parameters and initial conditions accurately, which may provide further avenues for research at RCEW.

2. Conclusions

The main contributions from this study are listed below:

- (1) A quantitative basis for delineation of watersheds into modeling elements at RCEW was established. Since the largest source of spatial variability in RCEW was due to surface water input, this delineation was based on the distribution of drift factors, which quantitatively describe the spatial variability of surface water input within the watershed.
- (2) It was shown that the drift factor concept could be used to parameterize wind-induced drifting of snow at RCEW. The drift factors obtained from a physically-based blowing snow model could also be used to decouple the process of drifting from the modeling of other components of the hydrologic fluxes, while keeping errors within reasonable bounds.
- (3) Understanding of small-scale hydrologic behavior was mostly transferable from a first-order watershed to a fourth-order watershed in the same region. Demonstration of this ability has significant consequences toward simplifying watershed-scale hydrologic modeling and upscaling.

3. Recommendations

Further study in RCEW should focus on determination of model parameters and initial conditions listed above. Some of these are expected to present significant challenges, especially at scales as large as that of Tollgate. Runoff from frozen ground

and partially saturated areas needs to be included in DZHM in order to better reproduce peaks in annual streamflow hydrograph.

The modeling philosophy presented here should also be applied to watersheds other than Reynolds Creek to validate the generality of the philosophic arguments made in this dissertation. The specific approach used here should at least be applicable to snow drift and melt dominated watersheds. The general idea of building simpler hydrologic models based on dominant processes should be of great interest to hydrologists because it allows us to capture the internal dynamics of the watershed processes in spite of simplifying assumptions. This capability is essential because hydrologists are increasingly being called upon to help facilitate decision making under uncertain and/or undocumented changes, often at scales as large as that of continents.

There are some issues that have a more general significance in hydrologic modeling:

- (1) Surface water input in this study was obtained by simulation of snow accumulation and melt on a grid scale, which was then aggregated to the zone scale to drive the hydrologic model at the zone scale. A better approach may include subzone parameterization of spatial variability to upscale the SWI modeling to the zone scale.
- (2) The validity of the drift factor concept, especially that of linearity in terms of interannual variability of precipitation needs to be determined. This issue may be of critical importance in terms of understanding the impacts of long-term

changes, such as climate warming or anthropogenic effects that change watershed properties.

APPENDICES

Appendix A: The Radiation Model

This appendix describes the methodology adopted for computing spatially distributed net radiation. The purpose of this method is to estimate direct shortwave, diffuse shortwave sky and net longwave radiation components accounting for the effects of terrain (i.e. slope, aspect and shading) so as to obtain spatially distributed radiation inputs suitable for spatially distributed snowmelt and evapotranspiration modeling.

A1. Shortwave Radiation

Observed global radiation (direct beam plus diffuse sky) measurements recorded by a horizontally mounted pyranometer are compared to extraterrestrial radiation (radiation without atmospheric effects) for each model time step to infer the absorption and scattering properties of the atmosphere. These inferred properties are then used to model radiation at each point in a spatially distributed model, accounting for the effects of terrain (slope, aspect and shading).

A1.1. Extraterrestrial Radiation

The instantaneous extraterrestrial radiation flux i_{et} on a horizontal surface is given by

$$i_{et} = I_0 \cdot \cos \psi \quad (\text{A1})$$

where I_0 is the solar constant (1367 W m^{-2}), and ψ is the solar zenith angle given by [Dingman, 1994]:

$$\cos \psi = \sin \phi \cdot \sin \delta + \cos \phi \cdot \cos \delta \cdot \cos \omega t \quad (\text{A2})$$

where ϕ is the latitude (radian), ω is the angular velocity of earth's rotation (0.2618 radian h⁻¹), t is the time in number of hours before (-ve) or after (+ve) true solar noon, and δ is the declination (radian) of the sun given by

$$\delta = \frac{23.5\pi}{180} \cdot \sin \left[\frac{2\pi}{365} \cdot (D - 82) \right] \quad (\text{A3})$$

where D is the Julian day ($1 \leq D \leq 365$ or 366).

The instantaneous extraterrestrial radiation flux is integrated over a time step (t_1 , t_2) to give the integrated extraterrestrial radiation flux on a horizontal plane I_{et} :

$$I_{et} = \frac{1}{(t_2 - t_1)} \cdot \int_{t_1}^{t_2} i_{et} dt = \frac{I_0}{(t_2 - t_1)} \cdot \int_{\text{Max}(t_1, t_{sr})}^{\text{Min}(t_2, t_{ss})} \cos \psi dt \quad (\text{A4})$$

where t_{sr} and t_{ss} denote sunrise and sunset times and the Max and Min operations ensure that the period of integration does not include time when the sun is below the horizon.

We use the analytical expression based on Dingman [1994, p535] to evaluate the above integral.

A1.2. Direct and Diffuse Components of Extraterrestrial Radiation

The hourly clearness index, k_t , is defined as [see page 77, *Duffie and Beckman*, 1991]:

$$k_t = \frac{I_{swobs}}{I_{et}} \quad (A5)$$

where I_{swobs} is the measured global radiation averaged over the measurement time period.

The diffuse fraction of global radiation is given by [*Erbs et al.*, 1982]:

$$\begin{aligned} f_{dif} &= 1.0 - 0.09 \cdot k_t && \text{for } k_t \leq 0.22 \\ &= 0.9511 - 0.1604 \cdot k_t + 4.3380 \cdot k_t^2 - \\ &\quad 16.6380 \cdot k_t^3 + 12.336 \cdot k_t^4 && \text{for } 0.22 < k_t \leq 0.80 \\ &= 0.165 && \text{for } k_t > 0.80 \end{aligned} \quad (A6)$$

and the direct and diffuse components of the measured global radiation are given as

$$\begin{aligned} I_{dif} &= f_{dif} \cdot I_{swobs} \\ I_{dir} &= (1 - f_{dif}) \cdot I_{swobs} \end{aligned} \quad (A7)$$

We note here that if the pyranometer location is significantly influenced by terrain shading (e.g., if the pyranometer is located in a valley), then the measured global

radiation $I_{s_{wobs}}$ will be reduced relative to an open horizontal location, resulting in reduction in k_t and increase in f_{dif} . This effect will be worse near sunrise and sunset. Since the radiation near sunrise and sunset is a small fraction of radiation received during the whole day, we neglect this effect.

A1.3. Estimation of Direct and Diffuse Radiation on Grid Cells

The extraterrestrial radiation flux on a sloping plane is computed by using the equivalent plane concept (Dingman, 1994). The difference in longitude between the location of the original slope and that of the equivalent plane is given by

$$\Delta\Omega = \tan^{-1}\left(\frac{\sin \beta \cdot \sin \alpha}{\cos \beta \cdot \cos \varphi + \sin \beta \cdot \sin \varphi \cdot \cos \alpha}\right) \quad (\text{A8})$$

where β is the slope of the plane (+ve downward), and α is the aspect (direction) of the slope (counterclockwise from south). The equivalent latitude for the sloping plane is given by

$$\phi_{eq} = \sin^{-1}(\cos \beta \cdot \sin \varphi - \sin \beta \cdot \cos \alpha \cdot \cos \varphi) \quad (\text{A9})$$

Now, the incidence angle of the direct solar beam on the sloping plane ψ_{eq} is given by

$$\cos \psi_{eq} = \sin \phi_{eq} \cdot \sin \delta + \cos \phi_{eq} \cdot \cos \delta \cdot \cos (\omega t + \Delta \Omega) \quad (\text{A10})$$

and the integrated extraterrestrial solar radiation flux over the time interval (t_1, t_2) per unit horizontal area at a location \bar{x} can be expressed as:

$$R_{et}(\bar{x}) = \frac{I_0}{(t_2 - t_1) \cdot \cos \beta} \cdot \int_{\text{Max}(t_1, t_{sr})}^{\text{Min}(t_2, t_{ss})} \cos \psi_{eq} dt \quad (\text{A11})$$

In evaluating the integral in equation (A11) t_{sr} and t_{ss} are evaluated based upon horizon angles to account for terrain shading where present. As before the analytical expression for this integral based on Dingman (1994 p535) is used. The global radiation at location \bar{x} now can be estimated by using the hourly clearness index as

$$R_{sw}(\bar{x}) = k_t \cdot R_{et}(\bar{x}) \quad (\text{A12})$$

The direct radiation at any grid cell \bar{x} is

$$R_{dir}(\bar{x}) = (1 - f_{dif}) \cdot R_{sw}(\bar{x}) \quad (\text{A13})$$

The diffuse radiation at the grid cell \bar{x} is adjusted for the sky view factor $V_d(\bar{x})$.

The sky view factor is based on the assumption of isotropic sky radiation and is defined

as the ratio of the radiation incident on a point accounting for slope, aspect and terrain obstructions, to the equivalent radiation incident on an unobstructed horizontal surface. The sky view factor and horizon angles are evaluated following methods given by [see *Dozier and Frew, 1990*]. The diffuse sky radiation flux at the grid cell \bar{x} is thus given by

$$R_{dif}(\bar{x}) = f_{dif} \cdot R_{sw}(\bar{x}) \cdot V_d(\bar{x}) \quad (\text{A14})$$

A2. Longwave Radiation

Incoming longwave radiation from the atmosphere at any location \bar{x} , is estimated using the air temperature T_a (K) adjusted for an average lapse rate, cloudiness factor (f_{cloud}), and the sky view factor.

$$R_{lwr}(\bar{x}) = \{f_{cloud} \cdot \varepsilon_{cloud} + (1 - f_{cloud}) \cdot \varepsilon_{air}\} \cdot \sigma \cdot T_a(\bar{x})^4 \cdot V_d(\bar{x}) \quad (\text{A15})$$

where σ is the Stefan-Boltzmann constant ($5.67 \times 10^{-8} \text{ W m}^{-2} \text{ K}^{-4}$). Emissivity of clouds (ε_{cloud}) is set to 1.0, and emissivity of air (ε_{air}) is computed using Satterlund's [1979] formula based on humidity:

$$\varepsilon_{air} = 1.08 \cdot \left[1 - \exp \left\{ - \left(\frac{e_a}{100} \right)^{T_a/2016} \right\} \right] \quad (\text{A16})$$

where e_a is the vapor pressure in Pa.

The cloudiness factor f_{cloud} is an estimate of the fraction of the sky that is cloud covered and is estimated as the ratio of the direct shortwave radiation to what would be possible under clear skies. We assume that the atmospheric transmission factor for extraterrestrial radiation does not exceed 0.8 [see for example, *Shuttleworth*, 1993 p4.5], the remainder of radiation being absorbed or back scattered into space. Equation (A9) gave the maximum fraction of direct radiation as 0.835. Combining this with the maximum transmission factor of 0.8 for extraterrestrial radiation suggests a maximum value for the transmission factor for direct radiation:

$$\tau_{dir,max} = 0.8 \times 0.835 = 0.668 \quad (A19)$$

The actual atmospheric transmission factor for direct radiation is estimated as

$$\tau_{dir} = k_t \cdot (1 - f_{dif}) \quad (A20)$$

Therefore the cloudiness factor can be estimated as:

$$f_{cloud} = 1 - \frac{\tau_{dir}}{\tau_{dir,max}} = 1 - \frac{\tau_{dir}}{0.668} \quad (A21)$$

The above approach to estimate the cloudiness factor cannot be used during nighttime because I_{et} is zero and k_t is not determinable. During nighttime we use the daytime average of k_t weighted by I_{et} .

Outgoing longwave radiation from the snow cover is estimated using a snow surface temperature T_s (K) set to the minimum of 273 K and the air temperature.

$$R_{lw,snow}(\bar{x}) = \varepsilon_{snow} \cdot \sigma \cdot T_s(\bar{x})^4 \quad (\text{A22})$$

Outgoing longwave radiation from the ground is computed based on a ground temperature assumed equal to the air temperature T_a (K).

$$R_{lw,ground}(\bar{x}) = \varepsilon_{ground} \cdot \sigma \cdot T_a(\bar{x})^4 \quad (\text{A23})$$

The emissivity of snow was taken as 0.99 [Tarboton and Luce, 1996], and that of the ground was taken as 0.97 [see Table D-1 in Appendix D, Dingman, 1994].

Terrain emitted longwave radiation incident on a given location is computed as a composite of longwave emission from the snow covered fraction (A_f) and bare ground fraction ($1-A_f$) adjusted for the ground view factor ($1-V_d$):

$$R_{lw,terrain}(\bar{x}) = \{A_f \cdot \varepsilon_{snow} \cdot \sigma \cdot T_s(\bar{x})^4 + (1 - A_f) \cdot \varepsilon_{ground} \cdot \sigma \cdot T_a(\bar{x})^4\} \cdot (1 - V_d(\bar{x})) \quad (\text{A24})$$

The net longwave radiation at any location \bar{x} , is then computed as

$$R_{lw,net}(\bar{x}) = R_{lw}(\bar{x}) - R_{lw,out}(\bar{x}) + R_{lw,terrain}(\bar{x}) \quad (A25)$$

where $R_{lw,out}(\bar{x})$ is equal to $R_{lw,snow}(\bar{x})$ if the location has snow on the ground, or equal to $R_{lw,ground}(\bar{x})$ if the location is bare of snow.

The net radiation R_n (W m^{-2}) at any location \bar{x} , is then computed as

$$R_n(\bar{x}) = (1 - A(\bar{x})) \cdot (R_{dir}(\bar{x}) + R_{dif}(\bar{x})) + R_{lw,net}(\bar{x}) \quad (A26)$$

where A is the albedo of the surface determined based on surface properties (snow or vegetation/bare ground).

References

- Dingman, S. L., *Physical Hydrology*, 575 pp., Macmillan, New York, 1994.
- Dozier, J., and J. Frew, Rapid calculation of terrain parameters for radiation modeling from digital elevation data, *IEEE Trans. on Geosci. and Rem. Sens.*, 28(5), 963-969, 1990.
- Duffie, J. A., and W. A. Beckman, *Solar Engineering of Thermal Processes*, Wiley-Interscience, 919 pp., John Wiley and Sons, Inc., New York, 1991.
- Erbs, D. G., S. A. Klein, and J. A. Duffie, Estimation of the diffuse radiation fraction for hourly, daily and monthly-average global radiation, *Solar Energy*, 28, 293, 1982.
- Satterlund, D. R., An improved equation for estimating long-wave radiation from the atmosphere, *Water Resour. Res.*, 15, 1643-1650, 1979.

Shuttleworth, W. J., Evaporation, in *Handbook of Hydrology*, edited by D. R. Maidment, pp. 4.1–4.53, McGraw-Hill, New York, 1993.

Tarboton, D. G., and C. H. Luce, *Utah Energy Balance Snow Accumulation and Melt Model (UEB), Computer Model Technical Description and Users Guide*, Utah Water Res. Lab., Logan, 1996.

Appendix B: Permission Letters

Date: Mon, 10 Sep 2001 11:23:14 -0400
 From: Allison Levine <ALevine@agu.org>
 Subject: Re: Copyright Permission
 To: David Tarboton <dtarb@cc.usu.edu>
 Organization: AGU
 X-Mailer: Mozilla 4.76 [en] (Windows NT 5.0; U)
 X-Accept-Language: en
 Original-recipient: rfc822;dtarb@cc.usu.edu

Dear David:

We are pleased to grant permission for the use of the material requested for inclusion in your thesis. The following non-exclusive rights are granted to AGU authors:

- . All proprietary rights other than copyright (such as patent rights).
- . The right to present the material orally.
- . The right to reproduce figures, tables, and extracts, appropriately cited.
- . The right to make hard paper copies of all or part of the paper for classroom use.
- . The right to deny subsequent commercial use of the paper.

Further reproduction or distribution is not permitted beyond that stipulated. The copyright credit line should appear on the first page of the article or book chapter. The following must also be included, "Reproduced by permission of American Geophysical Union." To ensure that credit is given to the original source(s) and that authors receive full credit through appropriate citation to their papers, we recommend that the full bibliographic reference be cited in the reference list. The standard credit line for journal articles is: "Author(s), title of work, publication title, volume number, issue number, page number(s), year. Copyright [year] American Geophysical Union."

If an article was placed in the public domain, in which case the words "Not subject to U.S. copyright" appear on the bottom of the first page or screen of the article, please substitute "published" for the word "copyright" in the credit line mentioned above.

I hope this will be sufficient.

Regards,

Allison Levine
 Program Manager, Publications Directorate

David Tarboton wrote:

- > Dear Alision,
- > This is to request permission to include a complete copy of the paper
- > Prasad, R., D. G. Tarboton, G. E. Liston, C. H. Luce and M. S.
- > Seyfried, "Testing a Blowing Snow Model Against Distributed Snow

> Measurements at Upper Sheep Creek, Idaho, USA," Water Resources
> Research, 37(5):1341-1356. 2001.
> as a chapter in Rajiv Prasad's PhD dissertation to be published at
> Utah State University. This paper was prepared as part of Rajiv's
> dissertation work. Please let me know if you need any additional
> information.
> Thank you.
> David Tarboton
>
> -----
> David Tarboton
> Professor, Civil and Environmental Engineering
> Water Program Coordinator, Utah Water Research Laboratory
> Utah State University, Logan UT 84322-8200
> Ph: (435) 797 3172 Fax: (435) 797 3663
> Email: dtarb@cc.usu.edu <http://www.engineering.usu.edu/dtarb/>
> -----

--

Allison Levine
Program Manager, Publications Directorate
Manager, Publications Administration
(t) 202-777-7380
(f) 202-328-0566
alevine@agu.org

Return-Path: <cluce@rmci.net>
 Received: from svl.boise.rmrs.fs.fed.us ([166.2.21.1])
 by out012.verizon.net (InterMail vM.5.01.04.01 201-253-122-
 122-101-20011014) with ESMTP id <20011221003419.NEH13990.
 out012.verizon.net@svl.boise.rmrs.fs.fed.us>
 for <rajiv.prasad@gte.net>; Thu, 20 Dec 2001 18:34:19 -0600
 Received: from pcl512.rmci.net (pcl512.boise.rmrs.fs.fed.us
 [166.2.21.101]) by svl.boise.rmrs.fs.fed.us
 (AIX4.3/8.9.3/8.7) with ESMTP id RAA67032 for
 <rajiv.prasad@gte.net>; Thu, 20 Dec 2001 17:33:54 -0700
 Message-Id: <5.1.0.14.0.20011220173426.00a8b2a0@rmci.net>
 X-Sender: cluce@rmci.net (Unverified)
 X-Mailer: QUALCOMM Windows Eudora Version 5.1
 Date: Thu, 20 Dec 2001 17:35:39 -0700
 To: "Rajiv Prasad" <rajiv.prasad@gte.net>
 From: Charlie Luce <cluce@rmci.net>
 Subject: Re: permission letter
 In-Reply-To: <005b01c1867f\$3cb618e0\$451dla3f@jeeves>
 Mime-Version: 1.0
 Content-Type: text/plain; charset="us-ascii"; format=flowed

Hi Rajiv,
 Congratulations on finishing up. You have my permission to include
 these papers in your dissertation.

Sincerely,
 Charles H. Luce

At 02:15 PM 12/16/2001 -0800, you wrote:

>Dear Charlie:

>

>This e-mail is to request permission to include in my dissertation,
 >complete copies of the following papers in which you appear as
 >coauthor:

>

> Prasad, R., D. G. Tarboton, G. E. Liston, C. H. Luce, and
 > M. S. Seyfried, "Testing a blowing snow model against
 > distributed snow measurements at Upper Sheep Creek, Idaho,
 > USA," Water Resources Research, 37(5): 1341-1356. 2001.

>

> Prasad, R., D. G. Tarboton, G. R. Flerchinger, Keith R. Cooley,
 > and C. H. Luce, "Understanding the hydrologic behavior of a
 > small semiarid mountainous watershed in Idaho, USA,"
 > Submitted to Hydrological Processes, 2000.

>

> Prasad, R., D. G. Tarboton, and C. H. Luce, "Hydrologic behavior
 > of a fourth-order watershed in Reynolds Creek, Idaho, USA,"
 > To be submitted to Hydrological Processes, 2002.

>

>Thanks for your help.

>

>Rajiv Prasad.

>(rajiv.prasad@gte.net)

Return-Path: <kroyco@sprintmail.com>
 Received: from swan.prod.itd.earthlink.net ([207.217.120.123]) by
 mta004.verizon.net (InterMail vM.5.01.04.01 201-253-122-122-
 101-20011014) with ESMTP id <20011222035454.HIRQ17629.
 mta004.verizon.net@swan.prod.itd.earthlink.net> for
 <rajiv.prasad@gte.net>; Fri, 21 Dec 2001 21:54:54 -0600
 from lcust200.tnt6.boise.id.da.uu.net ([63.39.113.200]
 helo=kroyco) by swan.prod.itd.earthlink.net with smtp (Exim
 3.33 #1) id 16HdFN-0005lq-00 for rajiv.prasad@gte.net;
 Fri, 21 Dec 2001 19:54:54 -0800
 Message-ID: <000701c18a9d\$b6a13000\$c871273f@earthlink.net>
 From: "Keith Cooley" <kroyco@sprintmail.com>
 To: "Rajiv Prasad" <rajiv.prasad@gte.net>
 References: <005d01c1867f\$46ba5630\$451dla3f@jeeves>
 Subject: Re: permission letter
 Date: Fri, 21 Dec 2001 21:04:10 -0700
 MIME-Version: 1.0
 Content-Type: text/plain; charset="iso-8859-1"
 Content-Transfer-Encoding: 7bit
 X-Priority: 3
 X-MSMail-Priority: Normal
 X-Mailer: Microsoft Outlook Express 5.50.4522.1200
 X-MimeOLE: Produced By Microsoft MimeOLE V5.50.4522.1200

Hi Rajiv

It was good to hear from you. You have my permission to use the paper
 as part of your dissertation. Hope all works out for you.

Keith R. Cooley

----- Original Message -----

From: "Rajiv Prasad" <rajiv.prasad@gte.net>
 To: <kroyco@sprintmail.com>
 Sent: Sunday, December 16, 2001 3:16 PM
 Subject: permission letter

> Dear Keith:
 >
 > This e-mail is to request permission to include in my dissertation,
 > complete copies of the following papers in which you appear as
 > coauthor:
 >
 > Prasad, R., D. G. Tarboton, G. R. Flerchinger, Keith R. Cooley,
 > and C. H. Luce, "Understanding the hydrologic behavior of a
 > small semiarid mountainous watershed in Idaho, USA," Submitted
 > to Hydrological Processes, 2000.
 >
 > Thanks for your help.
 >
 > Rajiv Prasad.
 > (rajiv.prasad@gte.net)

CURRICULUM VITAE

Rajiv Prasad
(December, 2001)

Education:

Doctor of Philosophy in Civil and Environmental Engineering
Utah State University, Logan, Utah (2001)
Master of Technology in Civil Engineering
Indian Institute of Technology, Madras, India (1992)
Bachelor of Engineering in Civil Engineering
Regional Engineering College, Durgapur, India (1990)

Job Experience:

Postdoctoral Research Associate, Hydrology Group
Pacific Northwest National Laboratory, Richland, Washington (August 2000
onwards)

Research Experience:

Graduate Research Assistant, Water Division, Utah Water Research Laboratory,
Utah State University, Logan, Utah (1993-2000)

Awards and Honors:

Dean's Merit List, Utah State University (1994)
Graduate Student Scholar, Indian Institute of Technology, Madras, India (1990-1992)
Gold Medalist, Civil Engineering, University of Burdwan, India (1990)
Merit Scholarship, Regional Engineering College, Durgapur, India (1986-1990)

Research Publications:

Prasad, R., D. G. Tarboton, and C. H. Luce, Application of a Spatially Distributed Hydrologic Model to Semi-Arid Mountainous Watersheds, 17th Annual AGU Hydrology Days, Fort Collins, Colorado, April 14-18, 1997.

Prasad, R., D. G. Tarboton, G. N. Flerchinger, K. R. Cooley, and C. H. Luce, Understanding the hydrologic behavior of a small semi-arid mountainous watershed, *Eos Trans. AGU*, Fall Meet. Suppl., 80(46), Abstract H21B-19, 1999.

Prasad, R., D. G. Tarboton, G. E. Liston, C. H. Luce, and M. S. Seyfried, Testing a Blowing Snow Model Against Distributed Snow Measurements at Upper

Sheep Creek, *Eos Trans. AGU*, Fall Meet. Suppl., 80(46), Abstract H11E-07, 1999.

Prasad, R., D. G. Tarboton, G. N. Flerchinger, K. R. Cooley, and C. H. Luce, Understanding the Hydrologic Behavior of a Small Semi-Arid Mountainous Watershed in Idaho, United States of America, *Submitted to Hydrological Processes*, 2000.

Prasad, R., D. G. Tarboton, G. E. Liston, C. H. Luce, and M. S. Seyfried, Testing a blowing snow model against distributed snow measurements at Upper Sheep Creek, Idaho, United States of America, *Water Resour. Res.*, 37(5), 1341-1356, 2001.

Prasad, R. and M. S. Wigmosta, Scalability issues in process-based hydrologic modeling, *Eos Trans. AGU*, Fall Meet. Suppl., 82(47), Abstract H12C-0312, 2001.